Understanding Cross-Polarization NMR Experiments Using Multi-Mode Floquet Theory

A thesis

submitted by

Zeba Qadri

for the partial fulfillment of the degree

of

DOCTOR OF PHILOSOPHY

Department of Chemical Sciences
Indian Institute of Science Education and Research Mohali
Mohali-140306
June 2015

Dedicated to My Grandfather

"Maulana Shah Fazle Ahmad Qadri"

Declaration

The work presented in this thesis entitled **"Understanding Cross-Polarization NMR Experiments Using Multi-Mode Floquet Theory"** has been carried out by me under the supervision of **Dr. Ramesh Ramachandran** in the Department of Chemical Sciences, Indian Institute of Science Education and Research (IISER) Mohali, Mohali.

This work has not been submitted in part or in full for a degree, diploma, or a fellowship to any other university or institute.

Whenever contributions of others are involved, every effort is made to indicate this clearly, with due acknowledgments of collaborative research and discussions. This thesis is a bona fide record of original work done by me and all sources listed within have been detailed in the bibliography.

Dated: November 18, 2015 **Zeba Qadri**

Place: Mohali (Candidate)

In my capacity as the supervisor of the candidate's thesis work, I certify that the above statements by the candidate are true to the best of my knowledge.

Dr. Ramesh Ramachandran

Assistant Professor
Department of Chemical Sciences
Indian Institute of Science Education and Research Mohali

Acknowledgements

I am extremely grateful to my supervisor, Dr. Ramesh Ramachandran for giving me the opportunity to work with him. I have high regards for his enthusiasm towards research and teaching. I would like to thank him for the guidance, encouragement and advice he has provided throughout my time as his student. I have been extremely lucky to have a supervisor who cared so much about my work, and who responded to my questions and queries so promptly. I also gratefully acknowledge his patience and endurance.

I would like to thank Prof. N. Sathyamurthy, Director, IISER Mohali for providing the infrastructure and all the necessary facilities to work in this institute. I would also like to thank my doctoral committee members, Prof. K. S. Viswanathan and Dr. Vinayak Sinha for their valuable comments.
I would like to take the opportunity to thank IISERM for providing me Fellowship and all kind of facilities and support during my Ph.D programme.

I am grateful to Dr. Manoj Kumar Pandey, Mr. Suba Rao and Mr. SivaRanjan for their immense support, kind help and useful discussions during my project. I would like to thank Deepansh for helping me with Latex whenever needed. Mr. Vinay is especially acknowledged for his compelling efforts towards improving my presentation skills. I am also thankful to Shivam for valuable discussions.

I am grateful to my parents and sister for encouraging me throughout my journey. I especially thank my husband for his continuous support, patience and encouragement. I would like to thank my friends Nidhi and Sadhika for their love and moral support.

List of Figures

List of Tables

Notations

I	Spin quantum number
h	Planck's constant
$\|IM\rangle$	Ket Eigen basis
I_x, I_y, I_z	Spin angular momentum operators
I^+, I^-	Lowering and Raising operators
Tr	Trace of matrix
$\left\langle \hat{O}_P \right\rangle$	Expectation value of corresponding observable
t	Time parameter
τ_{mix}	Mixing-time
i	Iota
$\rho(0)$	Initial density operator
$\rho(t)$	Evolved density operator
ω_0	Larmor frequency
ω_{RF}	Amplitude of oscillating RF field
${\omega_I}^{(0)}$	Isotropic chemical-shift
δ	Magnitude of Chemical-shift anisotropy
${\omega_I}^{(m)}$	Chemical-shift anisotropy in powder sample
$T^{(k)q}$	Spin Tensor
$R^{(k)-q}$	Spatial Tensor
ω_{ij}	Dipolar constant

RF	Oscillating magnetic field
H	Hamiltonian
H_{RF}	RF interaction Hamiltonian
H_I, H_S	Single-spin Hamiltonian
H_{IS}	Two-spin Hamiltonian
H_R	Hamiltonian in the rotating frame
H_{TR}	Hamiltonian in the Tilted Rotating frame
H_{TRF}	Hamiltonian in the Tilted RF interaction frame
U	Unitary transformation
S_1	Transformation function
k	rank
q	component
$\tilde{H}$	Hamiltonian after first transformation
$\tilde{\tilde{H}}$	Hamiltonian after second transformation
$H_0^{(1)}, H_1^{(1)}, H_2^{(1)}$	Zeroth, 1st, 2nd, order Hamiltonians respectively, after first Transformation
$H_0^{(2)}, H_1^{(2)}, H_2^{(2)}$	Zeroth, 1st, 2nd, order Hamiltonians respectively, after second Transformation
^1H	Proton
^{13}C	NMR active isotope of carbon (I=1/2)
^{15}N	NMR active isotope of nitrogen (I=1/2)

DQ	Double quantum
ZQ	Zero quantum
MHz	Mega Hertz
KHz	Kilo Hertz
PAS	Principle Axis System
LAS	Lab Axis System
$MolAS$	Molecular Axis System
RAS	Rotor Axis System
CP	Cross-polarization
$CWCP$	Continuous Wave Cross-polarization
$PMCP$	Phase Modulated Cross-polarization

Abstract

Magic Angle Spinning (MAS) is an important technique routinely employed for obtaining high resolution nuclear magnetic resonance (NMR) spectra in the solid state. In combination with MAS, the cross-polarization (CP) experiment (referred to as CPMAS) forms a vital building block in the design of multi-dimensional solid-state NMR (ssNMR) experiments for studying less sensitive/abundant nuclei. But efficient implementation of CP schemes at faster MAS remains a challenge. Since, the efficiency of CP under MAS depends on intrinsic parameters such as the orientation of the dipolar tensor, magnitude of the chemical shift anisotropy (CSA) interactions and other user control parameters such as the spinning frequency and RF amplitudes, quantitative description of the underlying spin dynamics has always remained elusive. So, along with the development of NMR experiments, refinements in NMR theory are also essential for designing sophisticated experiments and for extracting meaningful constraints from experimental data. To this end, a modified version of the CP experiment is proposed employing the concept of effective Hamiltonians based on multi-mode Floquet theory. In contrast to other existing schemes in the literature, the proposed schemes could be implemented at higher magnetic field strengths and at faster spinning frequencies. Since bio-molecular applications of solid-state NMR (ssNMR) entail the presence of faster spinning modules, we believe that the design of NMR experiments based on our approach would be beneficial. Additionally, the mechanism of polarization

transfer in CP experiments is described intuitively invoking the phenomenon of dipolar truncation. We believe that the current study would provide the necessary impetus for better design of ssNMR experiments and could be a guiding tool for quantifying the experimental data. The validity of the predictions emerging from our theory is verified with numerical simulations under different experimental conditions.

Contents

Chapter 1

Introduction

1.1 Background

Ever since its discovery in 1946[1–3], nuclear magnetic resonance (NMR) spectroscopy has become an indispensable tool for investigating molecular structure in wide range of systems of chemical, biological and medical relevance. In spite of its lower sensitivity, NMR enjoys wide popularity (as an analytic tool) mainly due to the flexibility that it offers in the design of experiments. Through careful manipulation of the nuclear spin interactions, structural constraints at the molecular level (both in the liquid and solid state) are obtained through sophisticated experiments. Unlike other forms of spectroscopy, the phenomenon of magnetic resonance (like NMR and Electron Spin Resonance (EPR)) results from a quantum property referred to as "spin". Just like charge, mass, etc., spin is also a fundamental property exhibited by all sub-atomic particles like electrons, protons, neutrons, etc. Being a quantum property, the spin of a nucleus is represented by the spin quantum number 'I' and is manifested as spin angular momentum. The charge distribution within the nucleus facilitates the interaction of matter with the magnetic field component of the electromagnetic (EM) radiation. In nuclei

with spherical symmetry (nuclei with $I = 1/2$ satisfy this criterion), the charge distribution is uniform and results in an intrinsic property commonly referred to as 'magnetic dipole moment'. Interestingly, nuclei with non-spherical distribution of charge (observed in nuclei with $I > 1/2$) result in both dipole as well as quadrupole moment. In contrast to the magnetic dipole moment, the quadrupole moment of a nucleus is larger in magnitude and interacts with the electric field gradient surrounding the nucleus resulting in quadrupolar interaction. A more detailed description of the various nuclear spin interactions are well-documented in the literature[4–7] and have been consciously omitted in this thesis to avoid repetition.

Similar to other forms of spectroscopy, the appearance of the NMR spectrum depends on the physical state of the sample under investigation. One of the prominent features being the broadened spectra in the solid state. The restricted mobility in the solid state renders the spin interactions anisotropic and is primarily responsible for the line broadening observed in the spectrum[5]. By contrast, the rapid isotropic motion inherent in the solution state averages the anisotropic interactions and effectively removes them from the spectrum. At first sight, this might force us to conclude that high resolution NMR spectroscopy would inevitably be confined to liquid samples. Such a restriction would have been a serious limitation, since interesting systems of chemical and biological relevance are either insoluble (in suitable organic solvents) or do not crystallize. However, with the combined efforts of several research groups[8–31], solid-state NMR (ssNMR) is rapidly emerging as a viable alternative to solution NMR spectroscopy for structural studies in

proteins. As in solution NMR, efforts to develop ssNMR techniques for proteins labeled uniformly with ^{13}C and ^{15}N are underway in several laboratories[8–31]. To determine the overall three-dimensional structure of peptides/proteins, it is essential to integrate different NMR experiments and apply them to ^{13}C, ^{15}N-labeled samples depending on the complexity of the system[24–29]. This requires sequence-specific assignment of NMR resonances and measurement of sufficient number of structural constraints (e.g. internuclear $^{13}C -^{13} C$ and $^{13}C -^{15} N$ distances and torsion angles) to obtain a high-resolution structure that is consistent with these constraints[30–32].

The initial breakthrough in solid-state NMR (ssNMR) was provided in 1958 by Andrew and coworkers[33] and independently by Lowe[34] in the form of 'magic angle spinning' (MAS) experiments. In their experiment, the sample under investigation was rotated along an axis (also referred to as rotor axis) inclined at an angle $\theta_m = 54.736^0$ with respect to the external magnetic field. On rapid rotation of the sample along this axis, the broadening effects due to the anisotropic interactions get minimized resulting in fine structures similar to those found in the solution state.

The next obstacle in the high-resolution NMR of solids was the sensitivity factor. In general, the sensitivity of a nucleus depends on two intrinsic properties: (1) natural abundance (2) gyromagnetic ratio. Accordingly, nuclei with lesser abundance and lower gyromagnetic ratios are often termed as dilute nuclei. Due to favourable chemical shift dispersion, the NMR spectra of dilute nuclei (such as ^{13}C, ^{15}N) are preferred (over ^{1}H-NMR) in structural investigations in the

solid state. To improve the sensitivity of dilute nuclei, Hartmann and Hahn[35] proposed a novel double resonance experiment (later referred to as 'Cross-polarization' (CP)), wherein, the polarization from a sensitive nucleus (nuclei with higher gyromagnetic ratio, γ and higher natural abundance) is transferred to the dilute nuclei of interest through the dipolar interactions. From an experimental perspective, the polarization transfer observed in CP experiments is facilitated through a resonance like phenomenon that involves careful matching of the amplitudes of the oscillating radio-frequency (RF) fields that are employed on the two channels. Hence, the combination of MAS with CP experiment seemed a probable solution for improving both the resolution and sensitivity of the spectrum in the solid state. In Fig. 1.1, the basic CP scheme is depicted.

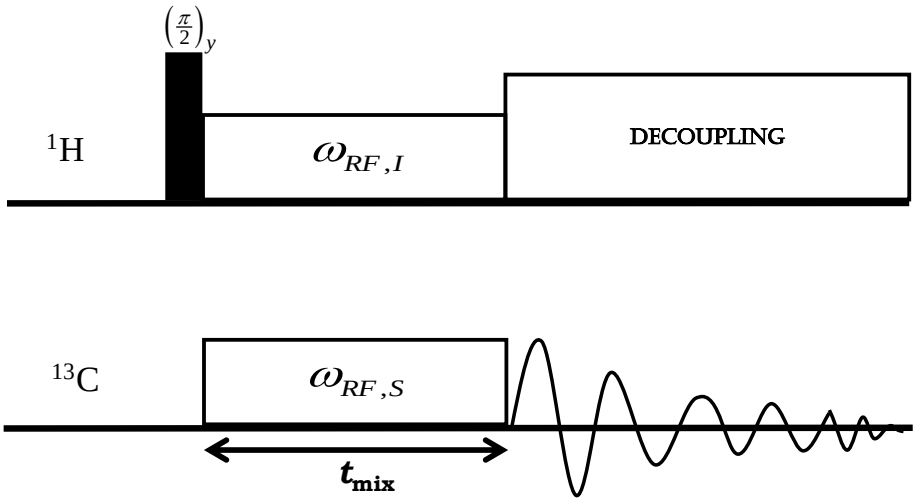

Figure 1.1: Pulse scheme for Continuous Wave CP

Interestingly, from a conceptual viewpoint, this initial line of thought seemed impractical owing to the averaging effect of MAS. Since dipolar interactions facili-

tate the transfer of polarization among spins, the CP experiment was expected to fail under MAS conditions. Nevertheless, in 1973 Waugh and coworkers successfully demonstrated the implementation of CP experiment under MAS conditions. In their implementation of the CP experiment, the averaging effect of MAS (on the dipolar interactions) was compensated temporarily during the CP period by a careful manipulation of the amplitudes of the RF fields employed on the two channels. Unlike the matching conditions in static CP experiments, the amplitudes of the RF field employed on the two channels are highly sensitive to the spinning frequency and are described in detail in the second chapter. Subsequently, the CPMAS experiment[36] has become an integral building block in the design of multi-dimensional solid state NMR experiments for studying dilute nuclei[8,37–53,53–65]. With the availability of higher magnetic field strengths and faster spinning modules, sophisticated variants to the original CP experiment have been developed in the past[37–53,53–63]. Consequently, suites of multi-dimensional experiments involving dilute nuclei (such as ^{13}C, ^{15}N) have emerged in ssNMR and have all been well documented in recent literature[8,64,65].

In spite of the tremendous progress made in the last two decades, ssNMR is still a developing field and methods towards structural characterization are just emerging. Similar to other spectroscopic methods, the success of ssNMR relies on the accuracy of the estimated molecular constraints such as inter-atomic distances, torsion angles etc. Since the number of molecular constraints estimated through ssNMR experiments is limited (due to resolution), the accuracy of the estimated constraints become important in the overall refinement of structure.

Hence, along with the progress on the experimental front, development of analytic theory/mathematical models is essential for both quantifying experiments and designing sophisticated variants to existing experiments. Since the molecular constraints in NMR spectroscopy are estimated through measurement of spin polarizations, understanding the mechanism of polarization transfer among nuclear spins is vital for developing mathematical models for quantifying experimental data. With this objective in mind, an analytic theory based on the concept of effective Hamiltonians is proposed in this thesis for elucidating the mechanism of polarization transfer in ssNMR experiments. A brief outline of the thesis is presented in the following sections.

1.2 Objectives and Motivation

Problem-1:

To develop an analytic theory/model for describing multiple-pulse sequences with cycle times occurring at competing timescales with respect to the MAS rotor period.

Motivation:

To extend the utility of ssNMR in studying biophysical systems, availability of higher magnetic field strengths and faster spinning modules are essential to improve the resolution of the spectrum. Very often, at faster spinning frequencies, the cycle time of a typical multiple-pulse sequence approaches to that of the MAS rotor period. From a theoretical standpoint, the averaging effects of MAS and multiple-pulse sequences become inseparable in the fast spinning regime and the

whole concept of a time-averaged Hamiltonian based on average Hamiltonian theory (AHT)[4,66] becomes invalid. Hence, development of analytic methods based on Floquet theory[67] are essential for describing periodic multiple-pulse sequences that are incommensurate with the MAS rotor period.

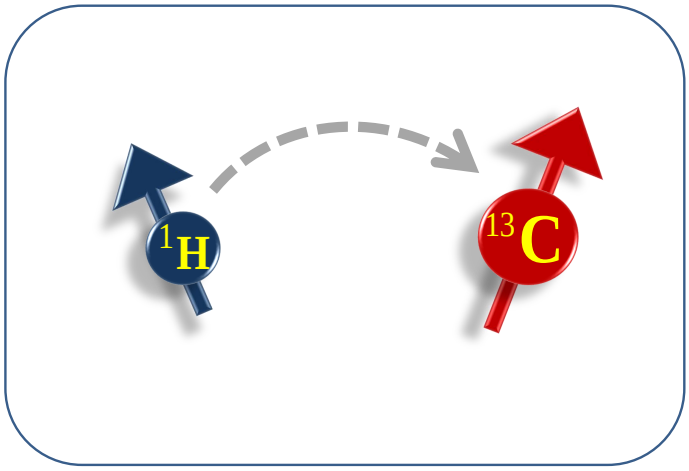

Figure 1.2: CP in an isolated two-spin system

Problem-2:

To understand the role of time-dependent oscillating fields (phase and amplitude modulation) in heteronuclear polarization transfer experiments.

Motivation:

In a typical multiple-pulse sequence, the phase and amplitude of the oscillating magnetic fields play an important role in the time-evolution of the spin system of interest. In particular, understanding the interconnection between spinning frequency, modulation frequency and RF amplitude is essential in the design of multiple-pulse sequences at faster MAS frequencies. Employing multimodal Flo-

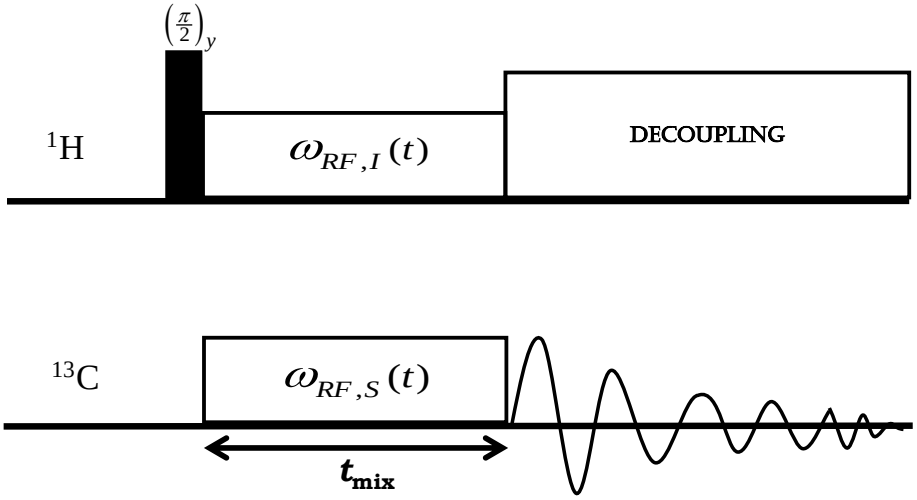

Figure 1.3: Phase/amplitude-modulated CP scheme

quet theory[68], we present an analytic theory for deducing the resonance conditions in CP experiments that employ phase/amplitude modulations that are incommensurate with the MAS rotor period.

Problem-3:

To develop a mathematical model for quantifying polarization transfer to a given target spin from multiple spin sites.

Motivation:

As discussed earlier, the number of molecular constraints (say interatomic distances, torsion angles, etc.) that could be estimated from ssNMR are limited due to poor resolution. Hence, the accuracy of the estimated constraints remain vital in the refinement of the three-dimensional structure of a typical biological system. Additionally, due to spectral crowding (a case often encountered in the study of

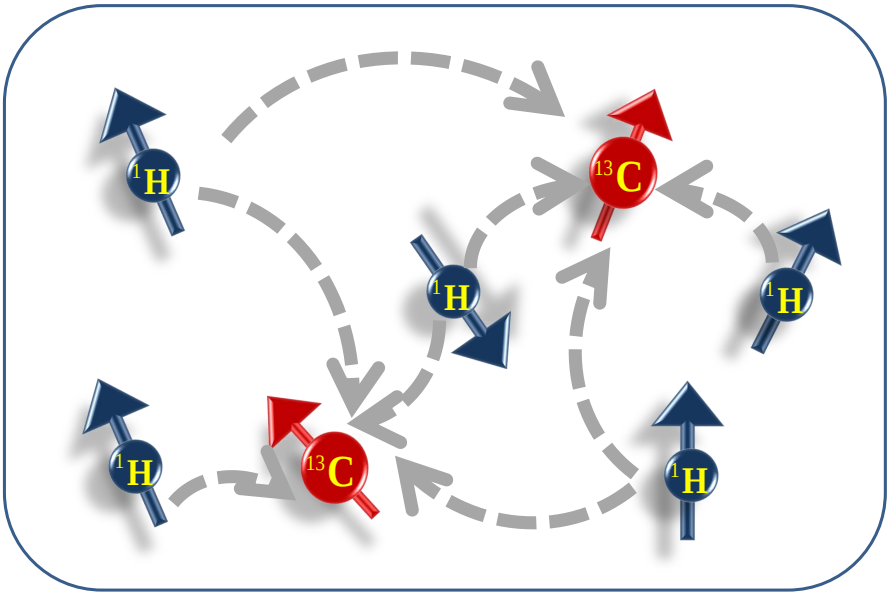

Figure 1.4: Polarization transfer from protons to carbons in CP experiments

proteins), selective transfer of polarization is hardly achieved in practice. In such cases, theoretical descriptions built on isolated spin pair models are of limited utility. As an alternative, models built on the concept of effective Hamiltonians seem to be an attractive solution and would be explored in this thesis.

1.3 Methodology

In the operator formulation of quantum mechanics, the time-evolution of a system is described by the Liouville-von Neumann equation,[69]

$$i\hbar\frac{\partial\rho(t)}{\partial t} = [H, \rho(t)] \tag{1.1}$$

where, $\rho(t)$ denotes the state of the system after some time 't'. The internal interactions of the system along with its interaction with the external fields (electric/or

magnetic) is included in the Hamiltonian operator, 'H'. When the Hamiltonian is time-independent, the state of a system at any instant of time 't' is given by the expression

$$\rho(t) = \exp\left\{-\frac{i}{\hbar}Ht\right\}\rho(0)\exp\left\{\frac{i}{\hbar}Ht\right\} \tag{1.2}$$

Subsequently, the expectation value of any observable is calculated by the expression given below:

$$\left\langle \hat{O}p(t)\right\rangle = Trace\left[\hat{O}p.\rho(t)\right] \tag{1.3}$$

However, as depicted in eq. 1.4, the solution gets quite complicated when the Hamiltonian is explicitly time-dependent,

$$\rho(t) = T\exp\left\{-\frac{i}{\hbar}\int_0^t H(t')dt'\right\}\rho(0)T\exp\left\{\frac{i}{\hbar}\int_0^t H(t')dt'\right\} \tag{1.4}$$

In the brute force approach, the solution to the above problem is obtained numerically by evaluating the time-evolution of the system at shorter time-periods by assuming a time-independent Hamiltonian. Although such approaches are quite useful, they are of lesser utility in understanding the nuances of experiments. To design new experiments or improve existing experiments, it is important to have a deeper understanding of the spin physics at the microscopic level. Hence, analytic methods based on average Hamiltonian theory (AHT)[4,66] and Floquet theory[67] were employed in the past to understand and design ssNMR experiments. In both these approaches, the time-evolution of a system is described through a time-averaged effective Hamiltonian employing different approximations. In the

AHT[4,66] approach, the cycle times of the multiple-pulse sequences are synchronized on purpose with the MAS rotor period and effective Hamiltonians to the desired order are derived through Magnus expansion[70]. By contrast, the Floquet approach presents a more general framework for describing ssNMR experiments without imposing any restriction on the time-modulations. With the availability of faster spinning modules, design of multiple-pulse experiments at faster spinning frequencies become quite daunting owing to the competing nature of the MAS and RF modulations. In such cases, Floquet theory[67] seems to be better suited for describing schemes that are incommensurate with the spinning frequency. A formal description of multiple-pulse experiments with cycle times incommensurate with the MAS rotor period is described in this thesis.

To begin with, the nuclear spin Hamiltonians under sample rotation is both time-dependent and periodic[5]. As often the case, the Hamiltonian in the rotating frame is expressed as a sum of single-spin and two-spin interactions represented by,

$$H(t) = H_{single-spin}(t) + H_{two-spin}(t) + H_{RF}(t) \tag{1.5}$$

The single-spin interaction comprises of the isotropic and anisotropic chemical shift interactions and is represented by,

$$H_{single-spin}(t) = \sum_{m=-2}^{2} \omega_I^{(m)} e^{im\omega_r t} I_z + \sum_{m=-2}^{2} \omega_S^{(m)} e^{im\omega_r t} S_z \tag{1.6}$$

The interaction among spins is depicted through two-spin Hamiltonians. Hence, in this thesis, we confine our discussion only to the dipolar interactions,

$$H_{two-spin}(t) = \sum_{\substack{m=-2,\\ m\neq 0}}^{2} \omega_{IS}^{(m)} e^{im\omega_r t} \left[2I_z S_z - \frac{1}{2} \left\{ I^+ S^- + I^- S^+ \right\} \right] \tag{1.7}$$

In the case of homonuclear dipolar interactions the flip-flop term ($I^+S^- + I^-S^+$) is retained while in heteronuclear dipolar interactions it is neglected.

The RF-Hamiltonian is represented by,

$$H_{RF}(t) = \omega_{RF,I}(t) I_x + \omega_{RF,S}(t) S_x \tag{1.8}$$

In the rotating frame, the RF-Hamiltonian could be time-dependent either due to variation in its amplitude or phase or both. Such modulations are always periodic and could be expressed as a Fourier series. To gain analytic insights, the Hamiltonian is transformed into the RF interaction frame wherein the evolution of the system is governed only by its internal Hamiltonian.

Although several descriptions based on AHT[4,66] exist in the literature, Floquet theory[67] presents a comprehensive framework for describing the dynamics of MAS experiments under oscillating RF fields. In the Floquet approach, the time-dependent Hamiltonian is transformed to a time-independent Hamiltonian through the use of a Fourier series expansion and Floquet theorem.

Consequently, both the nuclear spin states ($|IM\rangle$) and the operators ($T^{(k)q}$) are dressed with the Fourier indices associated with the various modulations in the system i.e., $|IM, m, n_1, n_2\rangle$ and $T^{(k)q}_{m,n_1,n_2}$. The periodic modulation imposed by sample rotation is depicted through the Fourier index 'm', while the indices

n_1, n_2 depict the modulations due to the oscillating RF fields on spins I and S, respectively. Employing the Floquet operators the Floquet Hamiltonian is defined as,

$$\begin{aligned} H_F =& \omega_r I_F^{(m)} + \omega_{RF,I} I_F^{(n_1)} + \omega_{RF,S} I_F^{(n_2)} \\ &+ \sum_{\substack{q=-1,\\ q\neq 0}}^{1} \sum_{m=-2}^{2} \left[\sum_{n_1=-\infty}^{\infty} G^{(1)q}_{m,n_1,0}(I) i T^{(1)q}_{m,n_1,0}(I) + \sum_{n_2=-\infty}^{\infty} G^{(1)q}_{m,0,n_2}(S) i T^{(1)q}_{m,0,n_2}(S) \right] \\ &+ \sum_{k=0}^{2} \sum_{q=-k}^{k} \sum_{\substack{m=-2,\\ m\neq 0}}^{2} \sum_{n_1,n_2=-\infty}^{\infty} \left[G^{(k)q}_{m,n_1,n_2}(IS) T^{(k)q}_{m,n_1,n_2}(IS) \right] \end{aligned} \tag{1.9}$$

To study the time evolution of a spin system, the Floquet Hamiltonian needs to be diagonalized. One of the standard approaches involves numerical diagonalization in which the eigenvalues are obtained by truncating the dimension of the Floquet matrix based on the convergence of the eigenvalues. Although, such an approach seems to be an attractive solution in simple problems, simulations involving multiple time-modulations are quite complicated. This problem is further accentuated with the increase in the number of spins in the system. To overcome this limitation, an analytic description of the underlying spin dynamics in the Floquet space is essential. In the past, this has been accomplished by employing the concept of effective Floquet Hamiltonians derived from the contact transformation method[71–74] (also known as the van Vleck transformation method). The contact transformation method is an operator equivalent of the standard perturbation theory in which all perturbation corrections are obtained in the form of operators resulting in effective, more nearly diagonal Hamiltonians[75].

To facilitate the implementation of the contact transformation procedure, the Floquet Hamiltonian is re-expressed as a sum, comprising of a zero-order (H_0)

and a perturbing Hamiltonian (H_1).

$$H_F = H_0 + H_1 \tag{1.10}$$

where,

$$H_0 = \omega_r I_F^{(m)} + \omega_{RF,I} I_F^{(n_1)} + \omega_{RF,S} I_F^{(n_2)} \tag{1.11}$$

$$H_1 = H_F^{(I)} + H_F^{(S)} + H_F^{(IS)} \tag{1.12}$$

In contrast to the standard perturbation theory, the perturbation corrections in the contact transformation method are derived through unitary transformations and expressed in terms of operators. The transformed Hamiltonian (referred to as effective Hamiltonian) to second-order after a single transformation is represented by,

$$\begin{aligned} H_F^{eff} &= \exp(iS_1) H_F \exp(-iS_1) \\ &= H_0^{(1)} + H_1^{(1)} + H_2^{(1)} \\ H_0^{(1)} &= H_0 \\ H_1^{(1)} &= H_1 + i\,[S_1, H_0] \\ H_2^{(1)} &= \tfrac{i}{2}\,[S_1, H_1] \end{aligned} \tag{1.13}$$

The final stage involves the description of the time-evolution of the system through the quantum-Liouville equation given below.

$$i\hbar \frac{\partial \rho(t)}{\partial t} = \left[H_F^{eff}, \rho(t) \right] \tag{1.14}$$

Here in this thesis, effective Hamiltonians are derived for multiple-pulse experiments that are incommensurate with the spinning frequency. The role of phase

and amplitude modulation is described employing multi-mode Floquet theory[68]. Through appropriately chosen model systems, polarization transfer in strongly coupled systems is described beyond the isolated two-spin framework.

1.4 Organization of the Thesis

Employing the cross-polarization experiment as a case study, an analytic model is proposed in this thesis to describe the mechanism of polarization transfer among heteronuclear spins in ssNMR. To unravel the mechanism of polarization transfer and quantify the experimental data in strongly coupled systems, models beyond the isolated two-spin framework are mandatory. With this objective, an analytical model based on effective Hamiltonians is proposed to describe the polarization transfer to a target spin arising from multiple spin sites. Through the concept of truncated effective Hamiltonians[76], the dimensionality of the problem is reduced in the spin space thereby facilitating an analytic description of the spin dynamics in a reduced subspace. Since bio-molecular applications of ssNMR entail the availability of higher magnetic field strengths and faster spinning modules, implementation of CP experiments at faster spinning frequencies become mandatory[51–54,56]. Consequently, design of experiments involving RF modulations occurring at competing timescales with respect to MAS modulations become inevitable.

In the second chapter, the theory of CP experiments under MAS conditions is described in terms of Floquet theory[67]. In the past, the Floquet approach has been successfully employed for describing pulse experiments employing modulations that are synchronized with the spinning frequency[65,77]. Alternatively, here

in this thesis, we present a framework for describing sequences that employ modulations that are incommensurate with the spinning frequency. Employing a model spin system comprising of two-spins, polarization transfer in both zero-quantum (ZQ) and double-quantum (DQ) experiments is described in terms of simple analytic expressions. The interplay between the various anisotropic interactions is illustrated through simulations by comparing the results obtained from exact numerical methods with those obtained from analytic methods based on effective Hamiltonians. Employing multi-mode Floquet theory[68], an analytic description of phase/amplitude modulated CP experiments is presented in the third chapter.

In the fourth chapter, the scope of the analytic description presented in the second chapter is extended beyond the isolated two-spin framework. Employing the concept of truncated effective Hamiltonians[76], the mechanism of polarization transfer among spins in a strongly coupled network is described. Through appropriate model systems, the important role of dipolar truncation[78] in the propagation of spin polarization in CP experiments is outlined through rigorous comparisons with numerical and analytic simulations.

Finally, the fifth chapter contains the summary of the research work with possible extensions of this work as future prospects.

Appendix-1

Theory (static case)

To describe the CP experiment, we begin our discussion with a model system comprising of two spins (I-S). In the laboratory frame, the Hamiltonian for such a system is represented by,

$$H = H_I + H_S + H_{IS} \tag{1.15}$$

where, H_I and H_S are single spin Hamiltonians, while H_{IS} denotes the interaction Hamiltonian between the spins. The single spin Hamiltonian depicts the interactions between the nuclear spin magnetic moment with both the static and oscillating magnetic fields.

$$H_I = -\hbar\omega_{0I} I_z - 2\hbar\omega_{RF,I}\cos(\omega_{spec,I}t)I_x \tag{1.16}$$

$$H_S = -\hbar\omega_{0S} S_z - 2\hbar\omega_{RF,S}\cos(\omega_{spec,S}t)S_x \tag{1.17}$$

In the above expressions (Eqns. 1.16 & 1.17) 'ω_{0I}' (or ω_{0S}) represents the Larmor frequency while $\omega_{RF,I}$ (or $\omega_{RF,S}$) and '$\omega_{spec,I}$' (or $\omega_{spec,S}$) denote the amplitude and frequency of the oscillating magnetic field. The interaction among the spins is denoted by the dipolar Hamiltonian given below,

$$H_{IS} = 2\omega_{IS} I_z S_z \tag{1.18}$$

where, 'ω_{IS}' is the dipolar constant represented by,

$$\omega_{IS} = \frac{\mu_0 \gamma_I \gamma_S \hbar}{4\pi r_{IS}^3} \left(1 - 3\cos^2\theta\right) \tag{1.19}$$

In the above equation θ denotes the angle between the dipolar vector and the static magnetic field. To describe the evolution of the system under its internal Hamiltonian, the Hamiltonian defined in Eq. 1.15 is transformed into a rotating frame through the transformation function $U_1 = \exp(i\omega_{spec,I} t I_z) \exp(i\omega_{spec,S} t S_z)$

$$H_{I,R} = U_1 H_I U_1^{-1} \tag{1.20}$$

In the rotating frame, the single spin Hamiltonian comprises of a static and a time-dependant terms,

$$H_{I,R} = \hbar(-\omega_{0I} + \omega_{spec,I}) I_z - 2\hbar\omega_{RF,I} \cos(\omega_{spec,I} t) \left[I_x \cos(\omega_{spec,I} t) - I_y \sin(\omega_{spec,I} t)\right] \tag{1.21}$$

Under secular approximation, the time-dependent terms in the above Hamiltonian are ignored and Eq. 1.21 reduces to a much simpler form given below,

$$H_{I,R} = -\hbar\Delta\omega_I I_z - \hbar\omega_{RF,I} I_x \tag{1.22}$$

where, '$\Delta\omega_I$' is the chemical-shift offset for spin-I.

Due to commuting nature of the transformation function U_1 and H_{IS}, the two-spin Hamiltonian remains invariant in the rotating frame.

$$H_{IS,R} = 2\omega_{IS} I_z S_z \tag{1.23}$$

When the oscillating fields on the two-channels are applied on resonance, the Hamiltonian in the rotating frame reduces to a much simpler form,

$$H_R = -\hbar\omega_{RF,I} I_x - \hbar\omega_{RF,S} S_x + 2\omega_{IS} I_z S_z \tag{1.24}$$

(A) Spin Dynamics in the Tilted Rotating Frame

Since the magnitude of the RF fields often exceeds the dipolar coupling constant, the Hamiltonian in the rotating frame is tilted through a unitary transformation, $U_2 = \exp(i\frac{\pi}{2}I_y)\exp(i\frac{\pi}{2}S_y)$ such that the effective fields on individual spins are quantized along the z-axis.

$$H_{TR} = U_2 H_R U_2^{-1} \tag{1.25}$$

Consequently, the dipolar Hamiltonian gets modified and is expressed in terms of zero-quantum (ZQ) and double-quantum (DQ) operators.

$$H_{TR} = \omega_{RF,I} I_z + \omega_{RF,S} S_z + \underbrace{\frac{\omega_{IS}}{2}\left[I^+S^- + I^-S^+\right]}_{ZQ} + \underbrace{\frac{\omega_{IS}}{2}\left[I^+S^+ + I^-S^-\right]}_{DQ} \tag{1.26}$$

To have a consistent description, both the initial density operator ($\rho(0) = I_x$) and the detection operator 'S_x' during the CP mixing period are transformed by the unitary transformations U_1 and U_2.

$$\rho_{TR}(0) = I_z \tag{1.27}$$

$$S_{x,TR} = S_z \tag{1.28}$$

Subsequently, the polarization transfer (from spin I to S) during the CP mixing period is calculated by evaluating the standard expression given below,

$$\langle S_z(t)\rangle = Tr\left[\rho_{TR}(t).S_z\right]$$

$$= Tr\left[\exp(-\tfrac{i}{\hbar}H_{TR}t)\rho_{TR}(0)\exp(\tfrac{i}{\hbar}H_{TR}t).S_z\right]$$

$$= \frac{(\omega_{IS})^2}{(\omega_{IS})^2+(\Delta)^2}\sin^2\left(\frac{\sqrt{(\omega_{IS})^2+(\Delta)^2}t}{2}\right)$$
$$- \frac{(\omega_{IS})^2}{(\omega_{IS})^2+(\sum)^2}\sin^2\left(\frac{\sqrt{(\omega_{IS})^2+(\sum)^2}t}{2}\right) \qquad (1.29)$$

$$\langle I_z(t)\rangle = Tr\left[\rho_{TR}(t).I_z\right]$$

$$= Tr\left[\exp(-\tfrac{i}{\hbar}H_{TR}t)\rho_{TR}(0)\exp(\tfrac{i}{\hbar}H_{TR}t).I_z\right]$$

$$=1 - \left[\begin{array}{l} \dfrac{(\omega_{IS})^2}{(\omega_{IS})^2+(\Delta)^2}\sin^2\left(\dfrac{\sqrt{(\omega_{IS})^2+(\Delta)^2}t}{2}\right) \\ -\dfrac{(\omega_{IS})^2}{(\omega_{IS})^2+(\sum)^2}\sin^2\left(\dfrac{\sqrt{(\omega_{IS})^2+(\sum)^2}t}{2}\right)\end{array}\right] \qquad (1.30)$$

where, $\Delta = \omega_{RF,I} - \omega_{RF,S}$ and $\sum = \omega_{RF,I} + \omega_{RF,S}$. Employing the above expressions, the optimal matching conditions for efficient polarization transfer in CP experiments could be deduced as described below,

(1) ZQ matching condition ($\omega_{RF,I} = \omega_{RF,S}$)

When the amplitude of the RF fields are identical, (i.e. $\Delta = 0$) the above Eqns (1.29 , 1.30) reduce to a much simpler form.

$$\langle S_z(t)\rangle = \sin^2\left(\frac{\omega_{IS}t}{2}\right) \qquad (1.31)$$

$$\langle I_z(t)\rangle = 1 - \sin^2\left(\frac{\omega_{IS}t}{2}\right) \tag{1.32}$$

(2) DQ matching condition ($\omega_{RF,I} = -\omega_{RF,S}$)

In a similar vein, when the amplitudes of the RF fields are phase-shifted (i.e. $\sum = 0$) we get the double-quantum matching condition.

$$\langle S_z(t)\rangle = -\sin^2\left(\frac{\omega_{IS}t}{2}\right) \tag{1.33}$$

$$\langle I_z(t)\rangle = 1 + \sin^2\left(\frac{\omega_{IS}t}{2}\right) \tag{1.34}$$

Based on the above analytic results, it is clear that the exchange trajectories in CP experiments depend on both the matching conditions as well as the magnitude of the dipolar coupling constant. Employing the above expressions (eqns. 1.31 and 1.33) polarization transfer in CP experiments are calculated and is depicted below through simulations.

As depicted in eq. 1.33, when the mismatch between the RF amplitudes increases, (Δ in the ZQ-CP and $\sum$ in the case of DQ-CP), the efficiency of polarization transfer decreases in CP experiments.

(B) Spin Dynamics in the Tilted RF interaction frame

The calculations in the tilted rotating frame could further be simplified by transforming into an interaction frame defined by the transformation function, $U_3 = \exp(i\omega_{RF,I}tI_z)\exp(i\omega_{RF,S}tS_z)$

$$H_{TRF} = U_3 H_{TR} U_3^{-1} \tag{1.35}$$

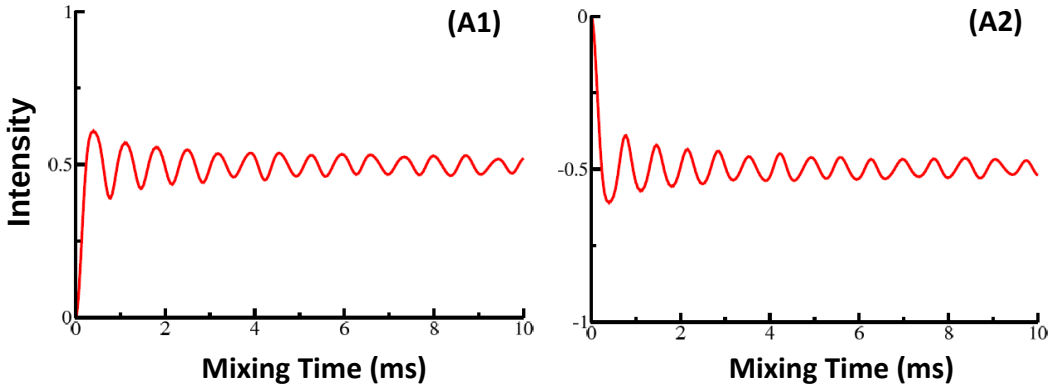

Figure 1.5: Simulations depicting polarization transfer from spin-I (^1H) to spin-S (^{13}C) in CP (static) experiments under (A) ZQ and (B) DQ matching conditions at 600MHz ^1H Larmor frequency. For the sake of simplicity, the chemical shift anisotropy is ignored in the simulations. The dipolar coupling between the spins was set to 2901 Hz and the RF field employed on both the channels was 10kHz

In the tilted 'RF' interaction frame the Hamiltonian of the system is purely dipolar in nature and is represented by,

$$H_{TRF} = \underbrace{\frac{\omega_{IS}}{2}\left[I^+S^+\exp\{-i(\omega_{RF,I}+\omega_{RF,S})t\} + I^-S^-\exp\{i(\omega_{RF,I}+\omega_{RF,S})t\}\right]}_{DQ} + \underbrace{\frac{\omega_{IS}}{2}\left[I^+S^-\exp\{-i(\omega_{RF,I}-\omega_{RF,S})t\} + I^-S^+\exp\{i(\omega_{RF,I}-\omega_{RF,S})t\}\right]}_{ZQ} \tag{1.36}$$

When the 'ZQ' matching condition is satisfied ($\omega_{RF,I} = \omega_{RF,S}$) the above Hamiltonian reduces to a time-independent Hamiltonian containing only the ZQ operators.

$$H_{eff} = \frac{\omega_{IS}}{2}\left[I^+S^- + I^-S^+\right] \tag{1.37}$$

Employing the transformed density operator and detection operator (eqns. 1.27 and 1.28), the polarization transfer from I to S is given by,

$$\begin{aligned} \langle S_z(t) \rangle &= Tr\left[\rho_{TRF}(t).S_z\right] \\ &= \sin^2\left(\frac{\omega_{IS}t}{2}\right) \end{aligned} \tag{1.38}$$

In a similar vein, when $(\omega_{RF,I} = -\omega_{RF,S})$, the effective Hamiltonian reduces to a much simpler form comprising of DQ operators,

$$H_{eff} = \frac{\omega_{IS}}{2}\left[I^+S^+ + I^-S^-\right] \tag{1.39}$$

Subsequently, the polarization transfer to spin 'S' is given by,

$$\begin{aligned} \langle S_z(t) \rangle &= Tr\left[\rho_{TRF}(t).S_z\right] \\ &= -\sin^2\left(\frac{\omega_{IS}t}{2}\right) \end{aligned} \tag{1.40}$$

A thorough description of the CP experiment under MAS conditions in the presence of anisotropic interactions will be presented in the second chapter of this thesis.

References

[1] E. M. Purcell, H. C. Torrey and R. V. Pound, *Phys. Rev.*, 1946, **69**, 37–38.

[2] F. Bloch, W. W. Hansen and M. Packard, *Phys. Rev.*, 1946, **69**, 127–127.

[3] F. Bloch, W. W. Hansen and M. Packard, *Phys. Rev.*, 1946, **70**, 474–485.

[4] U. Haeberlen, *High-Resolution NMR in Solids: Selective Averaging*, Academic, New York, 1976.

[5] M. Mehring, *Principles of High Resolution NMR in Solids*, Springer Verlag, Berlin, 1999.

[6] A. Abragam, *The Principles of Nuclear Magnetism*, Clarendon, Oxford, 1961.

[7] C. P. Slichter, *Principles of Magnetic Resonance*, Springer-Verlag Berlin, 1978.

[8] A. E. Bennett and S. Griffin, R. G.and Vega, *In Solid State NMR IV: Methods and Applications of Solid-State NMR*, 1994, **33**, 1.

[9] C. P. Jaroniec, *J. Magn. Reson.*, 2015, **253**, 50 – 59.

[10] C. P. Jaroniec, *Solid State Nucl. Magn. Reson.*, 2012, **43–44**, 1 – 13.

[11] H. R. Patel, A. S. Pithadia, J. R. Brender, C. A. Fierke and A. Ramamoorthy, *J. Phys. Chem. Lett.*, 2014, **5**, 1864–1870.

[12] S. A. Kotler, P. Walsh, J. R. Brender and A. Ramamoorthy, *Chem. Soc. Rev.*, 2014, **43**, 6692–6700.

[13] B. H. Meier and A. Böckmann, *Curr. Opin. Struct. Biol.*, 2015, **30**, 43 – 49.

[14] G. Zandomeneghi, W. Maas and B. H. Meier, *CHIMIA*, 2012, **66**, 798–800.

[15] M. Tang, G. Comellas and C. M. Rienstra, *Acc. Chem. Res.*, 2013, **46**, 2080–2088.

[16] E. D. Watt and C. M. Rienstra, *Anal. Chem.*, 2014, **86**, 58–64.

[17] G. Comellas and C. M. Rienstra, *Annu. Rev. Biophys.*, 2013, **42**, 515–536.

[18] L. Emsley and I. Bertini, *Acc. Chem. Res.*, 2013, **46**, 1912–1913.

[19] L. Emsley, *J. Am. Chem. Soc.*, 2013, **135**, 8089–8091.

[20] P. K. Madhu, *Isr. J. Chem.*, 2014, **54**, 25–38.

[21] D. Huster and P. K. Madhu, *Biophysical Journal*, 2014, **106**, 2083 – 2084.

[22] J. R. Lewandowski, *Acc. Chem. Res.*, 2013, **46**, 2018–2027.

[23] M. Baldus, *Prog. Nucl. Magn. Reson. Spectrosc.*, 2002, **41**, 1 – 47.

[24] C. M. Rienstra, M. Hohwy, M. Hong and R. G. Griffin, *J. Am. Chem. Soc.*, 2000, **122**, 10979–10990.

[25] A. Detken, E. Hardy, M. Ernst, M. Kainosho, T. Kawakami, S. Aimoto and B. Meier, *J. Biomol. NMR*, 2001, **20**, 203–221.

[26] A. McDermott, T. Polenova, A. Bockmann, K. Zilm, E. Paulsen, R. Martin and G. Montelione, *J. Biomol. NMR*, 2000, **16**, 209–219.

[27] T. Egorova-Zachernyuk, J. Hollander, N. Fraser, P. Gast, A. Hoff, R. Cogdell, H. de Groot and M. Baldus, *J. Biomol. NMR*, 2001, **19**, 243–253.

[28] J. Pauli, M. Baldus, B. van Rossum, H. de Groot and H. Oschkinat, *ChemBioChem*, 2001, **2**, 272–281.

[29] B. van Rossum, F. Castellani, K. Rehbein, J. Pauli and H. Oschkinat, *ChemBioChem*, 2001, **2**, 906–914.

[30] C. M. Rienstra, L. Tucker-Kellogg, C. P. Jaroniec, M. Hohwy, B. Reif, M. T. McMahon, B. Tidor, T. Lozano-Pérez and R. G. Griffin, *PNAS*, 2002, **99**, 10260–10265.

[31] C. P. Jaroniec, C. Filip and R. G. Griffin, *J. Am. Chem. Soc.*, 2002, **124**, 10728–10742.

[32] R. Tycko, *Curr. Opin Chem. Biol.*, 2000, **4**, 500 – 506.

[33] E. R. Andrew, A. Bradbury and R. G. Eades, *Nature*, 1958, **182**, 1659.

[34] I. J. Lowe, *Phys. Rev. Lett.*, 1959, **2**, 285–287.

[35] S. R. Hartmann and E. L. Hahn, *Phys. Rev.*, 1962, **128**, 2042–2053.

[36] A. Pines, M. G. Gibby and J. S. Waugh, *J. Chem. Phys.*, 1973, **59**, 569–590.

[37] E. Stejskal, J. Schaefer and J. Waugh, *J. Magn. Reson.*, 1977, **28**, 105 – 112.

[38] J. Schaefer and E. O. Stejskal, *J. Am. Chem. Soc.*, 1976, **98**, 1031–1032.

[39] J. Schaefer, E. Stejskal, J. Garbow and R. McKay, *J. Magn. Reson.*, 1984, **59**, 150 – 156.

[40] B. Sun, P. Costa and R. Griffin, *J. Magn. Reson., Series A*, 1995, **112**, 191 – 198.

[41] X. Wu and K. Zilm, *J. Magn. Reson., Series A*, 1993, **104**, 154 – 165.

[42] S. Hediger, B. Meier and R. Ernst, *Chem. Phys. Lett.*, 1993, **213**, 627 – 635.

[43] S. Hediger, B. H. Meier and R. R. Ernst, *J. Chem. Phys.*, 1995, **102**, 4000–4011.

[44] S. Hediger, B. Meier and R. Ernst, *Chem. Phys. Lett.*, 1995, **240**, 449 – 456.

[45] M. Baldus, D. Geurts, S. Hediger and B. Meier, *J. Magn. Reson., Series A*, 1996, **118**, 140 – 144.

[46] M. Baldus, A. T. Petkova, Herzfeld and R. G. Griffin, *Mol. Phys.*, 1998, **95**, 1197–1207.

[47] M. Bjerring and N. C. Nielsen, *Chem. Phys. Lett.*, 2003, **382**, 671 – 678.

[48] S. Laage, A. Marchetti, J. Sein, R. Pierattelli, H. J. Sass, S. Grzesiek, A. Lesage, G. Pintacuda and L. Emsley, *J. Am. Chem. Soc.*, 2008, **130**, 17216–17217.

[49] G. Metz, X. Wu and S. Smith, *J. Magn. Reson., Series A*, 1994, **110**, 219 – 227.

[50] J. P. Demers, V. Vijayan, S. Becker and A. Lange, *J. Magn. Reson.*, 2010, **205**, 216 – 223.

[51] G. D. Paepe, J. R. Lewandowski, A. Loquet, A. Bockmann and R. G. Griffin, *J. Chem. Phys.*, 2008, **129**, 245101.

[52] G. D. Paepe, J. R. Lewandowski, A. Loquet, M. Eddy, S. Megy, A. Bockmann and R. G. Griffin, *J. Chem. Phys.*, 2011, **134**, 095101.

[53] A. Lange, I. Scholz, T. Manolikas, M. Ernst and B. H. Meier, *Chem. Phys. Lett.*, 2009, **468**, 100 – 105.

[54] J. R. Lewandowski, G. De Paëpe and R. G. Griffin, *J. Am. Chem. Soc.*, 2007, **129**, 728–729.

[55] B. Meier, *Chem. Phys. Lett.*, 1992, **188**, 201 – 207.

[56] V. Vijayan, J. P. Demers, J. Biernat, E. Mandelkow, S. Becker and A. Lange, *ChemPhysChem*, 2009, **10**, 2205–2208.

[57] M. Bjerring, J. T. Rasmussen, R. Schultz Krogshave and N. C. Nielsen, *J. Chem. Phys.*, 2003, **119**, 8916–8926.

[58] C. P. Jaroniec, B. A. Tounge, C. M. Rienstra, J. Herzfeld and R. G. Griffin, *J. Am. Chem. Soc.*, 1999, **121**, 10237–10238.

[59] W. K. Peng, A. Samoson and M. Kitagawa, *Chem. Phys. Lett.*, 2008, **460**, 531 – 535.

[60] O. Peersen, X. Wu and S. Smith, *J. Magn. Reson., Series A*, 1994, **106**, 127 – 131.

[61] A. Kolbert and A. Bielecki, *J. Magn. Reson., Series A*, 1995, **116**, 29 – 35.

[62] O. Peersen, X. Wu, I. Kustanovich and S. Smith, *J. Magn. Reson., Series A*, 1993, **104**, 334 – 339.

[63] R. Verel, M. Ernst and B. H. Meier, *J. Magn. Reson.*, 2001, **150**, 81 – 99.

[64] D. Rovnyak, *Concepts Mag. Reson. A*, 2008, **32A**, 254–276.

[65] M. H. Levitt, *Encyclopedia of NMR*, 2002, **9**, 165.

[66] U. Haeberlen and J. S. Waugh, *Phys. Rev.*, 1968, **175**, 453–467.

[67] J. H. Shirley, *Phys. Rev. B*, 1965, **4**, 979.

[68] R. Ramachandran and R. G. Griffin, *J. Chem. Phys.*, 2005, **122**, 164502.

[69] J. V. Neumann, *Mathematical Foundations of Quantum Mechanics*, Princeton University Press, Princeton New Jersy, 1955.

[70] W. Magnus, *Comm. Pure Appl. Math.*, 1954, **7**, 649–673.

[71] J. H. Van Vleck, *Phys. Rev.*, 1929, **33**, 467–506.

[72] M. R. Aliev and V. T. Aleksanyan, *Opt. Spectrosc.*, 1968, **24**, 520.

[73] M. R. Aliev and V. T. Aleksanyan, *Opt. Spectrosc.*, 1968, **24**, 695.

[74] M. R. Aliev, *Molecular Vibrational-Rotational Spectra*, Elsevier, Amsterdam, 1982.

[75] R. Ramesh and M. S. Krishnan, *J. Chem. Phys.*, 2001, **114**, 5967–5973.

[76] M. K. Pandey, Z. Qadri and R. Ramachandran, *J. Chem. Phys.*, 2013, **138**, 114108.

[77] M. K. Pandey and R. Ramachandran, *Mol. Phys.*, 2011, **109**, 1545–1565.

[78] M. J. Bayro, M. Huber, R. Ramachandran, T. C. Davenport, B. H. Meier, M. Ernst and R. G. Griffin, *J. Chem. Phys.*, 2009, **130**, 114506.

Chapter 2

Analytic Theory of CPMAS Experiments

2.1 Background

After its successful demonstration in 1973, the CP-MAS experiment[1] has become an integral part of many multi-dimensional experiments. In a typical multi-dimensional experiment involving less sensitive nuclei, the initial cross-polarization step involves the transfer of the abundant ^1H polarization to one of the less abundant nuclei, say ^{15}N (or ^{13}C). Following this step, a sequential transfer of polarization from ^{15}N to ^{13}C (or ^{13}C to ^{15}N) is established through a second CP process. With the availability of faster spinning modules, sample heating and degradation has become an important issue to deal with in ssNMR experiments. To this end, several new approaches have emerged in recent years to address the above mentioned issues[2–7]. The sequences developed so far could be classified into two main categories (1) first order recoupling (2) second order recoupling. In the first order recoupling schemes, polarization transfer between two groups of spins is established (through the dipolar interactions) when one of the matching conditions $\left|\upsilon_{RF,S} \pm \upsilon_{RF,I}\right| = \upsilon_r$ or $2\upsilon_r$ is satisfied. Such schemes in principle

could be designed by employing either (a) higher RF powers at moderate spinning frequencies (b) higher spinning frequencies with lower RF powers. To facilitate analytic descriptions based on Average Hamiltonian theory (AHT)[8,9], the time-periods associated with the modulations (namely due to RF irradiation) are often synchronized with the sample spinning frequency i.e. $\upsilon_{RF,I} = p\upsilon_r$, $\upsilon_{RF,S} = r\upsilon_r$ (p and r are chosen to be integers).

Employing AHT formalism, suites of dipolar recoupling methods have emerged wherein, the amplitudes of the RF fields employed on the two channels are chosen carefully to avoid matching conditions that result in the reintroduction of the CSA interactions. When the sum ($\upsilon_{RF,I} + \upsilon_{RF,S} = m\upsilon_r$, (DQ matching condition) or the difference ($\left|\upsilon_{RF,I} - \upsilon_{RF,S}\right| = m\upsilon_r$ (ZQ matching condition) between the RF fields is matched to the spinning frequency, a time-independent dipolar Hamiltonian is obtained (See Eq. 2.12) suggesting the reintroduction of dipolar interactions under MAS. Since the time-period of the modulations employed on the two channels are commensurate ($\tau_c = N\tau_r$) with the rotor period, the DQ matching condition is never easily satisfied in MAS experiments. Consequently, dipolar recoupling experiments satisfying only the ZQ matching condition have emerged.[10–12] To prevent the reintroduction (or recoupling) of the CSA interactions, the indices p and r in ZQ experiments should differ by m (i.e., $p, r > 2$ and $|p - r| = 1$ or 2 . Hence, the amplitude of the RF fields employed on the two channels should be significantly greater than the sample spinning frequency (i.e. $\upsilon_{RF} \geq 3\upsilon_r$). Since bio-molecular applications of ssNMR necessitate higher magnetic field strengths and faster spinning frequencies[13,14] (for improved spectral

resolution), sequences that are synchronized with sample spinning frequency are of limited utility.

2.2 Definition of the Problem

With this objective, an analytic theory is proposed for designing CP experiments that employ modulations that are incommensurate with the spinning frequency. Since the RF and MAS modulations are incommensurate, we resort to Floquet theory[15]. In the Floquet treatment, the time-dependent Hamiltonian is transformed into a time-independent Hamiltonian via Fourier series expansion. Subsequently, the spin dynamics could be described either in the Floquet state space or the Floquet operator (Liouville) space. To present a general description of the spin dynamics, the multipole formulation of Floquet theory (MMFT)[16] is employed in the present study. In the past, the MMFT approach has been employed to describe the spin dynamics in the Floquet-Liouville space[16–19]. Alternatively, in this thesis we present a formalism to describe schemes that employ RF modulations that are incommensurate with the spinning frequency. Specifically, the polarization transfer in CP experiments is described in the Floquet-state space through simple analytic expressions.

2.3 Discussion

2.3.1 Spin Hamiltonians under MAS conditions

To explain the transformations of the internal spin Hamiltonians under rotations, spherical tensor operator basis is routinely employed in solid-state NMR[20,21]. Such a description, presents a suitable framework for understanding the effects of sample

spinning on the various interactions in the solid state. Following the standard procedure[20–22], the spatial and spin parts of the interactions are expressed in terms of irreducible spherical tensor operators, as given below,

$$H_\lambda = C^\lambda \sum_{k=0}^{2} \sum_{q=-k}^{k} (-1)^q R_\lambda^{(k)-q} T_\lambda^{(k)q} \tag{2.1}$$

In the above equation, 'λ' represents spin interactions (such as chemical shift, dipole-dipole interaction, spin-spin coupling, quadrupolar interaction etc.) and 'C^λ' the physical constants specific to a particular spin interaction 'λ'. The spatial and spin parts are expressed in terms of $R_\lambda^{(k)-q}$ and $T_\lambda^{(k)q}$ (wherein 'k' denotes the rank and 'q' the corresponding component) operators respectively. Since the nuclear spin interactions result from interactions among vector quantities, the spatial part of the interactions are expressed in terms of second rank tensors, $R_\lambda^{(2)-q}$. To minimize the complexity involved in the description, spatial tensors ($R_\lambda^{(k)-q}$) are often described in the principal axis system (PAS). Hence, a series of transformations is necessary for a unified description. Under secular approximation, the general form of the interaction Hamiltonian depicted in Eq. 2.1 is truncated to a set of terms/operators that commute with the Zeeman interaction i.e. $\left[I_z, T^{(k)q}\right] = 0$ (implies, $q = 0$)

$$H_\lambda = \sum_{k=0}^{2} \sum_{q=-k}^{k} (-1)^q R_\lambda^{(k)-q}(t)\, T_\lambda^{(k)q}$$

$$= R_\lambda^{(0)0} T_\lambda^{(0)0} + R_\lambda^{(1)0}(t)\, T_\lambda^{(1)0} + R_\lambda^{(2)0}(t)\, T_\lambda^{(2)0} \tag{2.2}$$

The first term '$R_\lambda^{(0)0}$' is isotropic and invariant under rotations, while the second term '$R_\lambda^{(1)0}(t)$' has no effect on the spectrum as only symmetric and traceless

quantities are measured in NMR spectroscopy. Hence, the only term that contributes to the spectrum in MAS experiments is '$R_{\lambda}^{(2)0}(t)$'[22]. Since, spatial tensor operators are described in the PAS, a series of coordinate transformations are performed to obtain the MAS Hamiltonian in the laboratory frame (from the PAS to Molecular Axis System (MolAS) to Rotor Axis System (RAS) and finally to Laboratory Axis System (LAS)).

$$PAS \xrightarrow{D^{(2)}(\Omega_{PM})} molAS \xrightarrow{D^{(2)}(\Omega_{MR})} RAS \xrightarrow{D^{(2)}(\Omega_{RL})} LAS$$

Employing the spatial tensor operators defined in the PAS the operators in the LAS are derived systematically using Wigner rotation matrices[23],

$$R_{\lambda,LAS}^{(k)0}(t) = \sum_{q,q_1,q_2=-k}^{k} D_{q_2q_1}^{(k)}(\Omega_{PM}) D_{q_1q}^{(k)}(\Omega_{MR}) D_{q0}^{(k)}(\Omega_{RL}) R_{\lambda,PAS}^{(k)q_2} \tag{2.3}$$

In the above equation, $D^{(k)}(\Omega_{AB})$ denotes the Wigner rotation matrix[23] of order 'k' which describes the transformations of irreducible spherical tensor components among various axis systems.

In the case of chemical shift anisotropy (CSA), the spatial component in the laboratory axis system for i^{th} nucleus is represented as,

$$\begin{aligned} R_{CS,LAS,i}^{(2)0}(t) &= \sum_{m,m_1,m_2=-2}^{2} D_{m_2m_1}^{(2)}(\Omega_{PM}) D_{m_1m}^{(2)}(\Omega_{MR}) D_{m0}^{(2)}(\Omega_{RL}) R_{CS,PAS,i}^{(2)m_2} \\ &= \sum_{m,m_1,m_2=-2}^{2} D_{m_2m_1}^{(2)}(\Omega_{PM}) D_{m_1m}^{(2)}(\Omega_{MR}) R_{CS,PAS,i}^{(2)m_2} e^{im\omega_r t} \\ &= \sum_{m=-2}^{2} \omega_i^{(m)} e^{im\omega_r t} \end{aligned} \tag{2.4}$$

In the case of CSA interactions, the following components of the spatial tensor are

non-zero in the PAS.

$$R^{(2)0}_{CS,PAS,i} = \delta_{anis} \tag{2.5}$$

$$R^{(2)\pm 2}_{CS,PAS,i} = -\tfrac{1}{\sqrt{6}}\delta_{anis}\eta \tag{2.6}$$

('δ_{anis}' and 'η' represent the 'chemical shift anisotropy' and 'asymmetry parameter' respectively).

In a similar vein, the transformation relating the spatial component of the dipolar interaction between i^{th} and j^{th} nuclei is represented by,

$$\begin{aligned} R^{(2)0}_{D,LAS,ij}(t) &= \sum_{m,m_1,m_2=-2}^{2} D^{(2)}_{m_2 m_1}(\Omega_{PM}) D^{(2)}_{m_1 m}(\Omega_{MR}) D^{(2)}_{m0}(\Omega_{RL}) R^{(2)m_2}_{D,PAS,ij} \\ &= \sum_{m,m_1,m_2=-2}^{2} D^{(2)}_{m_2 m_1}(\Omega_{PM}) D^{(2)}_{m_1 m}(\Omega_{MR}) R^{(2)m_2}_{D,PAS,ij} e^{im\omega_r t} \\ &= \sum_{m=-2}^{2} \omega^{(m)}_{ij} e^{im\omega_r t} \end{aligned} \tag{2.7}$$

where,

$$R^{(2)0}_{D,PAS,ij} = \sqrt{6}\omega_{ij} \tag{2.8}$$

($\omega_{ij} = \frac{\mu_0 \gamma_i \gamma_j \hbar}{4\pi r^3_{ij}}$ is the dipolar coupling constant) is the only non-zero term in the dipolar principal axis frame.

2.3.2 Theory of CP-MAS experiments at faster spinning frequencies

To deduce the matching conditions in CPMAS experiments, we begin our discussion employing a model system comprising of two-spins. In the rotating frame the MAS spin Hamiltonian for an isolated two-spin heteronuclear (I-S) system is represented by,

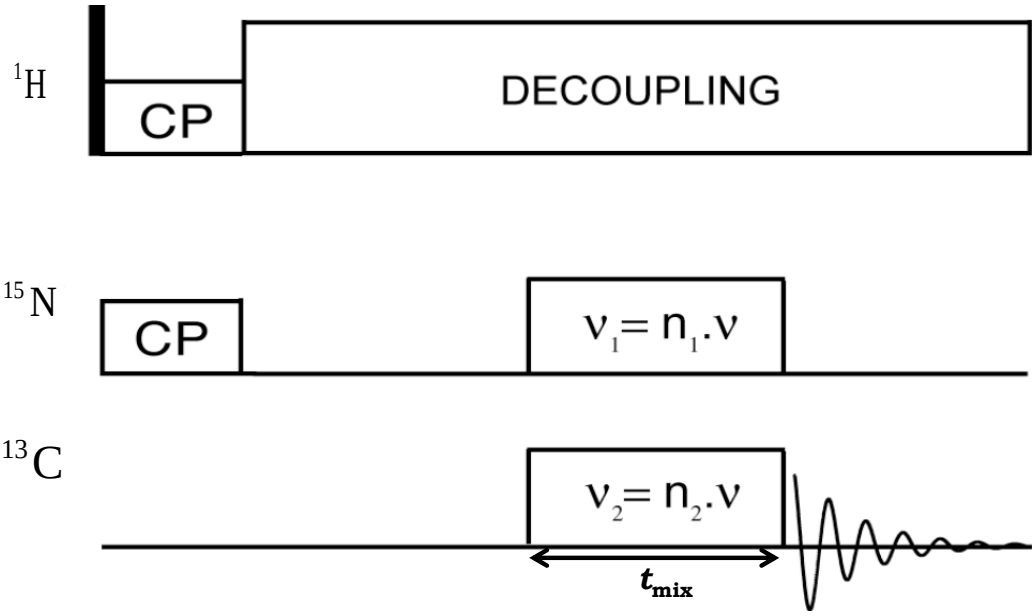

Figure 2.1: Pulse sequence depicting the polarization transfer in double cross-polarization (DCP)[24–27] experiments. The RF amplitude is not synchronized with the sample spinning frequency i.e., $\upsilon \neq N\upsilon_r$.

$$H(t) = \sum_{m=-2}^{2} \omega_I^{(m)} e^{im\omega_r t} I_z + \sum_{m=-2}^{2} \omega_S^{(m)} e^{im\omega_r t} S_z + \sum_{\substack{m=-2,\\ m\neq 0}}^{2} 2\omega_{IS}^{(m)} e^{im\omega_r t} I_z S_z + \omega_{RF,I} I_x + \omega_{RF,S} S_x \tag{2.9}$$

The spatial anisotropy associated with the chemical shift and dipolar interactions are represented by $\omega_\lambda^{(m)}$ ($\lambda = I, S$) and $\omega_{IS}^{(m)}$, respectively. For the sake of convenience, the isotropic part of the chemical shift interaction (represented by $\omega_\lambda^{(0)}$) is included along with the anisotropic part in our description. In the rotating frame, the oscillating radiofrequency (RF) field is time-independent, ($\omega_{RF,I}$ and $\omega_{RF,S}$ represent the RF amplitudes on the spins I and S, respectively). To simplify the description, the above Hamiltonian is transformed into a tilted frame (also described in Appendix-1) defined by the transformation operator, $U_1 = \exp(i\frac{\pi}{2}I_y)\exp(i\frac{\pi}{2}S_y)$ as,

$$\tilde{H}(t) = U_1 H(t) U_1^{-1} \tag{2.10}$$

$$\begin{aligned}\tilde{H}(t) =&\omega_{RF,I} I_z + \omega_{RF,S} S_z + \sum_{\substack{m=-2,\\ m\neq 0}}^{2} 2\omega_{IS}^{(m)} e^{im\omega_r t} I_x S_x \\ &- \omega_I^{(0)} I_x - \sum_{\substack{m=-2,\\ m\neq 0}}^{2} \omega_I^{(m)} e^{im\omega_r t} I_x \\ &- \omega_S^{(0)} S_x - \sum_{\substack{m=-2,\\ m\neq 0}}^{2} \omega_S^{(m)} e^{im\omega_r t} S_x \end{aligned} \tag{2.11}$$

In the tilted rotating frame the RF part of the Hamiltonian is quantized along the z-axis (i.e., diagonal) while the chemical shift and the dipolar interactions are off-diagonal. To deduce the optimum CP conditions (describe the recoupling process), the Hamiltonian in the tilted frame is further transformed into the RF interaction frame defined by the transformation operator $U_2 = \exp(i\omega_{RF,I} t I_z) \exp(i\omega_{RF,S} t S_z)$. Subsequently, the Hamiltonian in the tilted RF interaction frame is further split into single-spin and two-spin interactions . The single-spin Hamiltonian depicts both the isotropic and anisotropic chemical shift interactions and is expressed in terms of single-quantum (SQ) operators, while the two-spin Hamiltonian comprises of the dipolar-interactions and is expressed in terms of DQ and ZQ operators:

$$\begin{aligned}\tilde{\tilde{H}}(t) =& - \sum_{m=-2,}^{2} \tfrac{\omega_I^{(m)}}{2} e^{i(m\omega_r \pm \omega_{RF,I})t} I^{\pm} - \sum_{m=-2}^{2} \tfrac{\omega_S^{(m)}}{2} e^{i(m\omega_r \pm \omega_{RF,S})t} S^{\pm} \\ &+ \frac{1}{2} \sum_{\substack{m=-2,\\ m\neq 0}}^{2} \omega_{IS}^{(m)} \left[I^+ S^+ e^{i(\omega_{RF,I} + \omega_{RF,S})t} + I^- S^- e^{-i(\omega_{RF,I} + \omega_{RF,S})t} \right] e^{im\omega_r t} \\ &+ \frac{1}{2} \sum_{\substack{m=-2,\\ m\neq 0}}^{2} \omega_{IS}^{(m)} \left[I^+ S^- e^{i(\omega_{RF,I} - \omega_{RF,S})t} + I^- S^+ e^{-i(\omega_{RF,I} - \omega_{RF,S})t} \right] e^{im\omega_r t} \end{aligned} \tag{2.12}$$

In contrast to static CP experiments, the internal spin Hamiltonians in the tilted RF interaction frame are modulated by both MAS and the RF irradiation. When the amplitudes of the RF fields are adjusted to one of the matching conditions[28–30]

($|\upsilon_{RF,S} \pm \upsilon_{RF,I}| = \upsilon_r$ or $2\upsilon_r$), a part of the two-spin Hamiltonian (refer to Eq 2.12) becomes time-independent under MAS conditions (commonly referred to as 'recoupled Hamiltonian'). To maximize the polarization transfer among spins, the amplitudes of the RF fields are adjusted to avoid undesired matching conditions that result in the reintroduction of CSA interactions. In theoretical descriptions based on AHT[8,9], the undesirable matching conditions are avoided when the RF amplitudes exceed the spinning frequency (i.e., $\nu_{RF} > 2\nu_r$). From an experimental standpoint, the RF requirements on the probes increase with the MAS frequency, thereby limiting the implementation of first order CP experiments at faster spinning frequencies. Since, biomolecular applications of ssNMR entail the implementation of CP experiments at faster spinning frequencies, alternate strategies in the form of second-order CP experiments have emerged in recent past[31–34]. As an alternative to this current trend, we reinvestigate the entire CP process using Floquet theory with the objective of finding alternate recoupling conditions. In contrast to the AHT approach, Floquet theory presents a more general framework without any constraints on the magnitude of the RF modulations on the system. To facilitate analytic description, the Hamiltonian in the RF interaction frame (Eq. 2.12) is re-expressed in terms of multipole operators[20].

Table 2.1: Description of product operators in terms of Multipole operators [20,35]

Single-spin	$I_z = -iT^{(1)0}(I), I^{\pm 1} = \pm i\sqrt{2}T^{(1)\pm 1}(I)$
Two-spin (DQ)	$I^+S^+ = -T^{(2)2}(IS), I^-S^- = -T^{(2)-2}(IS)$
Two-spin (ZQ)	$I^+S^- = \frac{1}{\sqrt{3}}T^{(0)0}(IS) + \frac{1}{\sqrt{2}}T^{(1)0}(IS) + \frac{1}{\sqrt{6}}T^{(2)0}(IS)$ $I^-S^+ = \frac{1}{\sqrt{3}}T^{(0)0}(IS) - \frac{1}{\sqrt{2}}T^{(1)0}(IS) + \frac{1}{\sqrt{6}}T^{(2)0}(IS)$ $2I_zS_z = \frac{1}{\sqrt{3}}T^{(0)0}(IS) - \sqrt{\frac{2}{3}}T^{(2)0}(IS)$

$$
\begin{aligned}
\tilde{\tilde{H}}(t) = & \sum_{q=-1}^{1}\sum_{m=-2}^{2} \tfrac{-q}{\sqrt{2}}\omega_I^{(m)} e^{iq\omega_{RF,I}t} iT^{(1)q}(I) \\
& + \sum_{q=-1}^{1}\sum_{m=-2}^{2} \tfrac{-q}{\sqrt{2}}\omega_S^{(m)} e^{iq\omega_{RF,S}t} iT^{(1)q}(S) \\
& -\frac{1}{2}\sum_{m=-2,m\neq 0}^{2} \omega_{IS}^{(m)} \left[\begin{array}{l} T^{(2)2}(IS)e^{i(\omega_{RF,I}+\omega_{RF,S})t} \\ + \\ T^{(2)-2}(IS)e^{-i(\omega_{RF,I}+\omega_{RF,S})t} \end{array} \right] e^{im\omega_r t} \\
& +\frac{1}{2}\sum_{m=-2,m\neq 0}^{2} \omega_{IS}^{(m)} \left[\begin{array}{l} \left(\begin{array}{l} \frac{1}{\sqrt{3}}T^{(0)0}(IS)+ \\ \frac{1}{\sqrt{2}}T^{(1)0}(IS)+ \\ \frac{1}{\sqrt{6}}T^{(2)0}(IS) \end{array} \right) e^{i(\omega_{RF,I}-\omega_{RF,S})t} \\ + \\ \left(\begin{array}{l} \frac{1}{\sqrt{3}}T^{(0)0}(IS)- \\ \frac{1}{\sqrt{2}}T^{(1)0}(IS)+ \\ \frac{1}{\sqrt{6}}T^{(2)0}(IS) \end{array} \right) e^{-i(\omega_{RF,I}-\omega_{RF,S})t} \end{array} \right] e^{im\omega_r t}
\end{aligned}
\tag{2.13}
$$

The relation between the product operators and the spherical tensor operators [20,35] is described in table 2.1. A detailed description of the Spherical Tensor Operators in the multipole basis is given in Appendix-2. For convenience we follow the above convention. Employing Floquet theorem, the time-dependent Hamiltonian (as depicted in Eq. 2.13) is transformed into a time-independent Hamiltonian via Fourier series expansion. The transformed Hamiltonian (commonly referred to

as Floquet Hamiltonian) is defined in an infinite dimensional vector space using the irreducible Floquet tensor operator (IFT) basis[16].

$$
\begin{aligned}
H_F =& \omega_r I_F^{(m)} + \omega_{RF,I} I_F^{(n_1)} + \omega_{RF,S} I_F^{(n_2)} \\
&+ \sum_{q=-1,q\neq 0}^{1} \sum_{m=-2}^{2} \left[\sum_{n_1=-\infty}^{\infty} G^{(1)q}_{m,qn_1}(I) i T^{(1)q}_{m,qn_1}(I) + \sum_{n_2=-\infty}^{\infty} G^{(1)q}_{m,qn_2}(S) i T^{(1)q}_{m,qn_2}(S) \right] \\
&+ \sum_{m=-2,m\neq 0}^{2} \sum_{n_1,n_2=-\infty}^{\infty} \left[G^{(2)2}_{m,n_1,n_2}(IS) T^{(2)2}_{m,n_1,n_2}(IS) + G^{(2)-2}_{m,-n_1,-n_2}(IS) T^{(2)-2}_{m,-n_1,-n_2}(IS) \right] \\
&+ \sum_{k=0}^{2} \sum_{m=-2,m\neq 0}^{2} \sum_{n_1,n_2=-\infty}^{\infty} \left[G^{(k)0}_{m,n_1,-n_2}(IS) T^{(k)0}_{m,n_1,-n_2}(IS) + (-1)^k G^{(k)0}_{m,-n_1,n_2}(IS) T^{(k)0}_{m,-n_1,n_2}(IS) \right]
\end{aligned}
\tag{2.14}
$$

The IFT operator basis is constructed from a direct product between the spin ($T^{(k)q}(\alpha)$)[20] and the Fourier operators ($F^{(k)}_{n_k}$)[36]. The indices m, n_1, n_2 represent the Fourier indices associated with MAS, RF modulation on spin 'I' and RF modulation on spin 'S', respectively. The underlying theoretical framework and their utility in the description of ssNMR experiments are well documented and would not be elaborated upon any further in this thesis[17,18,37]. Since, the Hamiltonian is off-diagonal both in the spin ($q \neq 0$) and the Fourier dimension ($m, n_1, n_2 \neq 0$) , effective Hamiltonians based on the method of contact transformation have been employed in the present work to reduce the complexity in the Floquet space[17–19,38].

In the effective Hamiltonian approach based on contact transformation, the

Floquet Hamiltonian in Eq. 2.14 is re-expressed as a sum involving a zero order and a perturbing Hamiltonian. The zero order Hamiltonian comprises of operators that are diagonal in the Fourier dimension, while the perturbing Hamiltonian contains operators with off-diagonality in the Fourier dimensions as represented below. The non-zero coefficients involved in H_1 are tabulated in Table 2.2

$$H_0 = \omega_r I_F^{(m)} + \omega_{RF,I} I_F^{(n_1)} + \omega_{RF,S} I_F^{(n_2)} \tag{2.15}$$

$$\begin{aligned} H_1 = & \sum_{q=-1}^{1} \sum_{m=-2}^{2} \left[\begin{array}{l} \sum\limits_{n_1=-\infty}^{\infty} G_{m,qn_1}^{(1)q}(I) i T_{m,qn_1}^{(1)q}(I) + \\ \sum\limits_{n_2=-\infty}^{\infty} G_{m,qn_2}^{(1)q}(S) i T_{m,qn_2}^{(1)q}(S) \end{array} \right] \\ & + \sum_{\substack{m=-2 \\ m\neq 0}}^{2} \sum_{n_1,n_2=-\infty}^{\infty} \left[\begin{array}{l} G_{m,n_1,n_2}^{(2)2}(IS) T_{m,n_1,n_2}^{(2)2}(IS) + \\ \\ G_{m,-n_1,-n_2}^{(2)-2}(IS) T_{m,-n_1,-n_2}^{(2)-2}(IS) \end{array} \right] \\ & + \sum_{k=0}^{2} \sum_{\substack{m=-2 \\ m\neq 0}}^{2} \sum_{n_1,n_2=-\infty}^{\infty} \left[\begin{array}{l} G_{m,n_1,-n_2 r}^{(k)0}(IS) T_{m,n_1,-n_2}^{(k)0}(IS) + \\ \\ (-1)^k G_{m,-n_1,n_2}^{(k)0}(IS) T_{m,-n_1,n_2}^{(k)0}(IS) \end{array} \right] \end{aligned} \tag{2.16}$$

To reduce the complexity in the Floquet space, an effective Hamiltonian is proposed by transforming the original Floquet Hamiltonian (Eq. 2.14) through a unitary transformation defined by the operator, $U = e^{i\lambda S_1}$.

$$H_F^{eff} = U H_F U^{-1} = e^{i\lambda S_1} H_F e^{-i\lambda S_1} \tag{2.17}$$

$$H_n^{(1)} = H_n + \sum_{m=0}^{n-1} \frac{i^{n-m}}{(n-m)!} \underbrace{[S_1,[\, S_1 ...}_{n-m} [S_1, H_m] \ ...]] \tag{2.18}$$

In Eq. 2.18, S_1 represents the transformation function, H_m the various perturbation terms (arranged in the decreasing order of magnitude) and $H_n^{(1)}$ the perturbation corrections in terms of operators corresponding to a given order depicted

Table 2.2: The non-zero 'G' coefficients employed in the Floquet Hamiltonian

Single-spin	$G^{(1)q}_{m,qn_1}(I) = \frac{-q}{\sqrt{2}}\omega^{(m)}_I, G^{(1)q}_{m,qn_2}(S) = \frac{-q}{\sqrt{2}}\omega^{(m)}_S$
Two-spin (DQ)	$G^{(2)\pm 2}_{m,n_1,n_2}(IS) = \frac{-1}{2}\omega^{(m)}_{IS}$
Two-spin (ZQ)	$G^{(0)0}_{m,n_1,n_2}(IS) = \frac{1}{2\sqrt{3}}\omega^{(m)}_{IS}$
	$G^{(1)0}_{m,n_1,n_2}(IS) = \frac{1}{2\sqrt{2}}\omega^{(m)}_{IS}$
	$G^{(2)0}_{m,n_1,n_2}(IS) = \frac{1}{2\sqrt{6}}\omega^{(m)}_{IS}$

by 'n'. As a general procedure[38], the transformation function, S_1 is expressed in terms of a complete basis set of operators employed for describing H_1 and is chosen carefully to compensate the off-diagonality present in H_1 . Depending on the choice of the matching conditions, both zero-quantum (ZQ) and double-quantum (DQ) sequences could be developed in the double cross-polarization (DCP)[24–27] experiments. To minimize the complexity in the derivation of the transformation function in recoupling experiments, we express the recoupled part of the Hamiltonian as a diagonal term in H_1[19,39]. Consequently, the transformation function S_1 is chosen only to compensate the off-diagonality due to $H_{1,off-dia}$. Depending on the type of experiments (ZQ or DQ), the higher order corrections are calculated accordingly. For example, in the case of ZQ recoupling sequences, the second order corrections involve a complete set of operators $T^{(0)0}_{(0)}(IS), T^{(1)0}_{(0)}(IS), T^{(2)0}_{(0)}(IS)$, $T^{(1)0}_{(0)}(I)$ and $T^{(1)0}_{(0)}(S)$ that span the ZQ space, while in DQ experiments, the second order corrections comprise of the $T^{(2)\pm 2}_{(0)}(IS)$, $T^{(1)0}_{(0)}(I)$ and $T^{(1)0}_{(0)}(S)$ operators. A brief description of the underlying spin dynamics in ZQ and DQ recoupling experiments is presented in the next sub-section.

Zero-quantum recoupling sequences

In the first order ZQ recoupling experiments, the difference in the RF fields ($\left|\upsilon_{RF,I} - \upsilon_{RF,S}\right| = m\upsilon_r$) is matched to the spinning frequency. As described in the earlier section, the Floquet Hamiltonian is rewritten as a sum comprising of $H_0, H_{1,dia}$ and $H_{off-dia}$,

$$H_0 = \omega_r I_F^{(m)} + \omega_{RF,I} I_F^{(n_1)} + \omega_{RF,S} I_F^{(n_2)} \tag{2.19}$$

$$H_{1,dia} = G_{(0)}^{(0)0}(IS) T_{(0)}^{(0)0}(IS) + G_{(0)}^{(1)0}(IS) T_{(0)}^{(1)0}(IS) + G_{(0)}^{(2)0}(IS) T_{(0)}^{(2)0}(IS) \tag{2.20}$$

The recoupled part of the Hamiltonian is included in $H_{1,dia}$, while, the off-diagonal terms are retained in $H_{1,off-dia}$ (Eq. 2.16). Depending on the indices 'p' and 'r' (in $\upsilon_{RF,I} = p\upsilon, \upsilon_{RF,S} = r\upsilon$), the Fourier coefficients in the Floquet Hamiltonian differ and could be deduced from Eq. 2.14. The 'G' coefficients present in the recoupled Hamiltonian $H_{1,dia}$, depend on the value of 'm' in the matching condition ($\left|\omega_{RF,I} - \omega_{RF,S}\right| = m\omega_r$) i.e. for $m = 1$, $G_{(0)}^{(k)0}(IS) \propto \omega_{IS}^{(1)}$, $m = 2$, $G_{(0)}^{(k)0}(IS) \propto \omega_{IS}^{(2)}$. The off-diagonal contributions/corrections emerging from $H_{1,off-dia}$ are folded by the transforming function S_1 as discussed below,

$$\begin{aligned} S_1 =& i \sum_{q=-1,q\neq 0}^{1} \left[\sum_{m,n_1} C_{m,qn_1}^{(1)q}(I) i T_{m,qn_1}^{(1)q}(I) + \sum_{m,n_2} C_{m,qn_2}^{(1)q}(S) i T_{m,qn_2}^{(1)q}(S) \right] \\ &+ i \sum_{k=0}^{2} \sum_{m,n_1,n_2} C_{m,n_1,n_2}^{(k)0}(IS) T_{m,n_1,n_2}^{(k)0}(IS) + \\ &i \sum_{m,n_1,n_2} \left[C_{m,n_1,n_2}^{(2)2}(IS) T_{m,n_1,n_2}^{(2)2}(IS) + C_{m,n_1,n_2}^{(2)-2}(IS) T_{m,n_1,n_2}^{(2)-2}(IS) \right] \end{aligned} \tag{2.21}$$

The 'C' coefficients corresponding to a particular operator $T_{m,n_1,n_2}^{(k)q}(IS)$ in the transformation function S_1 are obtained by solving Eq. 2.22 and are tabulated in

Table 2.3: The 'C' coefficients involved in the transformation function, S_1.

Single-spin	$C^{(1)\pm1}_{m,\pm n_1}(I) = \frac{G^{(1)\pm1}_{m,\pm n_1}(I)}{(m\omega_r \pm n_1\omega_{RF,I})}, C^{(1)\pm1}_{m,\pm n_2}(S) = \frac{G^{(1)\pm1}_{m,\pm n_2}(S)}{(m\omega_r \pm n_2\omega_{RF,S})}$
Two-spin (DQ)	$C^{(2)2}_{m,n_1,n_2}(IS) = \frac{G^{(2)2}_{m,n_1,n_2}(IS)}{(n_1\omega_{RF,I}+n_2\omega_{RF,S}+m\omega_r)}$ $C^{(2)-2}_{m,-n_1,-n_2}(IS) = \frac{G^{(2)-2}_{m,-n_1,-n_2}(IS)}{(-n_1\omega_{RF,I}-n_2\omega_{RF,S]}+m\omega_r)}$
Two-spin (ZQ)	$C^{(k)0}_{m,n_1,n_2}(IS) = \frac{G^{(k)0}_{m,n_1,n_2}(IS)}{(m\omega_r+n_1\omega_{RF,I]}-n_2\omega_{RF,S})}$

Table 2.3

$$0 = H_{1,off-dia} + i\left[S_1, H_0\right] \tag{2.22}$$

Subsequently, the second order corrections (represented by $H_2^{(1)}$) are obtained in terms of operators by evaluating Eq. 2.18,

$$\begin{aligned} H_2^{(1)} =& \tfrac{i}{2}\left[S_1, H_{1,off-dia}\right] \\ =& iT_0^{(1)0}(I)A_1 + iT_0^{(1)0}(S)A_2 \end{aligned} \tag{2.23}$$

To second-order, the effective Floquet Hamiltonian describing ZQ-CPMAS experiments (see Table 2.4 for coefficients) is represented by,

$$\begin{aligned} H_F^{eff} =& H_0 + H_{1,dia} + H_2^{(1)} \\ =& iT_0^{(1)0}(I)A_1 + iT_0^{(1)0}(S)A_2 + \\ & G_0^{(0)0}(IS)T_0^{(0)0}(IS) + G_0^{(1)0}(IS)T_0^{(1)0}(IS) + G_0^{(2)0}(IS)T_0^{(2)0}(IS) \end{aligned} \tag{2.24}$$

Employing the effective Floquet Hamiltonian, polarization transfer in ZQ experiments were described in the past using a set of differential equations in the Floquet-Liouville space. As an alternative, here in this thesis, the polarization transfer in CP-MAS experiments is described in the Floquet-state space through

the equations given below,

$$\langle S_z(t)\rangle = Tr\left[\rho_F^{eff}(t).S_{z,F}\right] \tag{2.25}$$

$$\langle S_z(t)\rangle = \frac{\omega_{IS}^2}{\omega_{IS}^2 + (A_1 - A_2)^2}\sin^2\left(\frac{\sqrt{\omega_{IS}^2 + (A_1 - A_2)^2}t}{2}\right) \tag{2.26}$$

In Eq. 2.26, 'ω_{IS}' represents the coefficient associated with the two-spin ZQ operators. In contrast to the result presented in Appendix-1 (see chapter-1) the 'dipolar coupling-constant' is an ensemble average over all possible orientations present in a powdered sample.

Double-quantum recoupling sequences

In DQ recoupling experiments, the sum of the RF fields employed on the two channels ($\left|\omega_{RF,I} + \omega_{RF,S}\right| = m\omega_r$) is matched to the spinning frequency. Experimentally, this is realized only when the amplitude of the RF modulations are incommensurate with the sample spinning frequency. Following the description in the ZQ case, the recoupled Hamiltonian in DQ experiments is represented by,

$$H_{1,dia} = G_0^{(2)2}(IS)T_0^{(2)2}(IS) + G_0^{(2)-2}(IS)T_0^{(2)-2}(IS) \tag{2.27}$$

Depending on the value of 'm' in the matching condition ($\left|\omega_{RF,I} + \omega_{RF,S}\right| = m\omega_r$), the '$G$' coefficients in $H_{1,dia}$ differ i.e. for $m = 1$, $G_0^{(2)\pm2}(IS) = -\frac{1}{2}\omega_{IS}^{(\mp1)}$, $m = 2$, $G_0^{(2)\pm2}(IS) = -\frac{1}{2}\omega_{IS}^{(\mp2)}$. The transformation function S_1 and the associated coefficients are derived in an identical fashion as represented in Eq. 2.22. Following the procedure described in the previous section, the effective Floquet Hamiltonian

Table 2.4: Coefficients involved in the effective Hamiltonian (Eq. 2.24 & 2.28)

A_1	$\underbrace{-\frac{q}{2}C^{(1)q}_{m,qn_1}(I)G^{(1)-q}_{-m,-qn_1}(I)}_{csa\times csa}$ $+\underbrace{\begin{pmatrix} \frac{q_1}{4}C^{(2)q_1}_{m,n_1,n_2}(IS)G^{(2)-q_1}_{-m,-n_1,-n_2}(IS) \\ -\frac{1}{2\sqrt{3}}\begin{pmatrix} C^{(2)0}_{m,n_1,n_2}(IS)G^{(1)0}_{-m,-n_1,-n_2}(IS) \\ -C^{(1)0}_{m,n_1,n_2}(IS)G^{(2)0}_{-m,-n_1,-n_2}(IS) \end{pmatrix} \\ +\frac{1}{\sqrt{6}}\begin{pmatrix} C^{(1)0}_{m,n_1,n_2}(IS)G^{(0)0}_{-m,-n_1,-n_2}(IS) \\ -C^{(0)0}_{m,n_1,n_2}(IS)G^{(1)0}_{-m,-n_1,-n_2}(IS) \end{pmatrix} \end{pmatrix}}_{dipolar\times dipolar}$
A_2	$\underbrace{-qC^{(1)q}_{m,qn_2}(S)G^{(1)-q}_{-m,-qn_2}(S)}_{csa\times csa}$ $+\underbrace{\begin{pmatrix} \frac{q_1}{4}C^{(2)q_1}_{m,n_1,n_2}(IS)G^{(2)-q_1}_{-m,-n_1,-n_2}(IS) \\ +\frac{1}{2\sqrt{3}}\begin{pmatrix} C^{(2)0}_{m,n_1,n_2}(IS)G^{(1)0}_{-m,-n_1,-n_2}(IS) \\ -C^{(1)0}_{m,n_1,n_2}(IS)G^{(2)0}_{-m,-n_1,-n_2}(IS) \end{pmatrix} \\ -\frac{1}{\sqrt{6}}\begin{pmatrix} C^{(1)0}_{m,n_1,n_2}(IS)G^{(0)0}_{-m,-n_1,-n_2}(IS) \\ -C^{(0)0}_{m,n_1,n_2}(IS)G^{(1)0}_{-m,-n_1,-n_2}(IS) \end{pmatrix} \end{pmatrix}}_{dipolar\times dipolar}$
$G^{(0)0}_0(IS)$	$\frac{1}{2\sqrt{3}}\left(\omega^{(-1)}_{IS}+\omega^{(1)}_{IS}\right)$
$G^{(1)0}_0(IS)$	$\frac{1}{2\sqrt{2}}\left(\omega^{(-1)}_{IS}-\omega^{(1)}_{IS}\right)$
$G^{(2)0}_0(IS)$	$\frac{1}{2\sqrt{6}}\left(\omega^{(-1)}_{IS}+\omega^{(1)}_{IS}\right)$
$G^{(2)2}_0(IS)$	$\frac{1}{2}\omega^{(-1)}_{IS}$
$G^{(2)-2}_0(IS)$	$\frac{1}{2}\omega^{(1)}_{IS}$

describing the spin dynamics in DQ CP-MAS experiment is represented by,

$$\begin{aligned} H^{eff}_F =& H_0 + H_{1,dia} + H^{(1)}_2 \\ =& iT^{(1)0}_0(I)A_1 + iT^{(1)0}_0(S)A_2 + G^{(2)2}_0(IS)T^{(2)2}_0(IS) + G^{(2)-2}_0(IS)T^{(2)-2}_0(IS) \end{aligned} \tag{2.28}$$

Similar to the description in the ZQ case, the polarization transfer in the case of DQ experiments is described in the Floquet-state space.

$$\langle S_z(t)\rangle = Tr\left[\rho^{eff}_F(t).S_{z,F}\right] \tag{2.29}$$

where,

$$\rho^{eff}_F(t) = \exp\left\{-\frac{i}{\hbar}H^{eff}_F t\right\}\rho_F(0)\exp\left\{\frac{i}{\hbar}H^{eff}_F t\right\} \tag{2.30}$$

In the above equation, $\rho_F(0) \simeq I_z$ represents the initial density operator in the Floquet-state space. Evaluating the above expression, results in a compact expression.

$$\langle S_z(t)\rangle = -\frac{\omega_{IS}^2}{\omega_{IS}^2 + (A_1 + A_2)^2}\sin^2\left(\frac{\sqrt{\omega_{IS}^2 + (A_1 + A_2)^2}t}{2}\right) \tag{2.31}$$

In contrast to the description in the Floquet-Liouville space, the analytic expressions presented in this section are computationally robust and provide better insights into the spin physics in CPMAS experiments. In the following section, the simulations emerging from the analytic theory are compared with numerical simulations based on SPINEVOLUTION[40].

2.3.3 Simulations

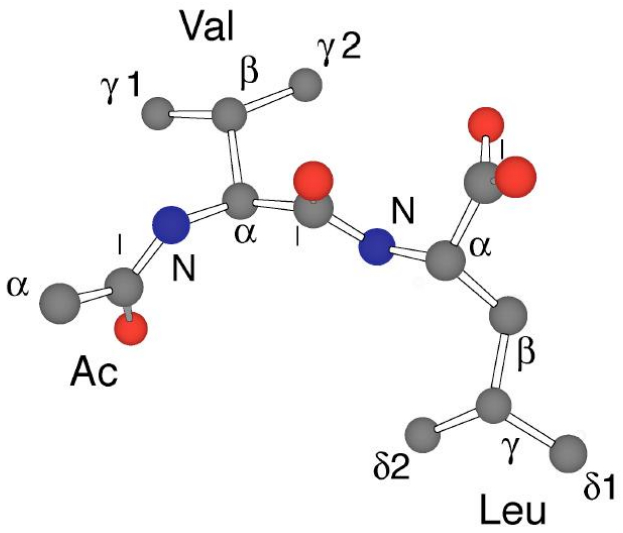

Figure 2.2: Crystal Structure of N-Acetyl-L-Valine-L-Leucine

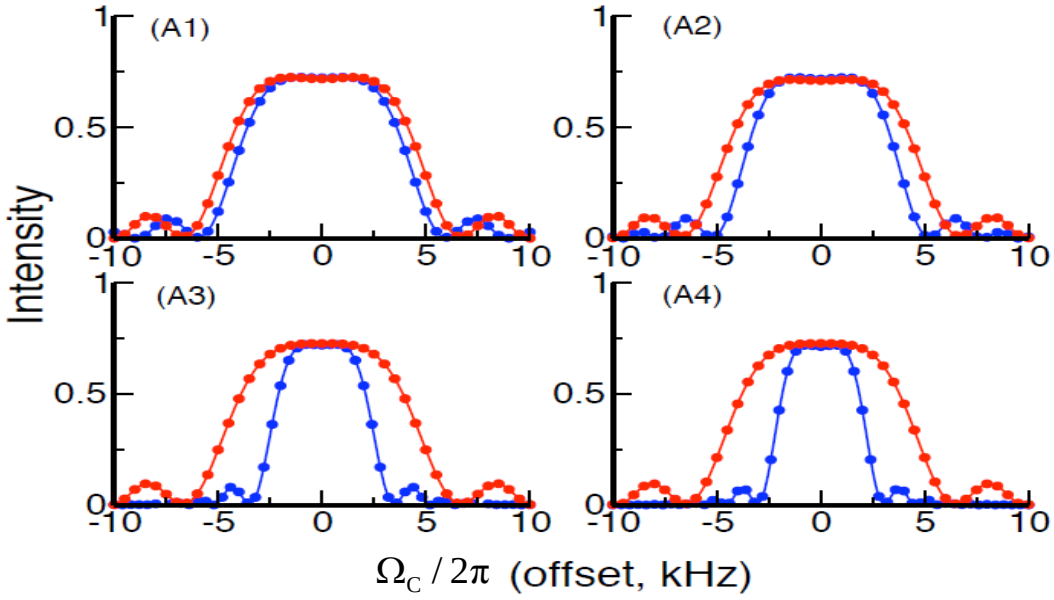

Figure 2.3: In the simulations presented, polarization transfer from ^{15}N to ^{13}C is calculated under constant mixing time, $\tau_{mix} = 2ms$. The RF amplitudes employed correspond to the ZQ matching condition $\left|\upsilon_{\mathrm{RF},^{13}\mathrm{C}} - \upsilon_{\mathrm{RF},^{15}\mathrm{N}}\right| = \upsilon_r$ with $\upsilon_{\mathrm{RF},^{13}\mathrm{C}} = p\upsilon, \upsilon_{\mathrm{RF},^{15}\mathrm{N}} = r\upsilon$. In panel (A1) υ_r = 10kHz , red (p=5, r=4), blue (p=4, r=5), (A2) υ_r = 20kHz , red (p=5/2, r=3/2), blue (p=3/2, r=5/2) (A3) υ_r = 40kHz , red (p=4/3, r=1/3), blue (p=1/3, r=4/3) and (A4) υ_r = 40kHz , red (p=5/4, r=1/4), blue (p=1/4, r=5/4). The following chemical shift parameters were employed in the simulations: $\alpha_{PM}^{(C)} = 64.9^0, \beta_{PM}^{(C)} = 37.5^0, \gamma_{PM}^{(C)} = -28.8^0$, $\eta_C = 0.98, \delta_C = 19.4$ppm; $\eta_N = 0.17, \delta_N = 10.1$ppm, $\alpha_{PM}^{(N)} = -83.3^0, \beta_{PM}^{(N)} = -79.0^0, \gamma_{PM}^{(N)} = 0.0^0$. The dipolar coupling between the spins was set to 890 Hz ($r_{12} = 1.5\mathrm{A}^0$) and correspond to the coupling found in glycine. The solid lines represent the analytic simulations while the circles represent the numerical simulations based on SPINEVOLUTION [40].

Following the theoretical description in the previous section, we outline the factors that govern the polarization transfer from $^{15}N \rightarrow ^{13}C$, (see Figure 2.1) in CP experiments. In all the simulations presented, polarization transfer from $^{15}N \rightarrow ^{13}C$ is calculated as a function of the frequency offset (under constant mixing time, 2ms) at a field strength of 11.7 T (500 MHz ^1H-Larmor frequency) under idealized decoupling conditions (i.e. the heteronuclear dipolar interactions between $^{13}C - ^1H$ and $^{15}N - ^1H$ is neglected). The amplitude of the RF powers employed in the simulations (constant phase) are in conformity with the current available

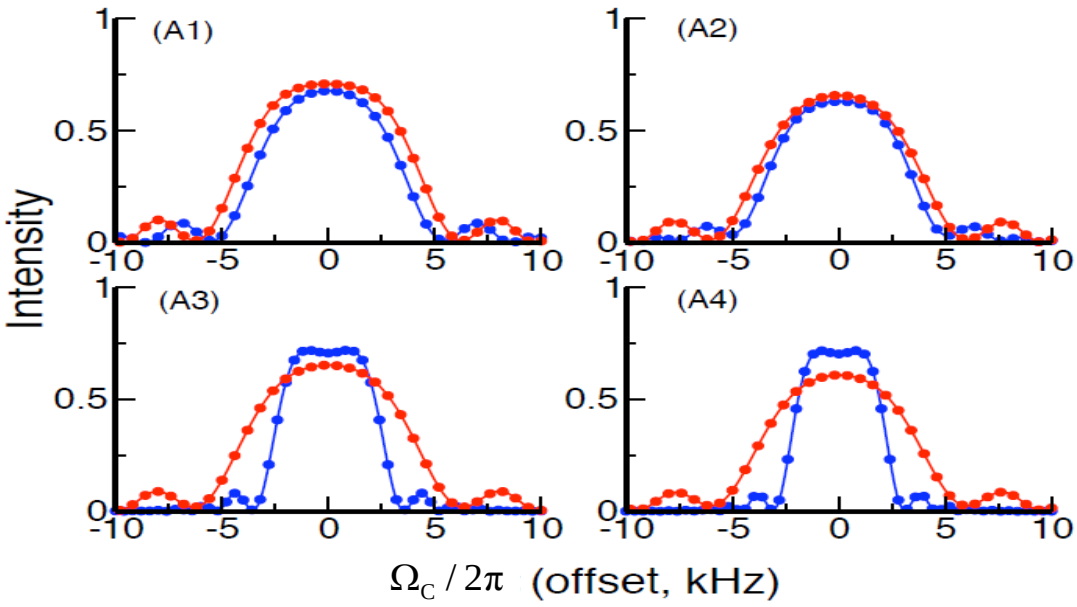

Figure 2.4: The notations and parameters employed are identical to the one employed in Figure except for δ_N = 99ppm and dipolar constant of 800 Hz (r_{12} = 1.56A^0). The simulations model the ^{15}N (Amide) $\rightarrow^{13} C_\alpha$ system. The solid lines represent the analytic simulations while the circles represent the numerical simulations based on SPINEVOLUTION[40].

technology and are chosen to be incommensurate with the spinning frequency. To illustrate the role of CSA interactions, simulations depicting the polarization transfer in ^{15}N(glycine)$\rightarrow^{13} C_\alpha$ (see Figure 2.3), ^{15}N (Amide) $\rightarrow^{13} C_\alpha$ (see Figure 2.4), and ^{15}N (Amide) $\rightarrow^{13} C_0$ (see Figure 2.5) resembling the spin pair in the peptide backbone[11] is presented at different spinning frequencies ranging from 10-40 kHz. For the sake of illustration, the results emerging from the standard experiments ($\upsilon_{\mathrm{RF},^{13}\mathrm{C}} = 50kHz$, $\upsilon_{\mathrm{RF},^{15}\mathrm{N}} = 40kHz$, panel A1 in Figure 2.3 - 2.5) are compared with schemes that employ modulations that are incommensurate with the spinning frequency.

Although, the recoupled dipolar Hamiltonian is identical in all of the ZQ schemes presented (Figures 2.3 - 2.5), the bandwidth of polarization transfer differs. This difference in the bandwidth is due to the presence of residual longi-

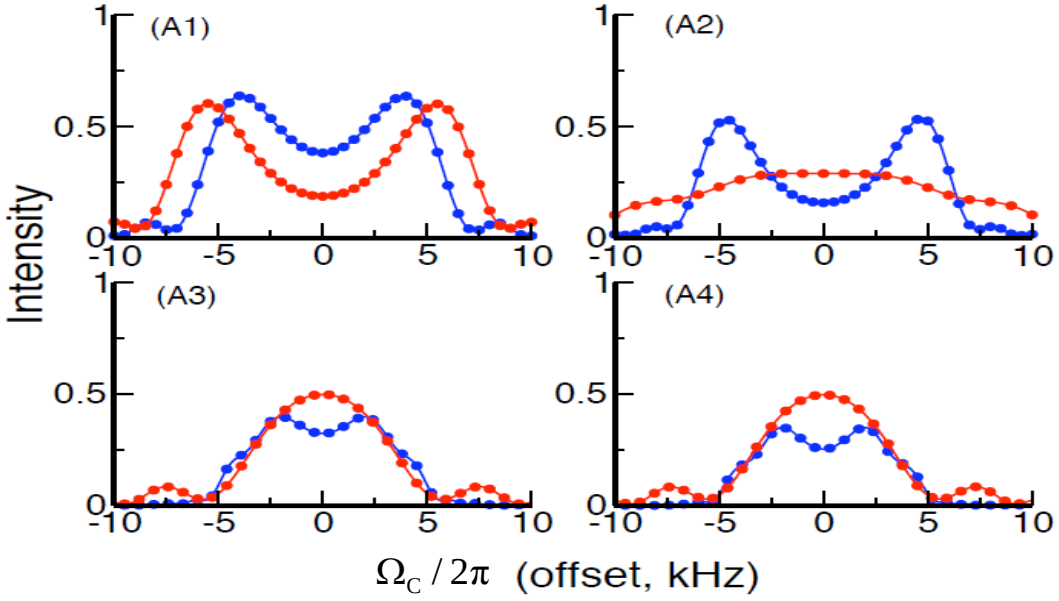

Figure 2.5: The notations and parameters employed are identical to the one employed in Figure 2.3 except for $\delta_C = -76$ppm,$\delta_N = 99$ppm and dipolar constant of 900 Hz ($r_{12} = 1.56\text{A}^0$). The simulations model the ^{15}N (Amide) $\rightarrow^{13} C_0$ system found in the peptide backbone. The solid lines represent the analytic simulations while the circles represent the numerical simulations based on SPINEVOLUTION[40].

tudinal single spin operators (say I_z), resulting from the second order contributions emerging from the cross terms between the chemical shift off set terms (say $[I^+, I^-] \propto I_z$). This behavior is prominently observed in schemes that employ modulations that are incommensurate with the spinning frequency and could also be deduced from the 'C' coefficients, $C^{(1)\pm1}_{m,\pm n_1}(I) = \frac{G^{(1)\pm1}_{m,\pm n_1}(I)}{(m\omega_r \pm n_1\omega_r)}$ (see Table 2.4) associated with single spin operators. Hence, the bandwidth decreases progressively as we go from $n_1 = 3/2, 1/3, 1/4$ as depicted in Figure 2.3 corresponding to the panels A2, A3 and A4 respectively. The decrease in the efficiency of transfer could be quantitatively explained based on the effective Hamiltonians and the analytic expressions presented in the previous section. As described in Eq. (2.26), when the magnitude of the coefficients associated with the longitudinal single spin operators (see A_1, A_2) in the effective Hamiltonian (see Eq. 2.24) are larger in comparison

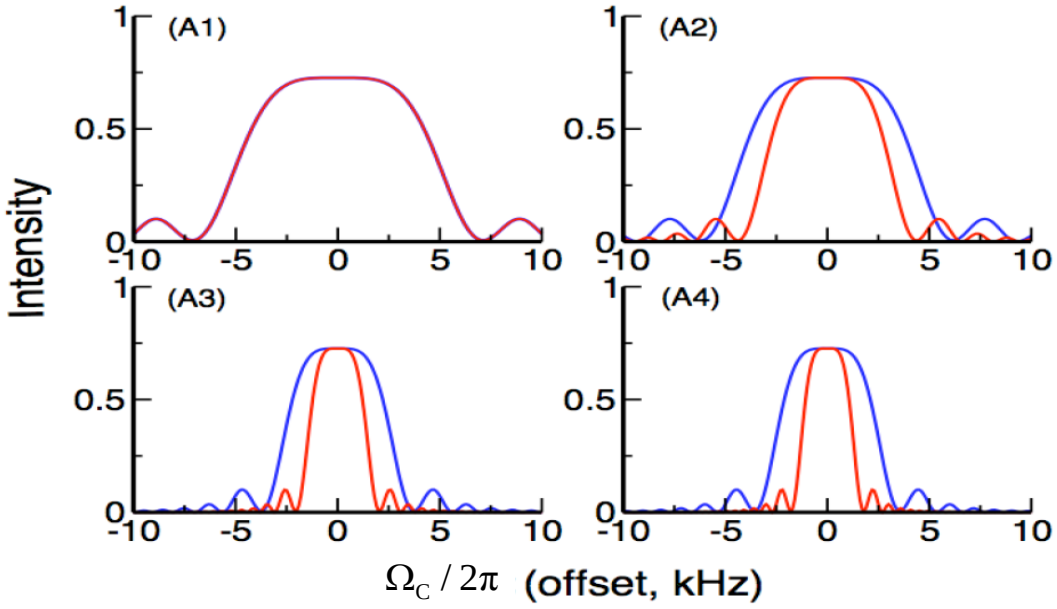

Figure 2.6: Analytic simulations depicting the polarization transfer in ^{15}N (Amide) $\rightarrow^{13} C_0$ system in the absence of the CSA x CSA cross terms. The notations and parameters employed are identical to the one employed in Figure 2.5.

to the recoupled dipolar Hamiltonian (dipolar coefficients), the prefactor in Eq. (2.26) decreases in magnitude. Hence, the efficiency of transfer decreases with increase in the off-sets.

To illustrate the effects of CSA interactions, additional simulations depicting polarization transfer in ^{15}N (Amide) $\rightarrow^{13} C_\alpha$ and ^{15}N (Amide) $\rightarrow^{13} C_0$ were performed. The ZQ matching conditions and other dipolar parameters are similar to the ones employed in the simulations depicted in Figure 2.3. As depicted in Figures 2.4 and 2.5, the efficiency of transfer decreases along with a dip in the exchange profile with increase in the magnitude of the CSA interactions. This dip is particularly severe (see Figure 2.5) when the magnitude of the CSA interactions of both ^{13}C and ^{15}N are dominant. To explain this observation, it is important to understand the other anisotropic contributions to the longitudinal single spin operators. To second order, the corrections to the longitudinal single spin oper-

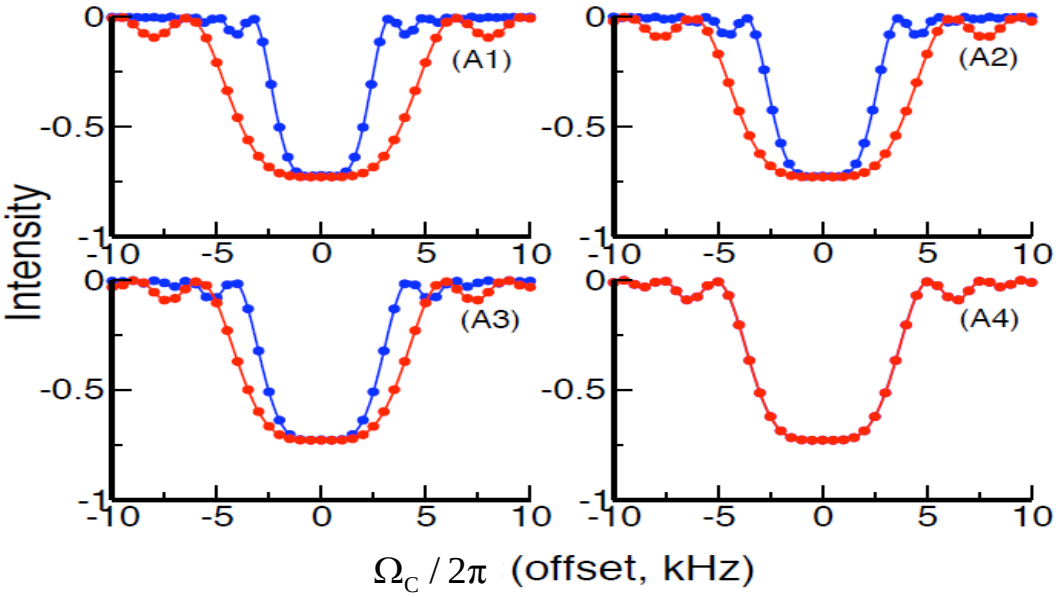

Figure 2.7: In the simulations presented, polarization transfer from ^{15}N to ^{13}C is calculated under constant mixing time, $\tau_{mix} = 2ms$. The RF amplitudes employed correspond to the DQ matching condition $\left|\upsilon_{\mathrm{RF},^{13}\mathrm{C}} + \upsilon_{\mathrm{RF},^{15}\mathrm{N}}\right| = \upsilon_r$ with $\upsilon_{\mathrm{RF},^{13}\mathrm{C}} = p\upsilon, \upsilon_{\mathrm{RF},^{15}\mathrm{N}} = r\upsilon$. In panel (A1) υ_r = 60kHz , blue (p=4/5, r=1/5), red (p=1/5, r=4/5), (A2) υ_r = 60kHz , blue (p=3/4, r=1/4), red (p=1/4, r=3/4) (A3) υ_r = 60kHz , blue (p=2/3, r=1/3), red (p=1/3, r=2/3) and (A4) υ_r = 60kHz , red (p=1/2, r=1/2). The CSA and dipolar parameters are identical to those employed in Figure 2.3. The solid lines represent the analytic simulations while the circles represent the numerical simulations based on SPINEVOLUTION[40].

ators result from (a) cross terms between the isotropic chemical shift terms (b) cross-terms between the CSA interactions (c) cross-terms between the dipolar interactions (see Table 2.4). In particular, the 'C' coefficients associated with the isotropic chemical shift and CSA interactions are dependent on the indices n_1 and n_2 (i.e. $C^{(1)\pm1}(I) \propto (m\upsilon_r \pm n_1\upsilon_1)^{-1}, C^{(1)\pm1}(S) \propto (m\upsilon_r \pm n_2\upsilon_2)^{-1}$ When the amplitudes of the RF modulations employed on the two channels are incommensurate with the spinning frequency, the magnitude of the cross-terms ($[I^+, I^-] \propto I_z$) increase, resulting in lower transfer of polarization. This is in agreement with the simulations depicted in Figures 2.4 - 2.5. As depicted in Figure 2.5, with the increase in the magnitude of the CSA interactions, the dip observed is more pro-

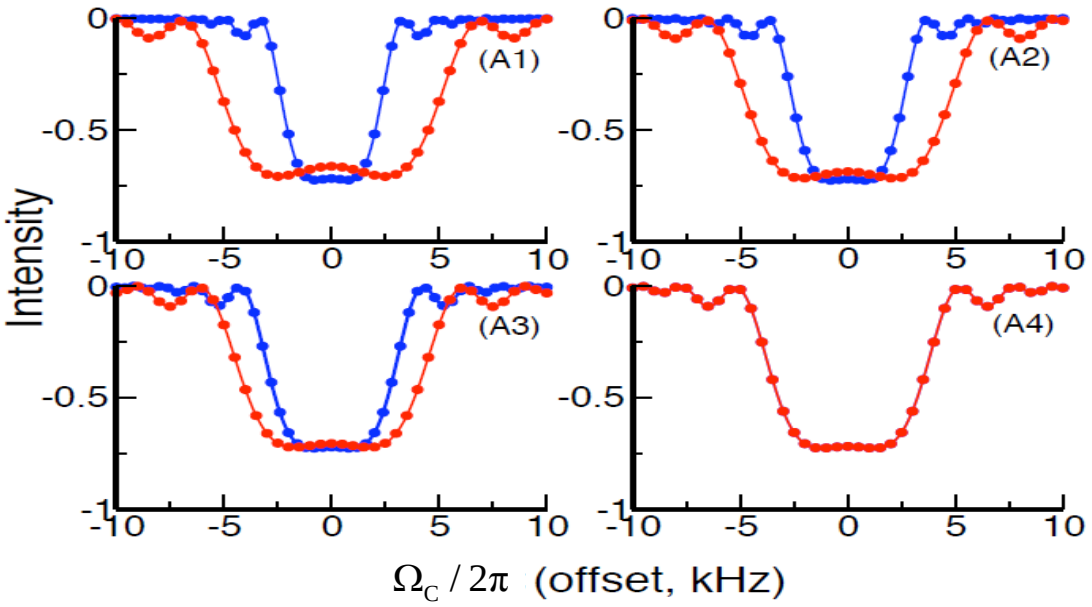

Figure 2.8: In the simulations presented, the DQ matching condition $\left|\upsilon_{\mathrm{RF},^{13}\mathrm{C}} + \upsilon_{\mathrm{RF},^{15}\mathrm{N}}\right| = \upsilon_r$ is satisfied. The value of 'p' and 'r' in the panels (A1-A4) are identical to the one employed in Figure 2.7. The CSA and dipolar parameters are identical to those employed in Figure 2.4. The solid lines represent the analytic simulations while the circles represent the numerical simulations based on SPINEVOLUTION [40].

found resulting in lesser transfer efficiencies. At the exact resonance condition (i.e. ^{13}C-offset frequency is zero) the magnetization exchange is diminished due to the presence of the non-zero cross-terms between the CSA interactions associated with the two spins. As the magnitude of the chemical shift off-set terms increase, the cross-terms between the chemical shift off-set terms compensate the cross-terms resulting from the CSA interactions of the two spins resulting in a symmetric pattern of transfer as depicted in Figure 2.5 (see panels A1, A2). This explanation is justified through analytic simulations (see fig 2.6) wherein, the cross-terms from the CSA interactions (both ^{13}C and ^{15}N) have been ignored. In ZQ experiments, the residual difference term $(A_1 - A_2)$ associated with the longitudinal single spin operators are primarily responsible for both depolarization and the observed dip in

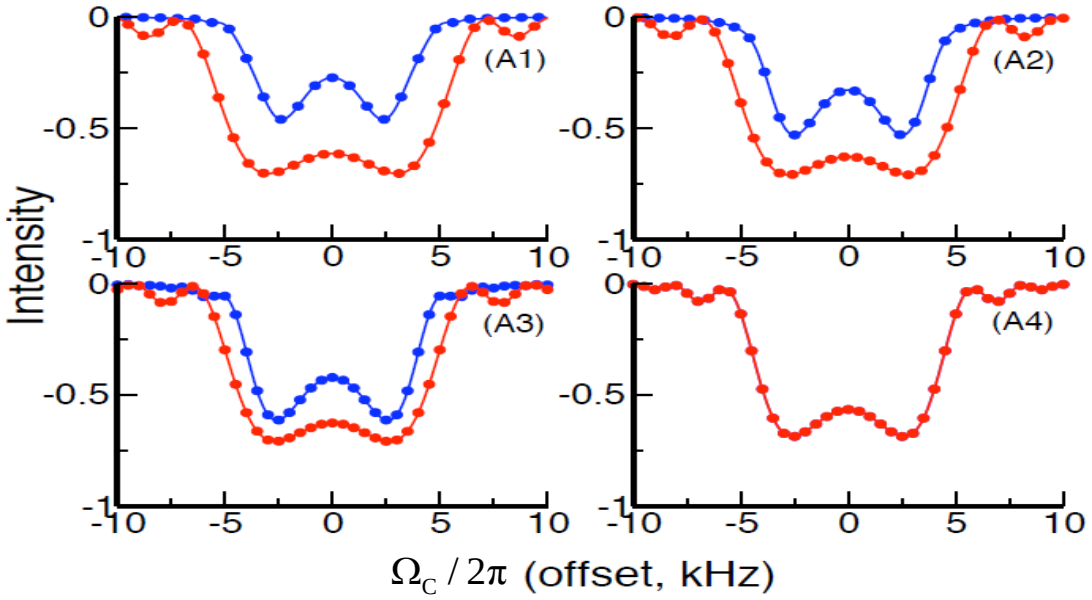

Figure 2.9: In the simulations presented, the DQ matching condition $\left|\upsilon_{\mathrm{RF},^{13}\mathrm{C}} + \upsilon_{\mathrm{RF},^{15}\mathrm{N}}\right| = \upsilon_r$ is satisfied. The value of 'p' and 'r' in the panels (A1-A4) are identical to the one employed in Figure 2.7. The CSA and dipolar parameters are identical to those employed in Figure 2.5. The solid lines represent the analytic simulations while the circles represent the numerical simulations based on SPINEVOLUTION [40].

the profile. As depicted in Figure 2.6, in the absence of the CSA cross-terms, there is no dip observed in the profile and the off-resonance behavior observed is solely due to the cross terms between the chemical shit off-set terms. In comparison to experiments that are chemical shift selective, the fractional matching conditions are suitable for studies in systems where broadband transfer is preferred in a controlled fashion. Such modifications are less feasible in the standard sequences ($p = 5$, $q = 4$) due to the synchronization conditions.[10] Hence, the bandwidth in ZQ experiments is mainly controlled by a residual term $(A_1 - A_2)$ proportional to the difference in the effective fields associated with longitudinal single spin operators resulting from the cross terms between the transverse components (inclusive of CSA and chemical shift off set) of the single spin interactions.

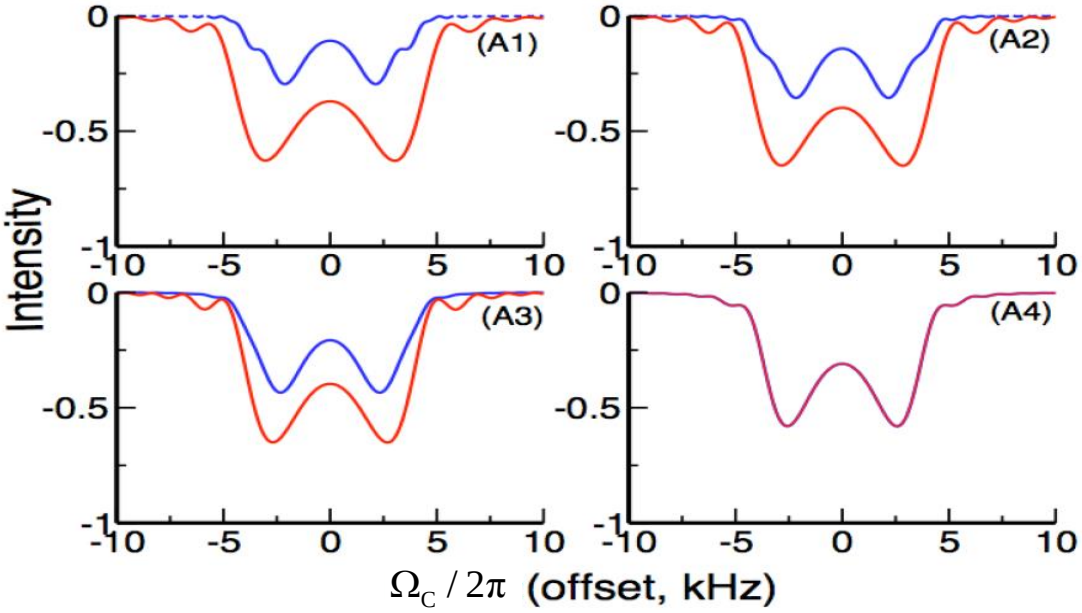

Figure 2.10: Analytic simulations depicting the polarization transfer in DQ experiments corresponding to $^{13}C_0 \rightarrow ^{15}N$ (Amide) system at $\upsilon_r = 30$kHz . The notations and parameters employed are identical to the one employed in Figure 2.9

To design experiments at faster spinning frequencies, we explore the double-quantum (DQ) matching condition. Although chemical shift selective versions of double quantum (DQ) homonuclear[27,41–43] and heteronuclear recoupling[44] schemes exist in the literature, the theory presented along with the simulations, predict the existence of a band-selective heteronuclear DQ recoupling scheme. As described in the previous section, the recoupling in DQ experiments is achieved by matching the sum of the RF fields to the spinning frequency. The polarization transfer in DQ experiments is depicted in Figures 2.6 - 2.8. In contrast to the ZQ recoupling schemes, the spinning frequencies employed in the DQ schemes are higher and are extremely useful for high field solid-state NMR experiments with faster MAS frequencies. Additionally, the efficiency of polarization transfer in the DQ sequences is much higher in all the CSA regimes (see Figures 2.7 - 2.9).

Analogous to the ZQ recoupling sequences (depicted in Figures 2.3 - 2.5), the

bandwidth in the DQ sequences could be altered by suitable choice of p and r as depicted in Figures 2.7 - 2.9. In the extreme CSA regimes, the efficiency of polarization transfer observed in the DQ experiments (Figure 2.9) is higher than those observed in ZQ experiments (Figure 2.5). Hence, the DQ experiments could be important at higher magnetic field strengths wherein the CSA interactions play an important role in the spin dynamics. To explain the better performance of DQ over ZQ recoupling sequences, simulations depicting the DQ polarization transfer at lower spinning frequency (say υ_r = 30kHz) is presented in Figure 2.10. The simulations depict the polarization transfer in the high CSA regime corresponding to the ^{15}N (Amide) $\rightarrow^{13} C_0$ system. As depicted, the efficiency of transfer decreases with a pronounced dip in the exchange profile. This decrease in the efficiency is due to the presence of the longitudinal single spin operators resulting from the cross terms between the CSA interactions. In contrast to the ZQ recoupling schemes, the coefficients associated with depolarization are proportional to the sum of the effective fields $(A_1 + A_2)$ resulting from the second order cross terms between single spin interactions (namely CSA, chemical shift off set). Since, the residual contributions to the depolarization emerging from the CSA interactions are additive, the efficiency of transfer is significantly diminished in DQ recoupling sequences. Hence, the implementation of DQ DCP experiments entails faster spinning frequencies. Depending on the spinning frequency, several ZQ and DQ matching conditions could be designed from the effective Hamiltonians and the 'C' coefficients presented in Table 2.4 and the theory presented herein could serve as a guiding tool to develop better schemes.

The analytic theory presented, provides a convenient framework for quantitative interpretation of the exchange trajectories in DCP experiments that employ modulations incommensurate with the spinning frequency and could be employed of measuring $^{13}C-^{15}N$ distances in uniformly labeled solids. The implementation of DCP experiments based on first order recoupling at faster spinning frequencies could be of extreme importance in the design of sequences without decoupling field on the proton channel. Such an approach minimizes sample-heating effects and could in principle improve the efficiency of polarization transfer.

2.4 Conclusions

In summary, a theoretical formalism for describing sequences that employ RF modulations that are incommensurate with the spinning frequency has been presented. The underlying spin physics in the ZQ and DQ case is thoroughly investigated in terms of effective Hamiltonians and could be employed as a tool for understanding the performance of DCP experiments at different conditions. The simulations predict the requirement of higher spinning frequencies for the implementation of DQ DCP experiments. The factors responsible for depolarization are outlined in terms of operators resulting in better understanding of the experiments. We believe, that the theory presented herein could be employed as a tool for quantitative interpretation of DCP experiments. The analytic model based on the Floquet approach presented in this article is suitable for describing the dynamics of spins subjected to multiple modulations and provides avenues for better design of sequences at higher magnetic field strengths with faster spinning frequencies.

Appendix-2

Table 2.5: Multipole Operators for coupled spin systems

Single spin system ($I = 1/2$)	$T^{(1)q}(1)\}$ Single spin Operators
Two - spin system ($I_1 = I_2 = 1/2$)	$T^{(1)q}(10), T^{(1)q}(01)\}$ Single spin Operators $T^{(2)q}(11), T^{(1)q}(11), T^{(0)0}(11)\}$ Two spin Operators
Three - spin system ($I_1 = I_2 = I_3 = 1/2$)	$T^{(1)q}_{\{1\}}(100), T^{(1)q}_{\{1\}}(010), T^{(1)q}_{\{0\}}(001)\}$ Single spin Operators $T^{(2)q}_{\{2\}}(110), T^{(1)q}_{\{1\}}(110), T^{(0)0}_{\{0\}}(110),$ $T^{(2)q}_{\{1\}}(101), T^{(1)q}_{\{1\}}(101), T^{(0)0}_{\{1\}}(101),$ $T^{(2)q}_{\{1\}}(011), T^{(1)q}_{\{1\}}(011), T^{(0)0}_{\{1\}}(011)$ } Two spin Operators $T^{(3)q}_{\{2\}}(111), T^{(2)q}_{\{2\}}(111), T^{(1)q}_{\{2\}}(111),$ $T^{(2)q}_{\{1\}}(111), T^{(1)q}_{\{1\}}(111), T^{(0)0}_{\{1\}}(111),$ $T^{(1)q}_{\{0\}}(111)$ } Three spin Operators

Note: $T^{(k)q}$ is representative of all operators ranging from $q = -k\ to + k$.

References

[1] A. Pines, M. G. Gibby and J. S. Waugh, *J. Chem. Phys.*, 1973, **59**, 569–590.

[2] M. Ernst, A. Samoson and B. H. Meier, *Chem. Phys. Lett.*, 2001, **348**, 293 – 302.

[3] M. Ernst, A. Samoson and B. H. Meier, *J. Magn. Reson.*, 2003, **163**, 332 – 339.

[4] M. Ernst, M. A. Meier, T. Tuherm, A. Samoson and B. H. Meier, *J. Am. Chem. Soc.*, 2004, **126**, 4764–4765.

[5] M. Kotecha, N. P. Wickramasinghe and Y. Ishii, *Magn. Reson. Chem.*, 2007, **45**, S221–S230.

[6] M. Weingarth, G. Bodenhausen and P. Tekely, *J. Magn. Reson.*, 2009, **199**, 238 – 241.

[7] V. Agarwal, T. Tuherm, A. Reinhold, J. Past, A. Samoson, M. Ernst and B. H. Meier, *Chem. Phys. Lett.*, 2013, **583**, 1 – 7.

[8] U. Haeberlen and J. S. Waugh, *Phys. Rev.*, 1968, **175**, 453–467.

[9] U. Haeberlen, *High-Resolution NMR in Solids: Selective Averaging*, Academic, New York, 1976.

[10] M. Bjerring and N. C. Nielsen, *Chem. Phys. Lett.*, 2003, **382**, 671 – 678.

[11] M. Bjerring, J. T. Rasmussen, R. Schultz Krogshave and N. C. Nielsen, *J. Chem. Phys.*, 2003, **119**, 8916–8926.

[12] M. Bjerring, A. B. Nielsen, Z. Tosner and N. C. Nielsen, *Chem. Phys. Lett.*, 2010, **494**, 326 – 330.

[13] S. Laage, A. Marchetti, J. Sein, R. Pierattelli, H. J. Sass, S. Grzesiek, A. Lesage, G. Pintacuda and L. Emsley, *J. Am. Chem. Soc.*, 2008, **130**, 17216–17217.

[14] S. Laage, J. R. Sachleben, S. Steuernagel, R. Pierattelli, G. Pintacuda and L. Emsley, *J. Magn. Reson.*, 2009, **196**, 133 – 141.

[15] J. H. Shirley, *Phys. Rev. B*, 1965, **4**, 979.

[16] R. Ramachandran and R. G. Griffin, *J. Chem. Phys.*, 2005, **122**, 164502.

[17] R. Ramachandran, J. R. Lewandowski, P. C. A. van der Wel and R. G. Griffin, *J. Chem. Phys.*, 2006, **124**, 214107.

[18] R. Ramachandran and R. G. Griffin, *J. Chem. Phys.*, 2006, **125**, 044510.

[19] M. K. Pandey and R. Ramachandran, *Mol. Phys.*, 2010, **108**, 619–635.

[20] B. C. Sanctuary, *J. Chem. Phys.*, 1976, **64**, 4352–4361.

[21] B. Silver, *Irreducible Tensor Methods*, Academic Press, 1st edn, 1976.

[22] M. Mehring, *Principles of High Resolution NMR in Solids*, Springer Verlag, Berlin, 1999.

[23] A. R. Edmonds, *Angular Momentum in Quantum Mechanics*, Princeton University Press, 1974.

[24] C. P. Jaroniec, B. A. Tounge, C. M. Rienstra, J. Herzfeld and R. G. Griffin, *J. Am. Chem. Soc.*, 1999, **121**, 10237–10238.

[25] C. P. Jaroniec, C. Filip and R. G. Griffin, *J. Am. Chem. Soc.*, 2002, **124**, 10728–10742.

[26] R. Ramachandran, V. Ladizhansky, V. S. Bajaj and R. G. Griffin, *J. Am. Chem. Soc.*, 2003, **125**, 15623–15629.

[27] V. Ladizhansky and R. G. Griffin, *J. Am. Chem. Soc.*, 2004, **126**, 948–958.

[28] E. Stejskal, J. Schaefer and J. Waugh, *J. Magn. Reson.*, 1977, **28**, 105 – 112.

[29] J. Schaefer and E. O. Stejskal, *J. Am. Chem. Soc.*, 1976, **98**, 1031–1032.

[30] J. Schaefer, E. Stejskal, J. Garbow and R. McKay, *J. Magn. Reson.*, 1984, **59**, 150 – 156.

[31] A. Lange, I. Scholz, T. Manolikas, M. Ernst and B. H. Meier, *Chem. Phys. Lett.*, 2009, **468**, 100 – 105.

[32] J. R. Lewandowski, G. De Paëpe and R. G. Griffin, *J. Am. Chem. Soc.*, 2007, **129**, 728–729.

[33] I. Hung and Z. Gan, *J. Magn. Reson.*, 2015, **256**, 23 – 29.

[34] J.-P. Demers, V. Chevelkov and A. Lange, *Solid State Nucl. Magn. Reson.*, 2011, **40**, 101 – 113.

[35] B. C. Sanctuary and T. K. Halstead, *Advances in Magnetic and Optical Resonance*, Academic Press, 1990, vol. 15, pp. 79 – 161.

[36] G. D. Boender, S. Vega and H. J. M. D. Groot, *Mol. Phys.*, 1998, **95**, 921–934.

[37] R. Ramachandran, V. S. Bajaj and R. G. Griffin, *J. Chem. Phys.*, 2005, **122**, 164503.

[38] R. Ramesh and M. S. Krishnan, *J. Chem. Phys.*, 2001, **114**, 5967–5973.

[39] M. K. Pandey and M. S. Krishnan, *J. Chem. Phys.*, 2010, **133**, 174121.

[40] M. Veshtort and R. G. Griffin, *J. Magn. Reson.*, 2006, **178**, 248 – 282.

[41] N. C. Nielsen, H. Bildsoe, H. J. Jakobsen and M. H. Levitt, *J. Chem. Phys.*, 1994, **101**, 1805–1812.

[42] K. Takegoshi, K. Nomura and T. Terao, *Chem. Phys. Lett.*, 1995, **232**, 424 – 428.

[43] K. Takegoshi, K. Nomura and T. Terao, *J. Magn. Reson.*, 1997, **127**, 206 – 216.

[44] M. Baldus, A. T. Petkova, Herzfeld and R. G. Griffin, *Mol. Phys.*, 1998, **95**, 1197–1207.

Chapter 3

Description of phase-modulations in heteronuclear recoupling experiments in solid-state NMR

3.1 Background

Following the description presented in the previous section, the next stage in our study was to develop a formalism for describing multiple pulse experiments in ssNMR using Floquet theory[1]. In the past, multiple pulse experiments in ssNMR were extensively designed using AHT[2,3]. To facilitate analytic description, the cycle time of the multiple pulse scheme is synchronized with the MAS rotor period. Subsequently, employing Magnus expansion[4], a time averaged Hamiltonian to the desired order of accuracy is derived over the MAS rotor period. Although the AHT approach has been quite successful in the design of sophisticated pulse schemes[3,5,6], its extension to pulse schemes at faster spinning frequencies is less straightforward. Specifically, at faster spinning frequencies, the concept of a time-averaged Hamiltonian breaks down due to competing nature of the MAS rotor period and the cycle time of a multiple pulse scheme. Under such conditions, the analytic insights emerging from AHT[2,3] could be misleading. From an experimen-

tal perspective, implementation of ssNMR experiments (as described in chapter-2) at faster spinning frequencies is essential for both improving the resolution as well as extending its utility in the study of biological systems. With this objective, an analytic framework is presented in the following sections to elucidate the effects of multiple pulses in MAS NMR experiments. Specifically, we confine our discussion to multiple-pulse based implementation of CP experiments.

3.2 Definition of the problem

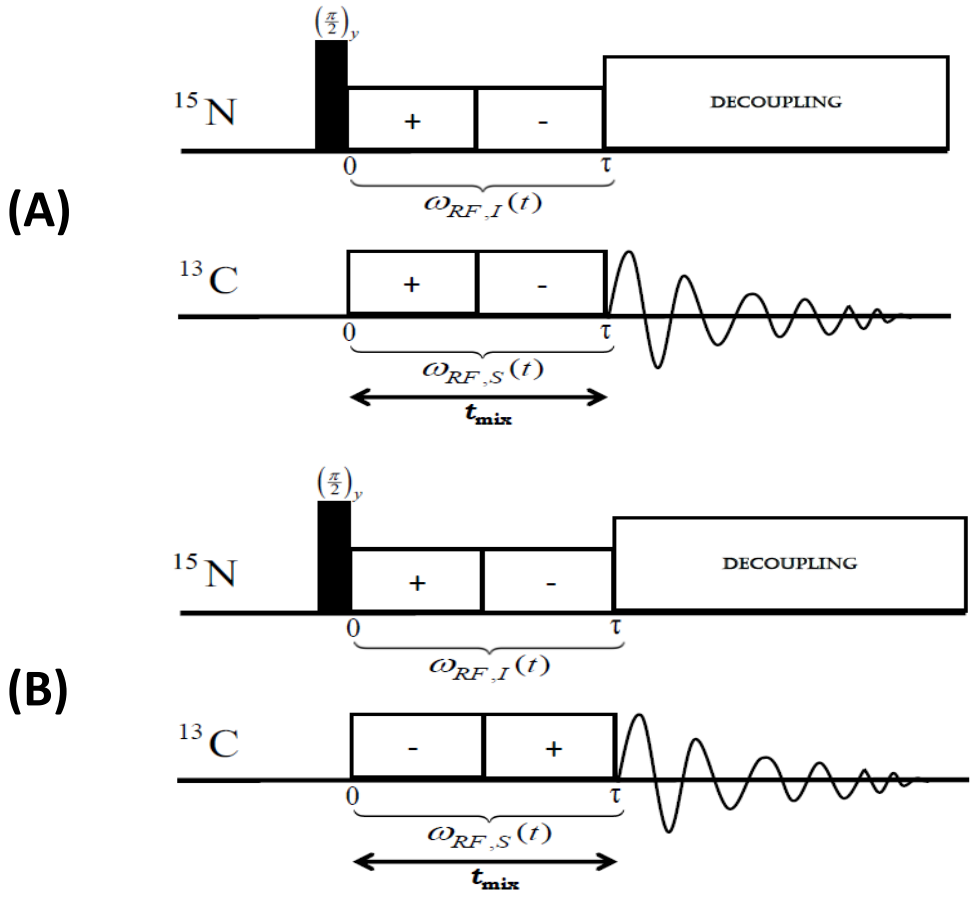

Figure 3.1: Pulse sequence depicting the polarization transfer in CP experiments with phase-modulated RF amplitudes. (A) No phase difference between the RF amplitudes on the two channels, (B) phase difference of 180^0 between the RF amplitudes on the two channels.

As described in chapter-2, the CP-matching conditions under MAS are ex-

tremely sensitive to the sample spinning frequency. Depending on the amplitudes of the RF fields employed on the two channels, the sample spinning frequency is adjusted to satisfy one of the matching conditions corresponding to the first and second-sidebands in a typical CP profile. Although, such an approach facilitates the reintroduction of the dipolar interactions under MAS, they are extremely sensitive to the RF inhomogeneities present in the system. Hence, alternate strategies in the form of amplitude and phase modulations were developed in the past to broaden the CP matching condition in addition to improving the matching condition corresponding to the centre band in the CP profile[7–18]. From a conceptual viewpoint, the theory of multiple-pulse based CP schemes remains a challenge owing to the complexity introduced by the time-dependent RF fields in the rotating frame. This aspect has been the main motivation behind our investigation. For demonstrative purposes, we employ the phase modulated version of the CP experiment in our study. The utility of the synchronisation condition (imposed by AHT) in PM-CP MAS experiments is thoroughly investigated to elucidate the mechanism of polarization transfer in CP experiments. To realize this objective, we employ the concept of effective Hamiltonians based on multimodal Floquet theory[19]. The theoretical framework presented in this chapter is quite general and could be extended to describe RF modulations that are independent of the MAS frequency.

3.3 Discussion

3.3.1 Theory

To illustrate the effects of phase modulated RF fields, we begin our discussion with a model system comprising of two spins. Following the description in chapter-2, the Hamiltonian in the rotating frame is transformed into a tilted frame defined by the transformation function, U_1. Although the form of the internal Hamiltonians are identical to those depicted in chapter-2, the amplitude of the RF fields in the tilted rotating frame are time-dependent. Hence, the transformation into the RF interaction frame is less straight forward. To facilitate analytic description, and elucidate the role of the time-dependent fields on the internal Hamiltonians, the amplitude of the RF modulation in the rotating frame is expanded and expressed in terms of a Fourier series. In the rotating frame, the amplitude of the RF field resembles a square-wave modulation and is conveniently expressed in terms of a Fourier series expansion, as illustrated below.

$$\omega_{RF,I}(t) = \frac{4}{\pi}\omega_{RF,I} \sum_{n_1=1,3,5}^{\infty} \tfrac{1}{n_1} \sin n_1\omega_I t \tag{3.1}$$

(where, $\omega_{RF,I}$ denotes the amplitude of the RF field and ω_I the frequency of the modulation on the i^{th} channel). The methodology presented in this chapter is equally applicable to any kind of periodic modulations (either phase or amplitude or both). In a similar vein, the RF modulation on the S channel is expressed by,

$$\omega_{RF,S}(t) = \frac{4}{\pi}\omega_{RF,S} \sum_{n_2=1,3,5}^{\infty} \tfrac{1}{n_2} \sin n_2\omega_S t \tag{3.2}$$

To describe the evolution of the system under RF fields, the Hamiltonian is further transformed into the RF interaction frame. In the RF interaction frame, the internal Hamiltonians are modulated by both the sample spinning frequency as well as the modulation frequency of the RF fields. The final form of the various spin Hamiltonians in the RF interaction frame are illustrated below.

$$\tilde{\tilde{H}}_I(t) = \sum_{q=-1,\neq 0}^{1} \sum_{m=-2}^{2} \sum_{n_1=-\infty}^{\infty} \frac{-q}{\sqrt{2}} \omega_I^{(m)} i T^{(1)q}(I) e^{im\omega_r t} e^{in_1\omega_I t} e^{iq\omega_{RF,I} t} g_{n_1}^{(1)q}(I) \qquad (3.3)$$

$$\tilde{\tilde{H}}_S(t) = \sum_{q=-1,\neq 0}^{1} \sum_{m=-2}^{2} \sum_{n_2=-\infty}^{\infty} \frac{-q}{\sqrt{2}} \omega_S^{(m)} i T^{(1)q}(S) e^{im\omega_r t} e^{in_2\omega_S t} e^{iq\omega_{RF,S} t} g_{n_2}^{(1)q}(S) \qquad (3.4)$$

The terms $g_{n_1}^{(1)q}(I)$ and $g_{n_2}^{(1)q}(S)$ represent the coefficients in the RF interaction frame and are derived using the Bessel function approach[20,21]. In the case of the dipolar interactions, the Hamiltonian in the RF interaction frame is modulated by the two modulation frequencies (ω_I, ω_S) in addition to the MAS frequency (ω_r).

$$\tilde{\tilde{H}}_{Dip}(t) = \tilde{\tilde{H}}_{ZQ}(t) + \tilde{\tilde{H}}_{DQ}(t) \qquad (3.5)$$

$$\tilde{\tilde{H}}_{ZQ}(t) = \frac{1}{2} \sum_{m=-2,m\neq 0}^{2} \sum_{k=0}^{1} \sum_{n_1,n_2=-\infty}^{\infty} \begin{bmatrix} \omega_{IS}^{(m)} T^{(k)0}(IS) * \\ \begin{pmatrix} e^{im\omega_r t} e^{in_1\omega_I t} e^{in_2\omega_S t} * & \\ & e^{i(\omega_{RF,I} - \omega_{RF,S})t} \end{pmatrix} \end{bmatrix} g_{n_1,n_2}^{(k)0}(IS) \qquad (3.6)$$

$$\tilde{\tilde{H}}_{DQ}(t) = -\frac{1}{2} \sum_{m=-2,m\neq 0}^{2} \sum_{q=-2}^{2} \sum_{n_1,n_2=-\infty}^{\infty} \begin{bmatrix} \omega_{IS}^{(m)} T^{(2)q}(IS) * \\ \begin{pmatrix} e^{im\omega_r t} e^{in_1\omega_I t} e^{in_2\omega_S t} * & \\ & e^{i\frac{q}{2}(\omega_{RF,I} + \omega_{RF,S})t} \end{pmatrix} \end{bmatrix} g_{n_1,n_2}^{(2)q}(IS) \qquad (3.7)$$

As an alternative to the AHT approach, we employ multimode Floquet theory to describe phase modulated CP experiments. Such an approach provides a framework for describing modulations that are commensurate/incommensurate with the spinning frequency.

Extending the procedure described in chapter-2, the Floquet Hamiltonian for the PM-CP experiment comprising of three modulations is derived and is represented below.

$$
\begin{aligned}
H_F &= \omega_r I_F^{(m)} + \omega_I I_F^{(n_1)} + \omega_S I_F^{(n_2)} \\
&+ \sum_{q=-1,q\neq 0}^{1} \sum_{m=-2}^{2} \left[\sum_{n_1=-\infty}^{\infty} G^{(1)q}_{m,n_1,0}(I) i T^{(1)q}_{m,n_1,0}(I) + \sum_{n_2=-\infty}^{\infty} G^{(1)q}_{m,0,n_2}(S) i T^{(1)q}_{m,0,n_2}(S) \right] \\
&+ \sum_{m=-2,m\neq 0}^{2} \sum_{n_1,n_2=-\infty}^{\infty} \left[G^{(2)2}_{m,n_1,n_2}(IS) T^{(2)2}_{m,n_1,n_2}(IS) + G^{(2)-2}_{m,n_1,n_2}(IS) T^{(2)-2}_{m,n_1,n_2}(IS) \right] \\
&+ \sum_{k=0}^{2} \sum_{m=-2,m\neq 0}^{2} \sum_{n_1,n_2=-\infty}^{\infty} \left[\begin{array}{l} G^{(k)0}_{m,n_1,n_2}(IS) T^{(k)0}_{m,n_1,n_2}(IS) + \\ (-1)^k G^{(k)0}_{m,n_1,n_2}(IS) T^{(k)0}_{m,n_1,n_2}(IS) \end{array} \right]
\end{aligned}
\tag{3.8}
$$

In the above equation the Fourier indices, m, n_1, n_2 represent the coefficients associated with MAS, RF modulations on channels I and S respectively. In contrast to the CWCP experiment, the Floquet Hamiltonian in PM-CP experiments is highly off-diagonal and as such is unsuitable for any analytic description. To this end, we propose an effective Floquet Hamiltonian based on the method of contact transformation procedure. As discussed in the previous chapter, the zero order Hamiltonian mainly comprises of operators that are diagonal in the Fourier dimension. The off-diagonal contributions due to MAS and RF modulations are incorporated along H_1. Subsequently, employing the standard procedure the effec-

tive Floquet Hamiltonian to the desired order is derived systematically as described below,

$$\begin{aligned} H_0^{(1)} &= H_0 \\ H_1^{(1)} &= H_1 + i\,[S_1, H_0] \\ H_2^{(1)} &= H_2 + i\,[S_1, H_1] - \frac{1}{2}\,[S_1, [S_1, H_0]] \\ H_3^{(1)} &= -\frac{1}{2}\,[S_1, [S_1, H_1]] - \frac{i}{6}\,[S_1, [S_1, [S_1, H_0]]] \end{aligned} \tag{3.9}$$

In cases where the off-diagonal contributions to second order are significant, a second transformation in the form of $\exp(i\lambda^2 S_2)$ is applied to the Hamiltonian. The transformation function 'S_2 is chosen to compensate the off-diagonal contributions to order λ^2 and does not affect the corrections to order λ.

$$H_{eff} = e^{(i\lambda^2 S_2)} e^{(i\lambda S_1)} H_F e^{(-i\lambda S_1)} e^{(-i\lambda^2 S_2)} \tag{3.10}$$

$$H_{eff} = e^{(i\lambda^2 S_2)} \left[H_0^{(1)} + \lambda H_1^{(1)} + \lambda^2 H_2^{(1)} + \lambda^3 H_3^{(1)} \right] e^{(-i\lambda^2 S_2)} \tag{3.11}$$

Equating like powers of 'λ' the following relations are obtained.

$$\begin{aligned} \lambda^0 \rightarrow H_0^{(2)} &= H_0^{(1)} = H_0 \\ \lambda^1 \rightarrow H_1^{(2)} &= H_1^{(1)} = H_1 + i\,[S_1, H_0] \\ \lambda^2 \rightarrow H_2^{(2)} &= H_2^{(1)} + i\,[S_2, H_0] \\ \lambda^3 \rightarrow H_3^{(2)} &= H_3^{(1)} + i\left[S_2, H_1^{(1)}\right] \\ \lambda^4 \rightarrow H_4^{(2)} &= H_4^{(1)} + i\left[S_2, H_2^{(1)}\right] - \frac{1}{2!}\,[S_2, [S_2, H_0]] \end{aligned} \tag{3.12}$$

In the above equations, the perturbation corrections are expressed in terms of Hamiltonians '$H_j^{(k)}$' with 'j' denoting the order and the super-script 'k' depicting the number of transformations.

Depending on the sample spinning frequency and the modulation frequencies employed on the two channels, the form of the effective Hamiltonian differs. For e.g, when the modulation frequency is equal to the spinning frequency ($\tau_c = \tau_r$), the effective Hamiltonian to zeroth-order comprises of both the dipolar and the CSA interactions as described below.

$$
\begin{aligned}
H_{eff} &= \omega_r I_F^{(m)} + \omega_I I_F^{(n_1)} + \omega_S I_F^{(n_2)} \\
&+ \sum_{q=-1,q\neq 0}^{1} \begin{bmatrix} G^{(1)q}_{-1,1}(I) i \left[T^{(1)q}(I)\right]_{0,0} + G^{(1)q}_{1,-1}(I) i \left[T^{(1)q}(I)\right]_{0,0} + \\ \\ G^{(1)q}_{-1,1}(S) i \left[T^{(1)q}(S)\right]_{0,0} + G^{(1)q}_{1,-1}(S) i \left[T^{(1)q}(S)\right]_{0,0} \end{bmatrix} \\
&+ \sum_{q=\pm 2} \begin{bmatrix} G^{(2)q}_{2,-1,-1}(IS) \left[T^{(2)q}(IS)\right]_{2,-1,-1} + \\ \\ G^{(2)q}_{-2,1,1}(IS) \left[T^{(2)q}(IS)\right]_{-2,1,1} \end{bmatrix} \\
&+ \sum_{k=0}^{2} \begin{bmatrix} G^{(k)0}_{2,-1,-1}(IS) \left[T^{(k)0}(IS)\right]_{2,-1,-1} + \\ \\ G^{(k)0}_{-2,1,1}(IS) \left[T^{(k)0}(IS)\right]_{-2,1,1} \end{bmatrix}
\end{aligned}
\tag{3.13}
$$

A detailed description of the various matching conditions along with simulations is described in the following section.

3.3.2 Simulations

To illustrate the role of phase modulations in CP experiments, a set of simulations under different experimental conditions is presented in this section. In all the simulations presented, polarization transfer from ^{15}N to ^{13}C is calculated as a function of mixing time under constant spinning frequency and RF amplitudes. As described in the previous section, the dipolar Hamiltonian in the RF interaction frame depends on the magnitudes of the sample spinning frequency (ω_r) and the modulation frequencies employed on the two channels (say ω_I and ω_S). Based

on this description, in the absence of CSA interactions, the efficiency of transfer should depend only on the matching condition and be independent of the magnitude of the RF amplitudes employed on the two channels. This result is verified through a set of simulations depicted in Figure 3.2.

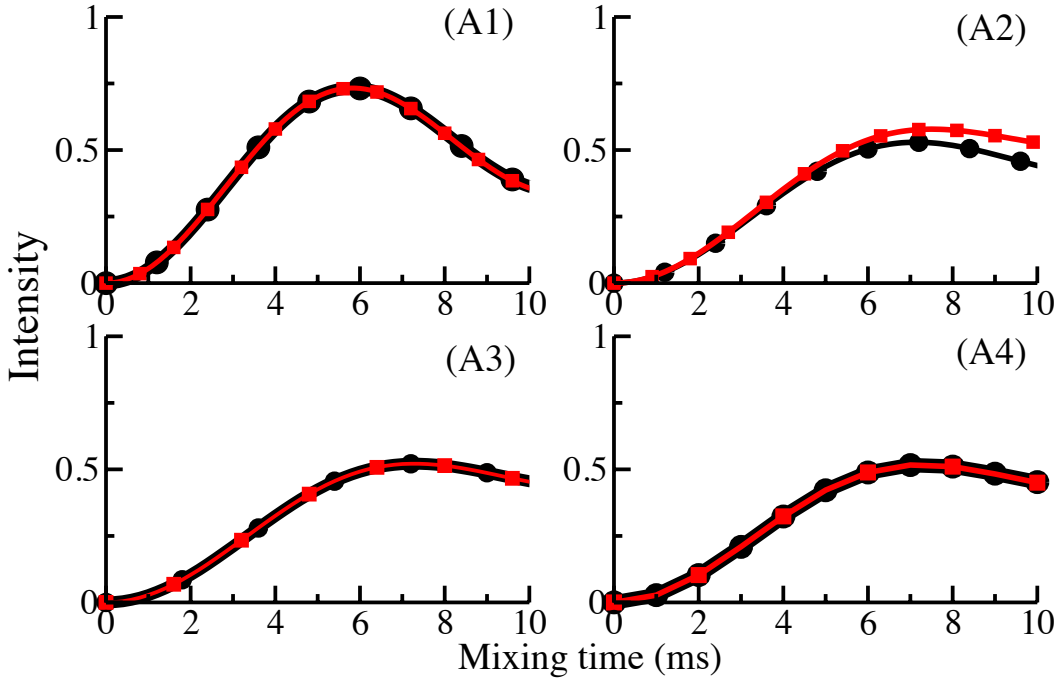

Figure 3.2: In the simulations presented, polarization transfer from ^{15}N to ^{13}C is calculated as a function of mixing time, τ_{mix}. The RF amplitudes employed correspond to the ZQ matching condition $\left|\upsilon_{\mathrm{RF},^{13}\mathrm{C}} - \upsilon_{\mathrm{RF},^{15}\mathrm{N}}\right| = \upsilon_r$. In all the panels, black corresponds to $\upsilon_r = 10$kHz, $\upsilon_{\mathrm{RF},^{13}\mathrm{C}} = 50$kHz, $\upsilon_{\mathrm{RF},^{15}\mathrm{N}} = 40$kHz, and red corresponds to $\upsilon_r = 10$kHz, $\upsilon_{\mathrm{RF},^{13}\mathrm{C}} = 30$kHz, $\upsilon_{\mathrm{RF},^{15}\mathrm{N}} = 20$kHz with variation in the modulation frequencies, (A1) $\omega_I = 0$, and $\omega_S = 0$ (CWCP), (A2) $\omega_I = \omega_r$, and $\omega_S = \omega_r$, (A3) $\omega_I = \frac{\omega_r}{2}$ and $\omega_S = \frac{\omega_r}{2}$, (A4) $\omega_I = \frac{\omega_r}{10}$ and $\omega_S = \frac{\omega_r}{10}$. The CSA interactions were ignored in the simulations and the dipolar coupling between the spins was set to 292 Hz ($r_{12} = 2.188\mathrm{A}^0$). The solid lines represent the simulations from SPINEVOLUTION[22], while the dots represent the analytic simulations.

For illustrative purposes, the simulations emerging from CW-CP experiments (see panel (A1)) are compared with PM-CP schemes employing modulation frequencies, ω_r panel (A2), $\frac{\omega_r}{2}$ panel (A3) and $\frac{\omega_r}{10}$ panel (A4). In the case of zero-quantum (ZQ) CW-CP experiments, the dipolar interactions are reintroduced

under MAS when the RF amplitudes are adjusted to satisfy one of the matching conditions given by the relation $\left|\omega_{RF,I} - \omega_{RF,S}\right| = \omega_r$ or $2\omega_r$. Interestingly, in the case of PM-CP experiments, the matching condition depends on both the RF amplitudes as well as the modulation frequencies. For example, in the case of ZQ PM-CP experiments, the matching condition in the RF interaction frame is governed by the relation, $m\omega_r + \omega_{RF,I} - \omega_{RF,S} + n_1\omega_I + n_2\omega_S$, while in the DQ version the matching condition is given by, $m\omega_r + \omega_{RF,I} + \omega_{RF,S} + n_1\omega_I + n_2\omega_S$. As depicted in Figure 3.2, the simulations emerging from our analytic theory (Eq. 2.26) are in excellent agreement with those emerging from exact numerical methods. In the absence of CSA interactions, the efficiency of transfer in PM-CP experiments is lower (0.5) than that of CW-CP experiments (0.7). This decrease in efficiency is attributed to the fact that the CW-CP experiment is γ encoded[23], whereas the PM-CP experiment in non-γ encoded (i.e. both the $m = 1$ and 2 components of the dipolar interaction are reintroduced under MAS).

The next stage in our study was to elucidate the role of CSA interactions in the exchange dynamics. In Figure 3.3 the effect of CSA interactions is illustrated through simulations depicting the polarization transfer fron ^{15}N to ^{13}C. The CSA parameters employed in the simulations correspond to the amine/amide nitrogens and aliphatic/aromatic carbon atoms encountered in a typical amino acid residue.

Although, the CSA matching conditions in the case of CW-CP experiments have been carefully avoided in the simulations, the efficiency of transfer decreases with increase in the magnitude of the CSA interactions. This decrease in efficiency is mainly due to the presence of longitudinal single-spin operators (refer to chapter-

2) resulting from second order cross-terms between the CSA interactions. By contrast, the CSA interactions in the case of PM-CP experiments seem to have a profound role in the exchange dynamics. As depicted in Figure 3.3 (panel (A2)), the efficiency of transfer decreases drastically when the magnitude of the modulation frequency is equal to the sample spinning frequency. This decrease in efficiency is due to the reintroduction of CSA interactions in the exchange dynamics and could be explained based on the analytic theory presented in the previous section. In the RF interaction frame, the CSA interactions in PM-CP experiments are introduced to first-order when the RF amplitudes and modulation frequencies satisfy one of the matching conditions i.e. $m\omega_r + \omega_{RF,I} + n_1\omega_I$. In the PM-CP schemes depicted in Figure 3.2 (see panels (A2), (A3) and (A4)), the CSA interactions are reintroduced to first order and are primarily responsible for the decrease in the efficiency of transfer. When the magnitude of the modulation frequency is comparable to the sample spinning frequency (see panel A2), the efficiency of transfer decreases drastically. At lower modulation frequencies (panels A3, A4), the scaling factor asssociated with the CSA Hamiltonian is reduced resulting in better transfer of polarization. As depicted, in the higher CSA regimes, the drop in efficiency is significant in all the four panels.

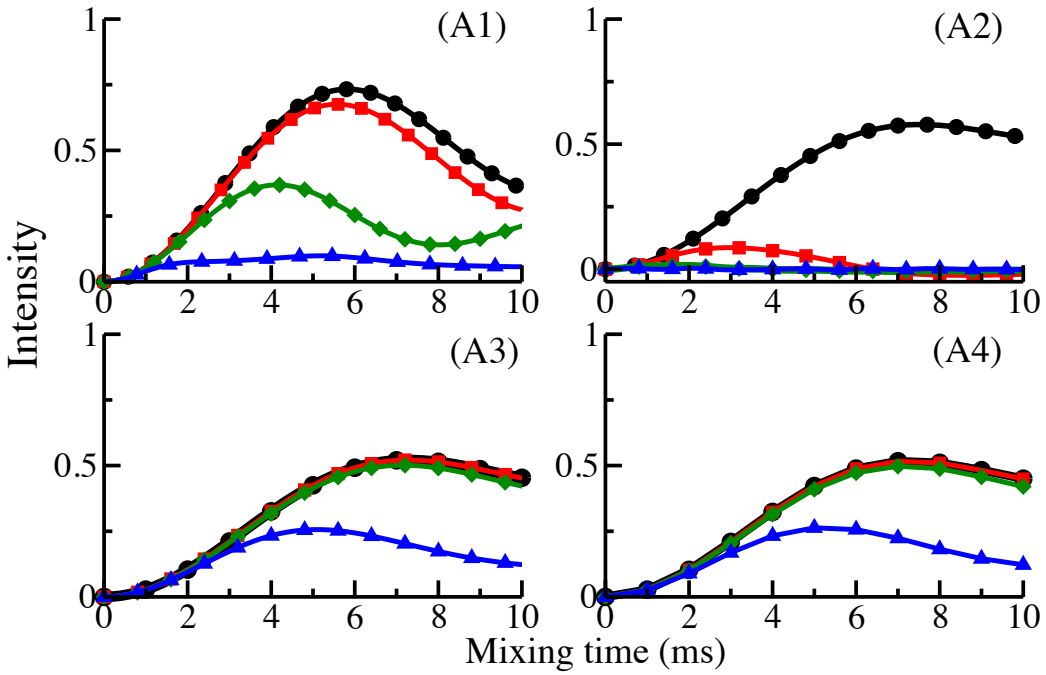

Figure 3.3: In the simulations presented, polarization transfer from ^{15}N to ^{13}C is calculated as a function of mixing time, τ_{mix}. The RF amplitudes employed correspond to the ZQ matching condition $\left|\upsilon_{\mathrm{RF},^{13}\mathrm{C}} - \upsilon_{\mathrm{RF},^{15}\mathrm{N}}\right| = \upsilon_r$. In all the panels, υ_r = 10kHz, $\upsilon_{\mathrm{RF},^{13}\mathrm{C}}$ = 50kHz, $\upsilon_{\mathrm{RF},^{15}\mathrm{N}}$ = 40kHz, with variation in the modulation frequencies, (A1) $\omega_I = 0$, and $\omega_S = 0$ (CWCP) (A2) $\omega_I = \omega_r$, and $\omega_S = \omega_r$, (A3) $\omega_I = \frac{\omega_r}{2}$ and $\omega_S = \frac{\omega_r}{2}$, (A4) $\omega_I = \frac{\omega_r}{10}$ and $\omega_S = \frac{\omega_r}{10}$. The following chemical shift parameters were employed in the simulations: black $\eta_C = 0.0, \delta_C = 0.0$ppm; $\eta_N = 0.0, \delta_N = 0.0$ppm, red $\eta_C = 0.98, \delta_C = 19.4$ppm; $\eta_N = 0.17, \delta_N = 10.1$ppm, green $\eta_C = 0.98, \delta_C = 19.4$ppm; $\eta_N = 0.17, \delta_N = 99$ppm, blue $\eta_C = 0.98, \delta_C = -76$ppm; $\eta_N = 0.17, \delta_N = 99$ppm. The following orientation parameters were employed for the CSA interactions in the simulations: $\alpha_{PM}^{(C)} = 64.9^0, \beta_{PM}^{(C)} = 37.5^0, \gamma_{PM}^{(C)} = -28.8^0$; $\alpha_{PM}^{(N)} = -83.3^0, \beta_{PM}^{(N)} = -79.0^0, \gamma_{PM}^{(N)} = 0.0^0$. The dipolar coupling between the spins was set to 292 Hz ($r_{12} = 2.188\mathrm{A}^0$). The solid lines represent the simulations from SPINEVOLUTION[22], while the dots represent the analytic simulations.

To minimize the role of CSA interactions, implementation of CP experiments at faster spinning frequencies seem mandatory. From an experimental aspect, this is accomplished when the amplitudes of the RF fields employed on the two channels are phase-shifted by 180^0 (see Figure 3.1, panel (B)). As depicted in Figure 3.4, the efficiency of transfer decreases in both CW (panel A1) and PM-CP (panels A2, A3) with the inclusion of the CSA interactions. In contrast to

CW-CP experiment, the depolarization effects due to CSA interactions are quite significant in the PM-CP schemes depicted in panels A2 and A3. At the outset, this result seems intriguing considering the observation that the CSA interactions remain unaveraged even at faster spinning frequencies (say 50 kHz).

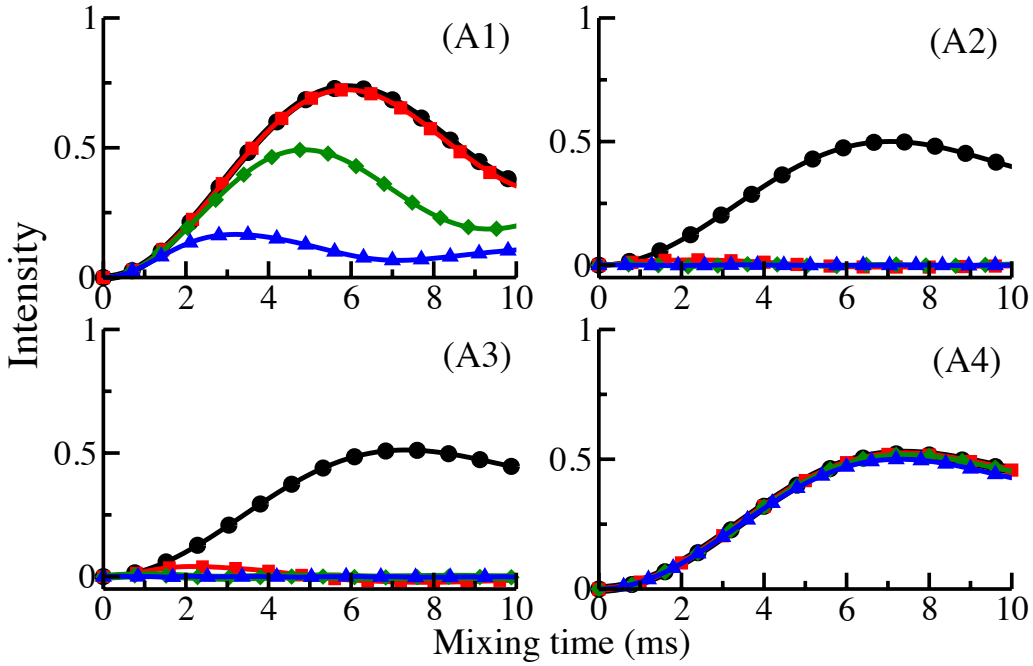

Figure 3.4: In the simulations presented, polarization transfer from ^{15}N to ^{13}C is calculated as a function of mixing time, τ_{mix}. The RF amplitudes employed correspond to the ZQ matching condition $\left|\upsilon_{\mathrm{RF},^{13}\mathrm{C}} - \upsilon_{\mathrm{RF},^{15}\mathrm{N}}\right| = \upsilon_r$. In all the panels, $\upsilon_r = 50$kHz, $\upsilon_{\mathrm{RF},^{13}\mathrm{C}} = 20$kHz, $\upsilon_{\mathrm{RF},^{15}\mathrm{N}} = 30$kHz, with variation in the modulation frequencies, (A1) $\omega_I = 0$, and $\omega_S = 0$ (CWCP) (A2) $\omega_I = \omega_r$, and $\omega_S = \omega_r$, (A3) $\omega_I = \frac{\omega_r}{2}$ and $\omega_S = \frac{\omega_r}{2}$, (A4) $\omega_I = \frac{\omega_r}{10}$ and $\omega_S = \frac{\omega_r}{10}$. The following chemical shift parameters were employed in the simulations: black $\eta_C = 0.0, \delta_C = 0.0$ppm; $\eta_N = 0.0, \delta_N = 0.0$ppm, red $\eta_C = 0.98, \delta_C = 19.4$ppm; $\eta_N = 0.17, \delta_N = 10.1$ppm, green $\eta_C = 0.98, \delta_C = 19.4$ppm; $\eta_N = 0.17, \delta_N = 99$ppm, blue $\eta_C = 0.98, \delta_C = -76$ppm; $\eta_N = 0.17, \delta_N = 99$ppm. The Euler angles and dipolar coupling employed correspond to those used in fig. 3.3. The solid lines represent the simulations from SPINEVOLUTION[22], while the dots represent the analytic simulations.

Since biophysical applications of ssNMR entail the availability of higher magnetic field strengths (for improved resolution), minimizing the role of CSA interactions is very essential in enhancing the overall polarization transfer in CP

experiments. Interestingly, the efficiency of polarization transfer in the simulations depicted in panel A4 remains unaffected in the presence of CSA interactions. This observation (through numerical simulations) could be explained by a comparison of the various coefficients present in effective Hamiltonian depicted in Eq. 3.13. When the modulation frequency is much lower than the sample spinning frequency (see panel A4), the CSA contributions in the effective Hamiltonian (Eq. 3.13) are scaled significantly (higher order Bessel functions), resulting in enhanced efficiency of polarization transfer. However, as the modulation frequency of the multiple-pulse scheme increases and competes with the sample spinning frequency (see panels A2, A3), the depolarization effects due to the recoupled CSA interactions become prominent (higher scaling factors) and are primarily responsible for the poor transfer efficiencies observed in the simulations. Hence, to maximize the efficiency of polarization transfer in CP experiments (at faster spinning freqeuncies), the modulation frequencies employed on the two channels have to be much smaller in comparison to the sample spinning frequency. This principle could be employed in the design of the cycle times in multiple pulse schemes and could be employed as an optimization procedure in the design of MAS experiments at faster spinning frequencies.

3.4 Conclusions

In summary, the analytic framework describing the effects of multiple-pulses in ssNMR experiments yields results in agreement with simulations emerging from exact numerical methods. In the rotating frame, the Fourier series expansion of

the RF interaction seems to be an attractive approach towards the derivation of effective Hamiltonians in the RF interaction frame. In contrast to the AHT approach, the framework presented in this chapter does not impose any restrictions on the choice of the cycle time of a typical multiple pulse scheme. We believe that the Fourier decomposition of the RF Hamiltonian in the rotating frame could be quite handful in the derivation of effective Hamiltonians in schemes that employ adiabatic and RAMP modulations of the RF fields. In contrast to constant amplitude CW-CP experiments, the phase-alternated PM-CP experiment seems to be a better alternative for improving the efficiency of polarization transfer at higher magnetic field strengths and faster spinning frequencies. In systems with larger chemical shift anisotropies, implementation of PM-CP depends on (a) the RF amplitudes (b) spinning frequency and (c) modulation frequency. The methodology presented in this chapter is quite general and could be extended for studying experiments that employ both phase as well as amplitude modulations.

References

[1] J. H. Shirley, *Phys. Rev. B*, 1965, **4**, 979.

[2] U. Haeberlen and J. S. Waugh, *Phys. Rev.*, 1968, **175**, 453–467.

[3] U. Haeberlen, *High-Resolution NMR in Solids: Selective Averaging*, Academic, New York, 1976.

[4] W. Magnus, *Comm. Pure Appl. Math.*, 1954, **7**, 649–673.

[5] M. Mehring, *Principles of High Resolution NMR in Solids*, Springer Verlag, Berlin, 1999.

[6] M. H. Levitt, *Encyclopedia of NMR*, 2002, **9**, 165.

[7] S. Hediger, B. Meier and R. Ernst, *Chem. Phys. Lett.*, 1993, **213**, 627 – 635.

[8] S. Hediger, B. H. Meier and R. R. Ernst, *J. Chem. Phys.*, 1995, **102**, 4000–4011.

[9] S. Hediger, B. Meier and R. Ernst, *Chem. Phys. Lett.*, 1995, **240**, 449 – 456.

[10] M. Bjerring and N. C. Nielsen, *Chem. Phys. Lett.*, 2003, **382**, 671 – 678.

[11] S. V. Dvinskikh, V. Castro and D. Sandstrom, *Phys. Chem. Chem. Phys.*, 2005, **7**, 3255–3257.

[12] T. M. Barbara and E. H. Williams, *J. Magn. Reson. (1969)*, 1992, **99**, 439 – 442.

[13] X. Wu and K. Zilm, *J. Magn. Reson., Series A*, 1993, **104**, 154 – 165.

[14] O. Peersen, X. Wu, I. Kustanovich and S. Smith, *J. Magn. Reson., Series A*, 1993, **104**, 334 – 339.

[15] O. Peersen, X. Wu and S. Smith, *J. Magn. Reson., Series A*, 1994, **106**, 127 – 131.

[16] A. C. Kolbert and S. L. Gann, *Chem. Phys. Lett.*, 1994, **224**, 86 – 90.

[17] R. Pratima and K. Ramanathan, *Chem. Phys. Lett.*, 1994, **221**, 322 – 326.

[18] H. Geen, J. J. Titman and H. W. Spiess, *Chem. Phys. Lett.*, 1993, **213**, 145 – 152.

[19] R. Ramachandran and R. G. Griffin, *J. Chem. Phys.*, 2005, **122**, 164502.

[20] J. Herzfeld and A. E. Berger, *J. Chem. Phys.*, 1980, **73**, 6021–6030.

[21] E. Kreyszig, *Advanced Engineering Mathematics*, John Wiley and Sons, 9th edn, 2006.

[22] M. Veshtort and R. G. Griffin, *J. Magn. Reson.*, 2006, **178**, 248 – 282.

[23] N. C. Nielsen, H. Bildsoe, H. J. Jakobsen and M. H. Levitt, *J. Chem. Phys.*, 1994, **101**, 1805–1812.

Chapter 4

Understanding Multispin effects in Cross-Polarization (CP) NMR experiments through Dipolar Truncation

4.1 Background

Understanding the mechanism of polarization transfer among nuclear spins remains an exciting area of research[1–3], primarily due to its utility in design and interpretation of NMR experiments/experimental data. Although, measurements in NMR are made in bulk, the underlying theory routinely employed to describe/interpret experiments, often comprises of finite number of spins. In general, analytic description of polarization transfer in a strongly coupled spin system is complicated due to the presence of non-commuting Hamiltonians in the system. From an experimental view-point, quantifying polarization transfer in strongly coupled systems is hindered owing to the co-existence of stronger and weaker couplings in the system. Consequently, polarization transfer to weakly coupled spins is diminished by the influence of other stronger couplings in the system, a phenomenon commonly referred to as dipolar truncation[4] in NMR. Hence, analytic

treatments based on isolated spin-pair models yield ambiguous results and are of limited utility in the weak-coupling regime. To this end, thermodynamic models[5] based on the concept of spin temperature[3,6] have also been invoked in the past to explain the experimental observations in CP experiments.

As an alternative to existing methods, an analytic model built on the concept of "dipolar truncation" is proposed to explain the propagation of spin polarization in CP experiments.

4.2 Definition of the Problem

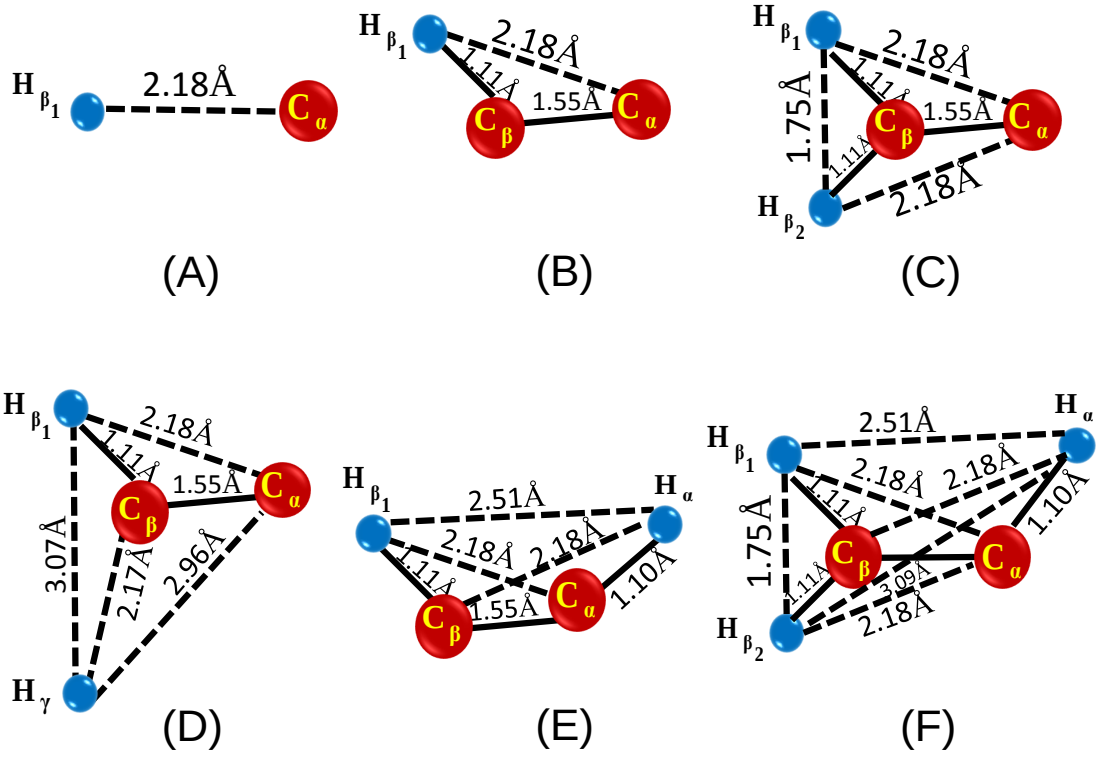

Figure 4.1: Model systems employed for describing the polarization transfer in CP experiments.

To describe the propagation of spin polarization from $^{1}H \rightarrow {}^{13}C$ in CP experi-

ment, a pedagogical description comprising of two ($C_\alpha H_{\beta_1}$), three ($C_\alpha C_\beta H_{\beta_1}$), four ($C_\alpha C_\beta H_{\beta_1} H_{\beta_2}$; $C_\alpha C_\beta H_{\beta_1} H_\gamma$; $C_\alpha H_\alpha C_\beta H_{\beta_1}$) and five ($C_\alpha H_\alpha C_\beta H_{\beta_1} H_{\beta_2}$) spin model systems is employed (See Figure 4.1. Since the $^{13}C-^1H$, $^1H-^1H$ dipolar coupling constants in the chosen model systems are prototypes of the coupling constants prevalent in typical amino acid residues/peptides, we believe that the current study would improve our understanding of the mechanism of polarization transfer among spins in ssNMR experiments.

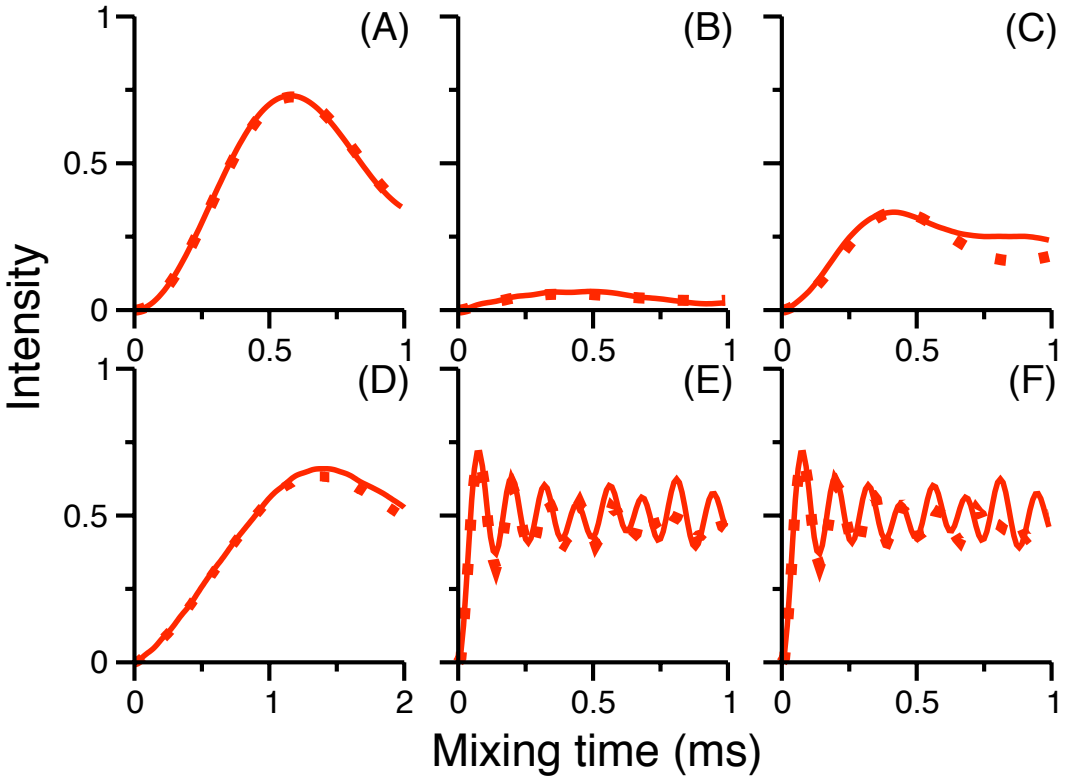

Figure 4.2: CP Simulations depicting the polarization transfer to C_α in the model systems presented in Figure 4.1. The RF amplitudes correspond to $\upsilon_{RF,S} = 40$kHz, $\upsilon_{RF,I} = 20$kHz and the phases shifted by 180^0. All the simulations were performed at $\upsilon_r = 60$kHz . The solid lines correspond to analytic simulations, while dots represent numerical simulations (6044 angle-sets) based on SPINEVOLUTION.[7]

To begin with, numerical simulations (based on SPINEVOLUTION[7]) depict-

ing polarization transfer from $^{1}H \rightarrow ^{13}C$ in first-order CP experiments are presented in Figure 4.2. To facilitate the implementation of experiments at faster spinning frequencies (for better resolution), the amplitudes of the RF fields employed in the simulations were adjusted to satisfy the ZQ matching condition $\left|\upsilon_{RF,S} - \upsilon_{RF,I}\right| = \upsilon_r$, i.e. $(\upsilon_r = 60kHz, \upsilon_{RF,I} = 20kHz, \upsilon_{RF,S} = 40kHz)$ and are phase shifted by 180^0 (i.e. the signs of the amplitudes differ in the rotating frame). To explain the nuances of polarization transfer in first-order based CP experiments, we begin our discussion with the profiles depicted in panels B and C (Figure 4.2). As depicted, polarization transfer to $^{13}C_\alpha$ in the three-spin system $C_\alpha C_\beta H_{\beta_1}$ (see panel B) is diminished significantly in contrast to the isolated spin pair system (panel A). This decrease in the CP efficiency is attributed to the presence of the stronger $C_\beta - H_{\beta_1}$ dipolar coupling and is commonly referred to as dipolar truncation[4] in ssNMR. Interestingly, inclusion of an additional proton to the beta carbon (C_β) (four spin model, Figure 4.1(C)) improves the overall transfer efficiency to C_α (see Figure 4.2(C)). This result seems counter-intuitive in view of the fact that the model three-spin system, $C_\alpha C_\beta H_{\beta_1}$ (Figure 4.1(B)) comprises of fewer stronger couplings ($C_\beta - H_{\beta_1}$) in comparison to the four-spin model $C_\alpha C_\beta H_{\beta_1} H_{\beta_2}$ (stronger couplings in the form of $C_\beta - H_{\beta_1}$ and $C_\beta - H_{\beta_2}$). Hence, an analytic theory is essential for understanding the mode of polarization transfer from multiple spin sites (say ^{1}H) to the desired target spin (say ^{13}C) in strongly coupled systems.

4.3 Discussion

4.3.1 Theory

To elucidate the mechanism of polarization transfer in CP-MAS experiments, a model system ($I_N S_M$) comprising of N-carbons ($I = ^{13}$ C) and M-protons ($S = ^{1}$ H) is employed. Under sample rotation, the nuclear spin Hamiltonian is time-dependent,[8] and is conveniently expressed in the rf interaction frame in terms of single-spin and two-spin interactions.

$$H(t) = \sum_{\lambda=I,S} H_\lambda(t) + H_{IS}(t) + H_{RF} \tag{4.1}$$

As discussed earlier, the single-spin Hamiltonian depicts both the isotropic and anisotropic chemical shift interactions and is expressed in terms of single-quantum (SQ) operators.

$$\begin{aligned}\tilde{H}_{Single}(t) = &- \tfrac{1}{\sqrt{2}} \cdot \left(\sqrt{2}\right)^{N+M-2} \\ &\sum_{m=-2}^{2} \sum_{i=1}^{N} \omega_{I_i}^{(m)} \left[\begin{array}{l} iT^{(1)1}(I_i) \exp\left(i\left[m\omega_r + \omega_{RF,I}\right]t\right) \\ \\ -iT^{(1)-1}(I_i) \exp\left(i\left[m\omega_r - \omega_{RF,I}\right]t\right) \end{array} \right]\end{aligned} \tag{4.2}$$

In a similar vein, the two-spin interactions comprising of Homonuclear and Heteronuclear dipolar interactions are expressed in terms of zero-quantum (ZQ) and double-quantum (DQ) operators.

$$\tilde{H}^{(DQ)}_{Hetero}(t) = -\tfrac{1}{2}\Big(\sqrt{2}\Big)^{N+M-2}$$
$$\sum_{i=1}^{N}\sum_{j=1}^{M}\sum_{\substack{m=-2,\\ m\neq 0}}^{2}\omega^{(m)}_{I_iS_j}\left[\begin{array}{l} T^{(2)2}(I_iS_j)\exp\left(i\left[\begin{array}{l} m\omega_r+\\ (\omega_{RF,I}+\omega_{RF,S})\end{array}\right]t\right)\\ +\\ T^{(2)-2}(I_iS_j)\exp\left(i\left[\begin{array}{l} m\omega_r-\\ (\omega_{RF,I}+\omega_{RF,S})\end{array}\right]t\right)\end{array}\right] \tag{4.3a}$$

$$\tilde{H}^{(ZQ)}_{Hetero}(t) = \big(\sqrt{2}\big)^{N+M-2}$$
$$\sum_{i=1}^{N}\sum_{j=1}^{M}\sum_{\substack{m=-2,\\ m\neq 0}}^{2}\tfrac{1}{2}\omega^{(m)}_{I_iS_j}\left[\begin{array}{l} \left[\begin{array}{l} \frac{1}{\sqrt{3}}T^{(0)0}(I_iS_j)\\ +\frac{1}{\sqrt{2}}T^{(1)0}(I_iS_j)\\ +\frac{1}{\sqrt{6}}T^{(2)0}(I_iS_j)\end{array}\right]*\\ \exp\left(i\left[\begin{array}{l} m\omega_r+\\ (\omega_{RF,I}-\omega_{RF,S})\end{array}\right]t\right)\\ +\\ \left[\begin{array}{l} \frac{1}{\sqrt{3}}T^{(0)0}(I_iS_j)\\ -\frac{1}{\sqrt{2}}T^{(1)0}(I_iS_j)\\ +\frac{1}{\sqrt{6}}T^{(2)0}(I_iS_j)\end{array}\right]*\\ \exp\left(i\left[\begin{array}{l} m\omega_r-\\ (\omega_{RF,I}-\omega_{RF,S})\end{array}\right]t\right)\end{array}\right] \tag{4.3b}$$

$$\tilde{H}^{DQ}_{Homo}(t) = -\tfrac{3}{4}.\Big(\sqrt{2}\Big)^{N+M-2}$$
$$\sum_{\substack{i,j=1\\ i<j}}^{N}\sum_{\substack{m=-2,\\ m\neq 0}}^{2}\omega^{(m)}_{I_iI_j}\left[\begin{array}{l} T^{(2)2}(I_iI_j)\exp\left(i\left[m\omega_r+2.\omega_{RF,I}\right]t\right)+\\ T^{(2)-2}(I_iI_j)\exp\left(i\left[m\omega_r-2.\omega_{RF,I}\right]t\right)\end{array}\right] \tag{4.4a}$$

$$\tilde{H}^{(ZQ)}_{Homo}(t) = \sqrt{\frac{3}{8}}.\Big(\sqrt{2}\Big)^{N+M-2}\sum_{\substack{i,j=1\\ i<j}}^{N}\sum_{\substack{m=-2,\\ m\neq 0}}^{2}\omega^{(m)}_{I_iI_j}T^{(2)0}(I_iI_j)\exp\left(im\omega_r t\right) \tag{4.4b}$$

Following the description in chapter-2, the corresponding Floquet Hamiltonian

for the above model system is derived.

$$H_F^{(I)} = \sum_{m,n_1}\sum_{i=1}^{N}\sum_{q=-1,q\neq 0}^{1} G_{m,n_1}^{(1)q}(I_i) iT_{m,n_1}^{(1)q}(I_i) + \sum_{\substack{i,j=1,\\ i<j}}^{N}\sum_{m,n_1}\sum_{k=0}^{2}\sum_{q=-k}^{k}\left[G_{m,n_1}^{(k)q}(I_iI_j)T_{m,n_1}^{(k)q}(I_iI_j)\right] \tag{4.5a}$$

$$H_F^{(S)} = \sum_{m,n_2}\sum_{i=1}^{M}\sum_{q=-1,q\neq 0}^{1} G_{m,n_1}^{(1)q}(S_i) iT_{m,n_2}^{(1)q}(S_i) + \sum_{\substack{i,j=1,\\ i<j}}^{M}\sum_{m,n_2}\sum_{k=0}^{2}\sum_{q=-k}^{k}\left[G_{m,n_2}^{(k)q}(S_iS_j)T_{m,n_2}^{(k)q}(S_iS_j)\right] \tag{4.5b}$$

$$H_F^{(IS)} = \sum_{m,n_1,n_2}\sum_{i=1}^{N}\sum_{j=1}^{M}\sum_{k=0}^{2}\sum_{q=-k}^{k}\left[G_{m,n_1,n_2}^{(k)q}(I_iS_j)T_{m,n_1,n_2}^{(k)q}(I_iS_j)\right] \tag{4.5c}$$

The 'G' coefficients in Eq. 4.5 could be deduced from the coefficients described in Eqns (4.2 - 4.4) inclusive of the numerical constants and are similar to our earlier descriptions in chapter-2.

4.3.2 Effective Floquet Hamiltonians for first-order and second-order CP experiments

As mentioned in the previous chapter, when the amplitudes of the RF fields are adjusted to one of the matching conditions[9–11] ($|\upsilon_{RF,S} \pm \upsilon_{RF,I}| = \upsilon_r$ or $2\upsilon_r$), a part of the two-spin Hamiltonian (refer to Eq. (4.3)) becomes time-independent under MAS conditions (commonly referred to as 'recoupled Hamiltonian') . In such cases, the recoupled Hamiltonian is included as a diagonal contribution[12,13] along H_1 and the transformation function is carefully chosen only to compensate the

off-diagonal contributions in H_1. The second-order corrections ($H_2^{(1)}$) to the zero-order Hamiltonian comprises of single-spin, two-spin and three-spin operators. For a given system, the single-spin operators (to second-order) result from cross-terms between (a) single-spin operators (say CSA X CSA) (b) two-spin operators associated with the same spin pair. The cross-terms between single-spin and two-spin operators in (CSA X dipolar interactions) result in two-spin operators. The cross-terms between different pairs of dipolar interactions (with at least one-spin being common) result in three-spin operators. A detailed description of the second-order contributions is summarized in Table 4.1 (Appendix-4), along with a generalization to N-coupled spin ($I = 1/2$) systems.

Employing the results summarized in Table 4.1(Appendix-4), the first-order contribution to the effective Hamiltonian in CP experiments is expressed in terms of two-spin operators.

$$H_1^{(1)} = H_{1,dia} = \underbrace{\sum_{i=1}^{N}\sum_{j=1}^{M}\sum_{k=0}^{2} A^{(k)0}(I_iS_j)T^{(k)0}(I_iS_j)}_{\text{Two-Spin}} \tag{4.6}$$

In a similar vein, the second-order contributions are composed of single spin and three-spin operators as represented below

$$H_2^{(1)} = \underbrace{\sum_{\lambda=I,S}\sum_{i} B^{(1)0}(\lambda_i).iT^{(1)0}(\lambda_i)}_{\text{Single-spin}} + \underbrace{\sum_{i}^{N}\sum_{\substack{r,j=1\\ j<r}}^{M} B_1^{(k)0}(I_iS_jS_r)T^{(k)0}(I_iS_jS_r) + \sum_{\substack{i,j=1\\ i<j}}^{N}\sum_{r=1}^{M} B_1^{(k)0}(I_iI_jS_r)T^{(k)0}(I_iI_jS_r)}_{\text{Three-Spin}} \tag{4.7}$$

Based on Eq. 2.24, the effective Hamiltonian describing first-order CP experiments

is represented by

$$H_F^{eff} = H_0^{(1)} + H_1^{(1)} + H_2^{(1)} \tag{4.8}$$

Depending on the choice of the model spin systems, the number of operators increases in the effective Hamiltonian framework. Consequently, descriptions based on the effective Hamiltonian approach are less suited for studying polarization transfer among strongly coupled spin systems. To alleviate this problem, an alternate approach in the form of "truncated effective Hamiltonians" employing fewer operators is proposed in the following section.

4.3.3 Concept of Truncated Effective Hamiltonians

To describe the mechanism of polarization transfer in strongly coupled systems, the effective Hamiltonians derived in the previous section are restructured based on the phenomenon of dipolar truncation. Employing this approach, truncated effective Hamiltonians are proposed by retaining only the dominant contributions in the effective Hamiltonians. Although, such an approach facilitates the description in the Floquet state-space, the validity of such approximations could only be verified through a comparison between analytic simulations emerging from the truncated Hamiltonians and the exact numerical simulations comprising of the entire spin system of interest. Employing the model systems depicted in Figure 4.1, truncated effective Hamiltonians are proposed for describing the polarization transfer observed in first-order and second-order CP experiments.

First-order CP experiments

As illustrated through the simulations depicted in Figure 4.2(B), the stronger dipolar interaction due to $C_\beta - H_{\beta_1}$ ($\omega_{C_\beta H_{\beta 1}}$) truncates the polarization transfer to C_α (i.e. $\omega_{C_\beta H_{\beta 1}} > \omega_{C_\alpha H_{\beta 1}}$) in the three-spin system $C_\alpha C_\beta H_{\beta_1}$. Consequently, a truncated effective Hamiltonian (in the form $H^{(eff)T}_{F,Three}$) comprising of $T^{(k)0}(C_\beta H_{\beta_1})$ and single-spin operators $T^{(1)0}(C_\beta), T^{(1)0}(H_{\beta_1})$ is proposed for describing the polarization transfer observed in $C_\alpha C_\beta H_{\beta_1}$ (Figure 4.1(B)). Due to the smaller magnitude of the second-order coefficients (see Table 4.1), the contributions from the three-spin operators are neglected and the truncated effective Hamiltonian comprises only of single-spin and two-spin operators:

$$H^{(eff)T}_{F,Three,C_\beta} = \sum_{k=0}^{2} A^{(k)0}(C_\beta H_{\beta_1}) T^{(k)0}(C_\beta H_{\beta_1}) + \sum_{\lambda = C_\beta, H_{\beta_1}} B^{(1)0}(\lambda).iT^{(1)0}(\lambda) \quad (4.9)$$

Such approximations simplify the description in the Floquet-state space and result in analytic expressions similar to those derived in chapter-2. To test the validity of this approach, analytic simulations based on Eq. 4.9 depicting polarization transfer from H_β to C_α and C_β in the model three-spin system $C_\alpha C_\beta H_{\beta_1}$ are compared in Figure 4.3 with exact numerical simulations (inclusive of all three-spins). For illustrative purposes, the analytic simulations emerging from truncated (panel B1) Hamiltonian is compared with exact numerical simulations. In contrast to the effective Hamiltonian approach, polarization transfer to C_β (depicted in panel B1) is simulated within a reduced subspace comprising of spins C_β and H_{β_1}. Hence, the truncated effective Hamiltonian approach provides an alternate framework

for describing the dipolar truncation effect observed in $C_\alpha C_\beta H_{\beta_1}$. To explain the enhanced polarization transfer observed in $C_\alpha C_\beta H_{\beta_1} H_{\beta_2}$(see Figure 4.2(C)), we propose a model, wherein, polarization transfer to C_β results from only one of the protons, say H_{β_1} in $C_\alpha C_\beta H_{\beta_1} H_{\beta_2}$. Consequently, the polarization from H_{β_2} is readily transferred to C_α without the destructive influence of the stronger $C_\beta - H_{\beta_2}$ dipolar coupling. Based on this model, the truncated effective Hamiltonians describing polarization transfer to C_β and C_α is derived and represented by

$$H^{(eff)T}_{F,Four,C_\beta} = \sum_{k=0}^{2} A^{(k)0}(C_\beta H_{\beta_1}) T^{(k)0}(C_\beta H_{\beta_1}) + \sum_{\lambda=C_\beta,H_{\beta_1}} B^{(1)0}(\lambda).iT^{(1)0}(\lambda) \quad (4.10)$$

$$H^{(eff)T}_{F,Four,C_\alpha} = \sum_{k=0}^{2} A^{(k)0}(C_\alpha H_{\beta_2}) T^{(k)0}(C_\alpha H_{\beta_2}) + \sum_{\lambda=C_\alpha,H_{\beta_2}} B^{(1)0}(\lambda).iT^{(1)0}(\lambda) \quad (4.11)$$

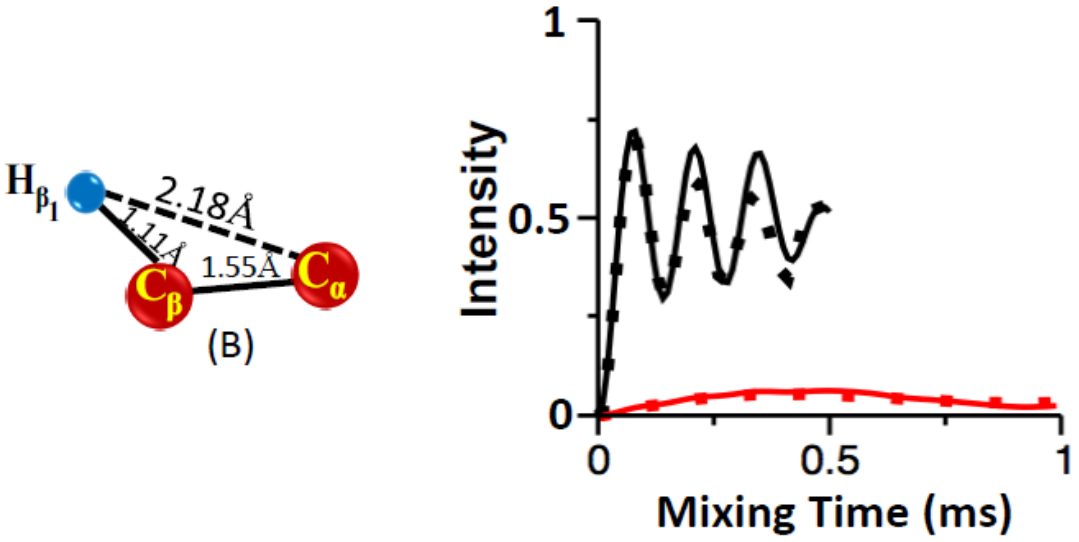

Figure 4.3: Simulations depicting the polarization transfer to C_α (red) and C_β (black) in the model three-spin system ($C_\alpha C_\beta H_{\beta_1}$). The analytic simulations from truncated Hamiltonian are compared with the numerical simulations (indicated by dots).

In a similar vein, the stronger coupling in the form of $C_\beta - H_{\beta_1}(\omega_{C_\beta H_{\beta 1}})$ truncates the $C_\beta - H_\gamma$ dipolar coupling in $C_\alpha C_\beta H_{\beta_1} H_\gamma$ (Figure 4.1(D)) and facilitates

the propagation of spin polarization to C_α. Hence, based on the truncated effective Hamiltonian approach, polarization transfer to C_β and C_α in the model four-spin system $C_\alpha C_\beta H_{\beta_1} H_\gamma$, should result primarily from H_{β_1} ($H_{\beta_1} \rightarrow C_\beta$ through $T^{(k)0}(C_\beta H_{\beta_1})$) and H_γ ($H_\gamma \rightarrow C_\alpha$ through $T^{(k)0}(C_\alpha H_\gamma)$), respectively.

To verify the validity of the proposed models based on truncated effective Hamiltonians, analytic simulations emerging from truncated Hamiltonians are compared with exact numerical simulations. Since the truncated effective Hamiltonians comprise of only single-spin and two-spin operators, the polarization transfer to the desired spin in the Floquet-state space is conveniently described using the analytic expressions derived in chapter-2 (see Eq. 2.26). In contrast to the Floquet-operator space approach, the analytic expressions in the Floquet-state space are computationally less intensive and could be beneficial in the fitting of experimental trajectories involving multiple fit parameters. In Figure 4.4, polarization transfer to C_α in $C_\alpha C_\beta H_{\beta_1} H_{\beta_2}$ is calculated from the truncated effective Hamiltonian and compared with exact numerical methods (indicated by dots). As depicted (in Figure 4.4), the analytic simulations emerging from the truncated effective Hamiltonians (comprising of C_α and H_{β_2}) are in good agreement with the four-spin numerical simulations in $C_\alpha C_\beta H_{\beta_1} H_{\beta_2}$. Hence, the truncation effect imposed by the stronger $C_\beta - H_{\beta_1}$ coupling on $C_\beta - H_{\beta_2}$, indirectly influences (facilitates) the transfer of polarization from H_{β_2} to C_α in $C_\alpha C_\beta H_{\beta_1} H_{\beta_2}$. While the efficiency of transfer from $H_{\beta_2} \rightarrow C_\alpha$ in $C_\alpha C_\beta H_{\beta_1} H_{\beta_2}$ is higher in contrast to the three-spin simulations depicted in Figure 4.1(B), it is still diminished in comparison to the simulations depicting polarization transfer in an isolated spin pair

(see Figure 4.2(A)). This reduction in efficiency is attributed to the influence of the passive spin H_{β_1} through the $H_{\beta_1} - H_{\beta_2}$ dipolar coupling in $C_\alpha C_\beta H_{\beta_1} H_{\beta_2}$. Although, matching conditions (say $\omega_{RF,S} = \frac{1}{2}\omega_r$) corresponding to the reintroduction of $H_{\beta_1} - H_{\beta_2}$ dipolar interactions are avoided in CP-MAS experiments, their manifestations through second-order cross-terms are inevitable in strongly coupled systems. As summarized in Table 4.2, second-order cross-terms between the $^1H-^1H$ dipolar interactions ($H_{H_{\beta 1}-H_{\beta 2}} \times H_{H_{\beta 1}-H_{\beta 2}}$) result in longitudinal single-spin operators $T^{(1)0}(H_{\beta_1})$ and have been incorporated in the truncated effective Hamiltonians (Eqns (4.7- 4.8)) for better agreements with exact numerical simulations. Hence, the truncated effective Hamiltonian approach provides an adequate framework for the inclusion of both passive and active spins in a reduced subspace within the Floquet-state space. In general, depending on the magnitude of the

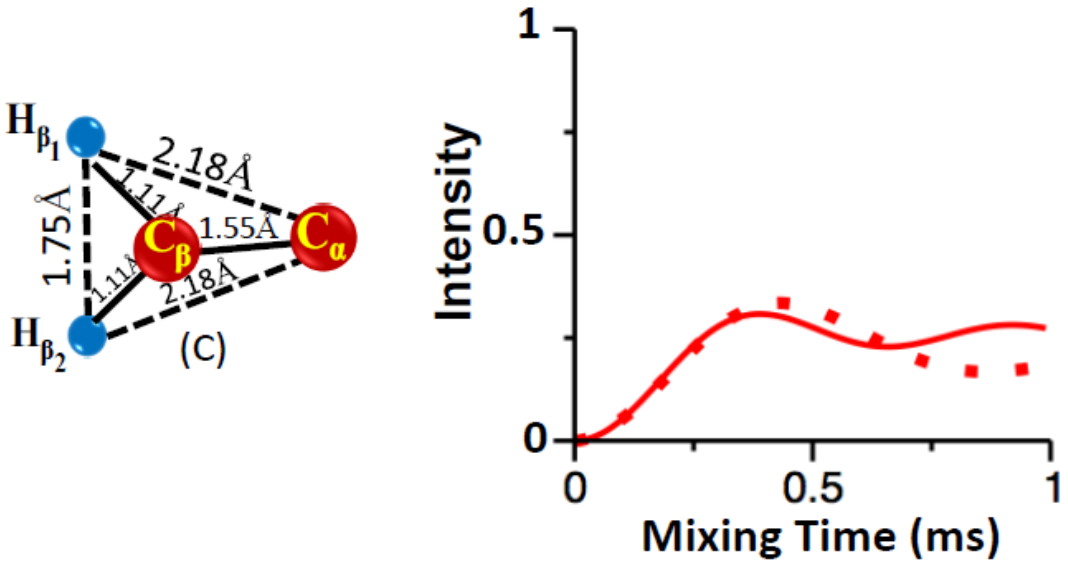

Figure 4.4: Simulations depicting polarization transfer to C_α in $C_\alpha C_\beta H_{\beta_1} H_{\beta_2}$. The analytic simulations emerging from the truncated effective Hami1tonian (comprising of only $C_\alpha H_{\beta_2}$) are compared with the exact numerical simulations (dots) involving all the four spins in $C_\alpha C_\beta H_{\beta_1} H_{\beta_2}$.

$^1H-^{13}C$ dipolar-coupling constants, the influence of passive spins in CP experiments varies. To illustrate this aspect, polarization transfer to C_α in $C_\alpha C_\beta H_{\beta_1} H_{\beta_2}$ (Figure 4.5(A1)), $C_\alpha C_\beta H_{\beta_1} H_\gamma$ (Figure 4.5(B1)) and $C_\alpha H_\alpha C_\beta H_{\beta_1}$ (Figure 4.5(C1)) is depicted (see Figure 4.5) both in the presence (indicated red) and absence (indicated in blue) of the second-order cross-terms resulting from the $^1H-^1H$ dipolar interactions. As depicted in Figure 4.5, the analytic simulations from the truncated effective Hamiltonians (indicated in red) are in good agreement with the numerical simulations (dots) in all the model four-spin systems. Due to smaller magnitude of the $C_\alpha - H_{\beta_2}$ dipolar coupling constant, the second-order cross terms resulting from $^1H-^1H$ dipolar interactions have a prominent role in the efficiency of polarization transfer in $C_\alpha C_\beta H_{\beta_1} H_{\beta_2}$(depicted in blue in panel A1). Hence, polarization transfer to C_α in the model four-spin systems (depicted through Figures 4.1(C-E)) could in principle be described within an isolated two-spin framework comprising of $C_\alpha - H_{\beta_2}$, $C_\alpha - H_\gamma$ and $C_\alpha - H_\alpha$ dipolar couplings, respectively. The truncated effective Hamiltonians are represented by,

$$H^{(eff)T}_{F,Four,C_\alpha} = \sum_{k=0}^{2} A^{(k)0}(C_\alpha H_\alpha) T^{(k)0}(C_\alpha H_\alpha) + \sum_{\lambda=C_\alpha,H_\alpha} B^{(1)0}(\lambda).iT^{(1)0}(\lambda) \quad (4.12)$$

$$H^{(eff)T}_{F,Four,C_\beta} = \sum_{k=0}^{2} A^{(k)0}(C_\beta H_{\beta_1}) T^{(k)0}(C_\beta H_{\beta_1}) + \sum_{\lambda=C_\beta,H_{\beta_1}} B^{(1)0}(\lambda).iT^{(1)0}(\lambda) \quad (4.13)$$

In a similar vein, polarization transfer to C_α in the model five-spin system $C_\alpha H_\alpha C_\beta H_{\beta_1} H_{\beta_2}$ was simulated using truncated effective Hamiltonians (see Figure 4.6). Based on the extensive analytic simulations, a schematic decomposition of polarization transfer in the chosen model systems is summarized through Fig-

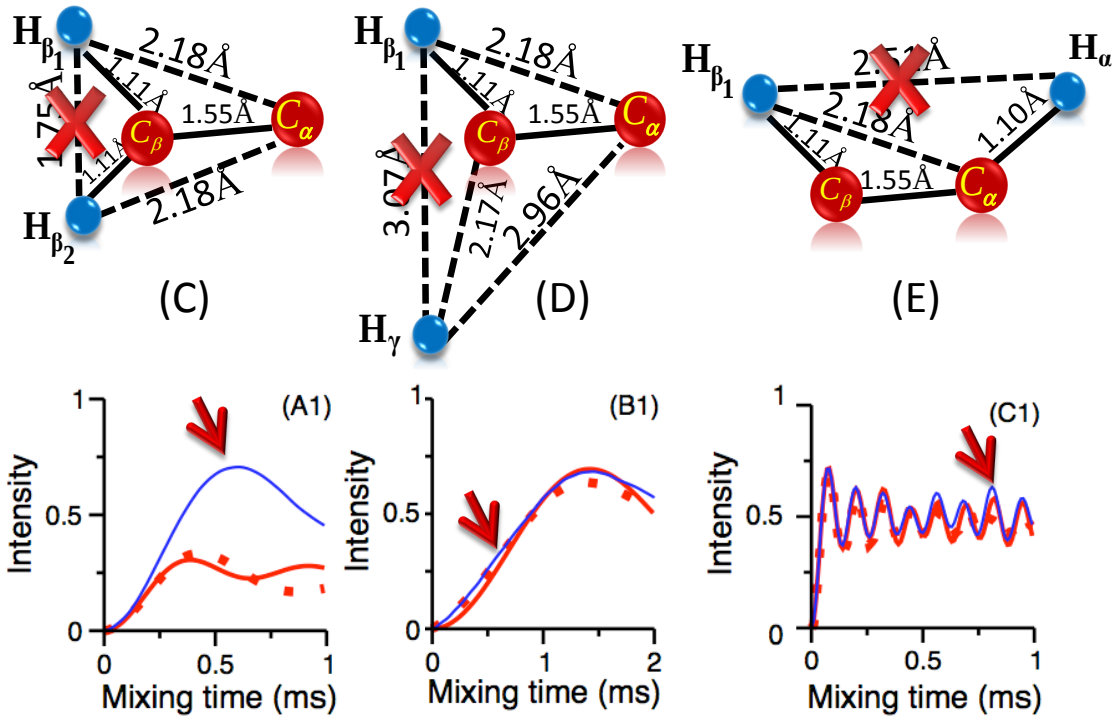

Figure 4.5: Simulations highlighting the role of ^{1}H$-^1$H-homonuclear dipolar interactions on polarization transfer to C_α in (A1) $C_\alpha C_\beta H_{\beta_1} H_{\beta_2}$ (B1) $C_\alpha H_\gamma C_\beta H_{\beta_1}$ and (C1) $C_\alpha H_\alpha C_\beta H_{\beta_1}$. The analytic simulations based on the truncated effective Hamiltonian (solid lines in red) are compared with the exact numerical simulations (dots) involving all the four spins in the chosen model systems. The analytic simulations depicted in blue represent the absence of second-order cross terms resulting from the ^{1}H$-^1$H dipolar interactions in the truncated Hamiltonian.

ure 4.7. Hence, in a strongly coupled system, dipolar truncation seems to be the driving force behind the propagation of spin polarization in first-order based CP experiments.In the following section, we explore the suitability of truncated effective Hamiltonians in understanding the propagation of spin polarization in second-order CP experiments[14].

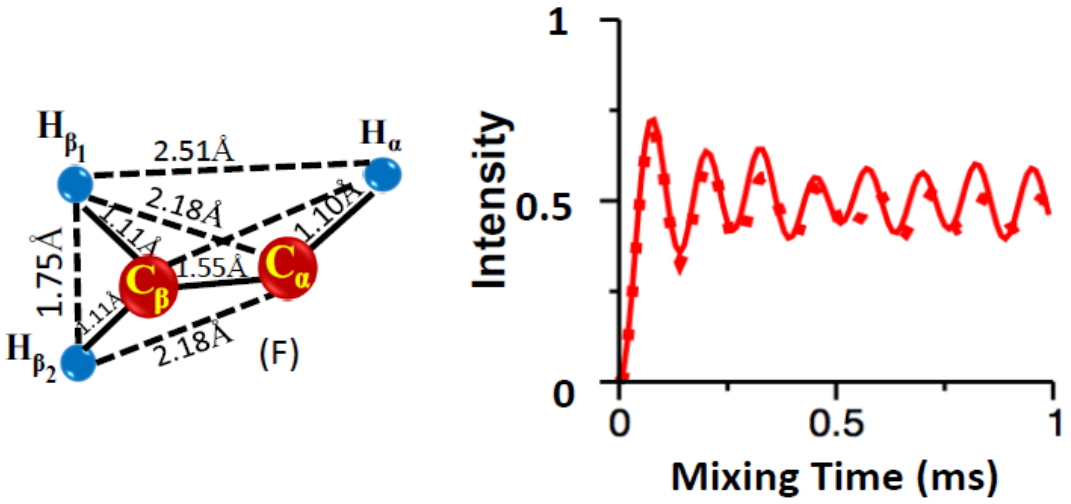

Figure 4.6: Simulations depicting polarization transfer to C_α in the model five-spin system ($C_\alpha H_\alpha C_\beta H_{\beta_1} H_{\beta_2}$). The analytic simulation (solid lines) comprising of the truncated effective Hamiltonians are compared with five-spin numerical simulations.

Second-order CP experiments

To minimize the effects of sample heating (due to RF fields) and facilitate implementation of CP-MAS experiments at faster spinning frequencies, schemes based on second-order recoupling were preferred over first-order CP experiments. In contrast to first-order based schemes, the three-spin operators (see Table 4.1) resulting from cross-terms between different pairs of dipolar interactions such as (a) Heternonuclear X Heteronuclear dipolar interactions (say $C_1{-}H_1XC_1{-}H_2$) (b) cross terms from Homonuclear X Heteronuclear interactions (such as $C_1{-}H_1XH_1{-}H_2$) facilitate the propagation of polarization in second-order based schemes. For e.g. in PAIN-CP[15] type experiments, polarization transfer from carbon to nitrogen is mediated through a proton that is coupled to both the spins (i.e. second-order cross-terms resulting from $C_1{-}H_1XN{-}H_1$), while in SOCP[14] experiments cross-

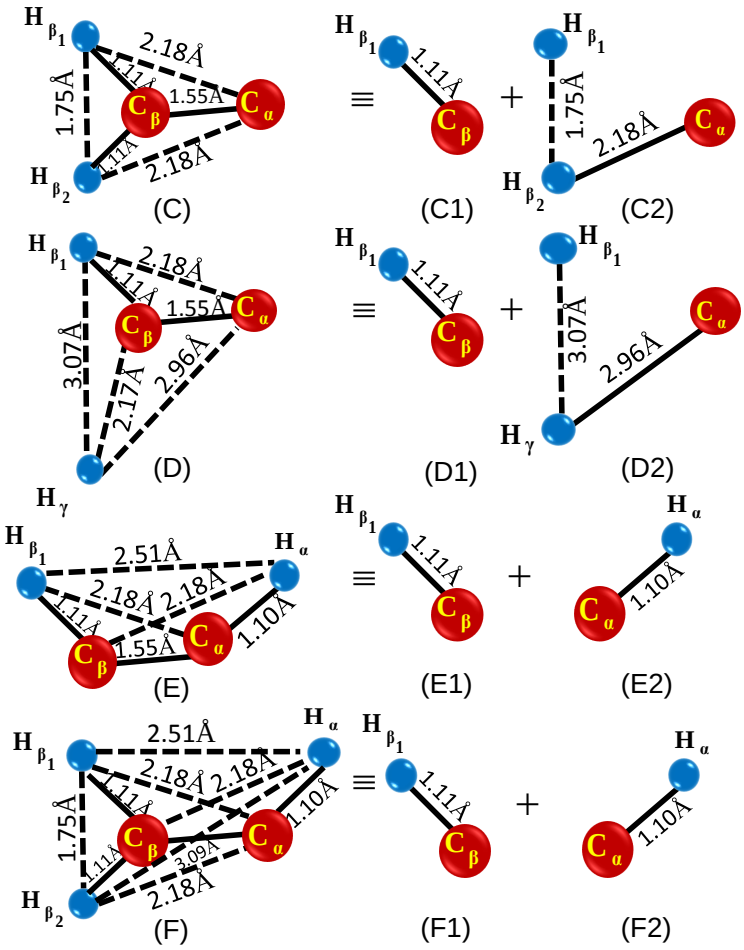

Figure 4.7: Schematic decomposition of polarization transfer in the model systems depicted in Figure 4.1.

terms from both (a) and (b) aid polarization transfer. In Figure 4.8, analytic simulations (based on effective Hamiltonians) depicting polarization transfer to C_α in SOCP experiments in model three ($C_\alpha H_{\beta_1} H_{\beta_2}$), four ($C_\alpha C_\beta H_{\beta_1} H_{\beta_2}$) and five-spin ($C_\alpha H_\alpha C_\beta H_{\beta_1} H_{\beta_2}$) systems is compared with exact numerical simulations (represented by dots).

Based on the effective Hamiltonian approach, polarization transfer in SOCP experiments is described in the Floquet-Liouville space through differential equations comprising of single-spin (e.g.$\Phi_0^{(1)}(\lambda, t), \lambda = I_1, I_2, S$) and three-spin polarizations

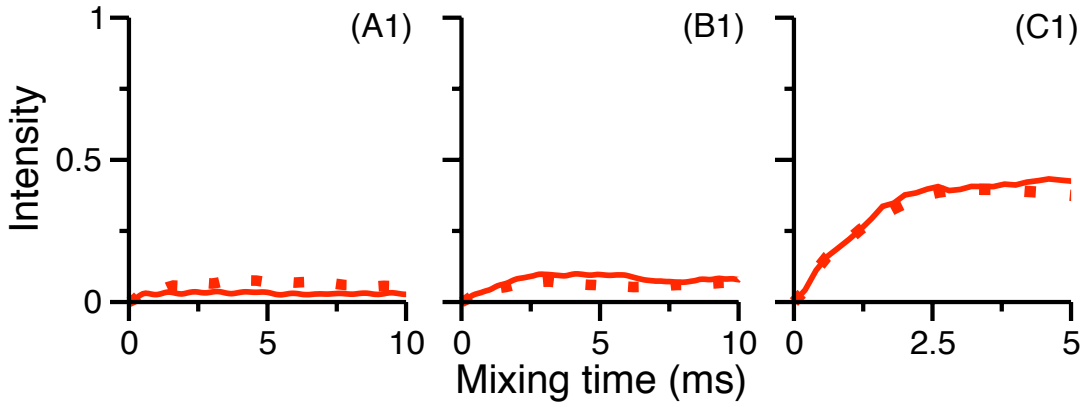

Figure 4.8: Simulations depicting the polarization transfer to C_α in (A1) $C_\alpha H_{\beta_1} H_{\beta_2}$ (B1) $C_\alpha C_\beta H_{\beta_1} H_{\beta_2}$ and (C1) $C_\alpha H_\alpha C_\beta H_{\beta_1} H_{\beta_2}$ based on second-order recoupling (SOCP). The simulations were performed at $\upsilon_r = 60$kHz and $\upsilon_{RF,C} = \upsilon_{RF,H} = 18$kHz.

$(\Phi_0^{(k)}(I_i I_j S, t))$

$$i\hbar \frac{d}{dt}\Phi_0^{(1)}(\lambda, t) = \sum P^{(k)0}(I_i I_j S)\Phi_0^{(k)}(I_i I_j S, t)$$

$$i\hbar \frac{d}{dt}\Phi_0^{(k)}(I_i I_j S, t) = \sum P^{(k_1)0}(I_i I_j S)\Phi_0^{(1)}(\lambda, t) + \sum P^{(1)0}(\lambda)\Phi_0^{(k_1)}(I_i I_j S, t) \tag{4.14}$$

Since polarization transfer in SOCP experiments is facilitated through three-spin operators, analytic descriptions based on the concept of effective Hamiltonians become less insightful when extended to larger groups of spin systems.

To explore the utility of truncated effective Hamiltonians in SOCP experiments, we begin our discussion with numerical simulations depicting polarization transfer to C_α in (A1) $C_\alpha H_{\beta_1} H_{\beta_2}$ (B1) $C_\alpha H_{\beta_1} H_\gamma$ and (C1) $C_\alpha H_\alpha H_{\beta_1}$ in Figure 4.9. The above three-spin models have been carefully chosen to illustrate the combined effects of homonuclear and heteronuclear dipolar couplings in the propagation of spin polarization in second-order CP experiments. Since three-spin operators (resulting from (a) $C_1{-}H_1$ X $C_1{-}H_2$) (b) $C_1{-}H_1$ X $H_1{-}H_2$)) facilitate the propa-

gation of spin polarization in SOCP experiments, the simulations depicting the polarization transfer to C_α in $C_\alpha H_{\beta_1} H_{\beta_2}$ are bit counter-intuitive, given that the magnitude of the second-order three-spin coefficients (refer Table 4.1) in $C_\alpha H_{\beta_1} H_{\beta_2}$ is greater in comparison to the three-spin models depicted in panels B1 and C1. To explain this anomalous result, we revisit the differential equations presented in Eq. 4.15.

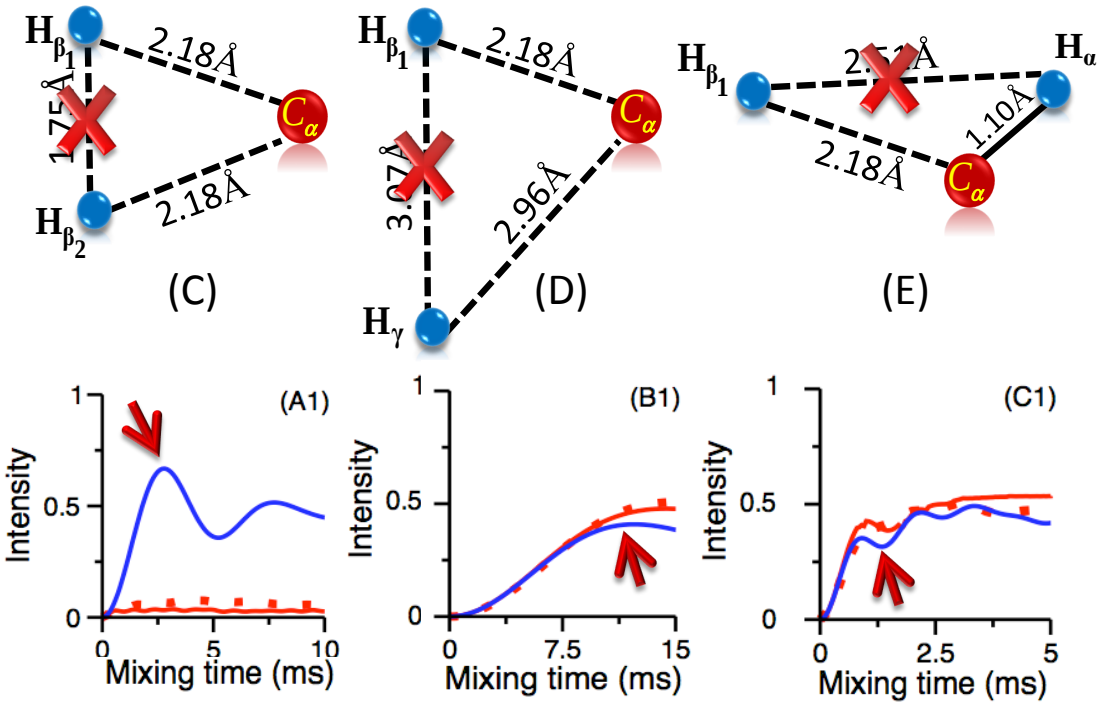

Figure 4.9: Simulations depicting the polarization transfer to C_α in model three-spin systems (A1) $C_\alpha H_{\beta_1} H_{\beta_2}$ (B1)$C_\alpha H_{\beta_1} H_\gamma$ and (C1) $C_\alpha H_\alpha H_{\beta_1}$ based on second-order recoupling (SOCP). The simulations were performed at $\upsilon_r = 60$kHz and $\upsilon_{RF,C} = \upsilon_{RF,H} = 18$kHz.The analytic simulations depicted in blue represent the absence of second-order cross-terms resulting from $^1H-^1H$ dipolar interactions in the truncated effective Hamiltonian.

In accord with the description of first-order based schemes[16–22], the coupled differential equations (see Eq. 4.15) reduce to a much simpler form, when the

magnitude of the coefficients associated with single-spin operators exceeds the magnitude of the three-spin coefficients (i.e.$P^{(1)0}(I_i) > P^{(k)0}(I_iI_jS)$).

$$i\hbar\frac{d}{dt}\Phi_0^{(1)}(\lambda,t) = 0$$

$$i\hbar\frac{d}{dt}\Phi_0^{(k)}(I_iI_jS,t) = \sum P^{(1)0}(I_i)\Phi_0^{(k_1)}(I_iI_jS,t) \tag{4.15}$$

Consequently, transfer of polarization among spins is inhibited in CP experiments. This aspect is exemplified in Figure 4.9 through a series of analytic simulations both in the presence (red) and absence of (depicted in blue) the second-order cross-terms resulting from the ^{1}H$-^1$H dipolar interactions. As illustrated (see panels 4.9(B1), 4.9(C1)), in strongly coupled systems (a condition satisfied in systems comprising of directly bonded ^{13}C and ^1H) the second-order cross-terms due to ^{1}H$-^1$H dipolar interactions are of lesser consequence. Hence, in the weak-coupling limit, the stronger homonuclear coupling (^{1}H$-^1$H) truncates the heteronuclear coupling ($^{13}C-^1H$) and is primarily responsible for the depolarization observed in both first-order and second-order CP experiments. The above observations are in accord with our earlier description of polarization transfer from carbon to nitrogen in presence of protons[13]. Hence, the magnitude of the single-spin operators, have a profound effect on the efficiency of polarization transfer in both first-order and second-order schemes. To further substantiate the utility of the truncated effective Hamiltonians, polarization transfer to C_α in model four-spin systems (depicted in Figure 4.10) were investigated.

To minimize the complexity in the description, truncated effective Hamilto-

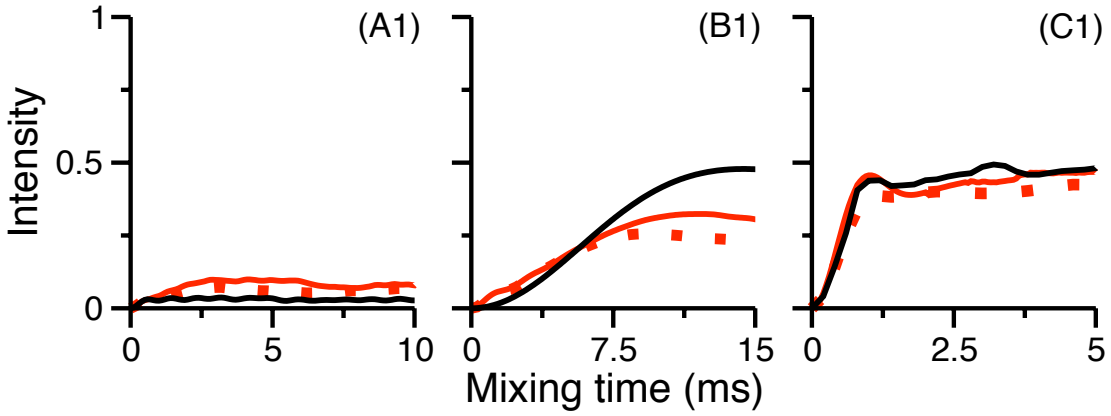

Figure 4.10: Simulations depicting the polarization transfer to C_α in model four-spin systems (A1) $C_\alpha C_\beta H_{\beta_1} H_{\beta_2}$ (B1)$C_\alpha C_\beta H_{\beta_1} H_\gamma$ and (C1) $C_\alpha H_\alpha C_\beta H_{\beta_1}$ based on second-order recoupling (SOCP). The simulations were performed at $\upsilon_r = 60$kHz and $\upsilon_{RF,C} = \upsilon_{RF,H} = 18$kHz.The analytic simulations depicted in black are derived from the three-spin model based on reduced effective Hamiltonian. The simulations depicted in red correspond to the four-spin model with solid lines depicting the analytic simulations (complete effective Hamiltonian) and dots denoting four-spin numerical simulations.

nians comprising of $T^{(k)0}(C_\beta H_{\beta 2} H_{\beta 1})$ and single-spin operators (i.e. the stronger coupling due to $T^{(k)0}(C_\beta H_{\beta 2} H_{\beta 1})$ (resulting from cross-terms between $C_\beta H_{\beta_1} \times H_{\beta_1} H_{\beta_2}$) truncates ((resulting from cross-terms between $C_\alpha H_{\beta_1} \times H_{\beta_1} H_{\beta_2}$)) were employed to describe the polarization transfer observed in $C_\alpha C_\beta H_{\beta_1} H_{\beta_2}$. As depicted in Figure 4.10, the analytic simulations based on the truncated effective Hamiltonians (indicated in black) are in better agreement in $C_\alpha C_\beta H_{\beta_1} H_{\beta_2}$ (panel A1) and $C_\alpha H_\alpha C_\beta H_{\beta_1}$(panel C1)). The deviations observed in $C_\alpha C_\beta H_{\beta_1} H_\gamma$ (panel B1), may be due to stronger correlations among protons and are of lesser consequence in real systems. Hence, the polarization transfer to C_α in $C_\alpha H_\alpha C_\beta H_{\beta_1}$ is modeled by

$$H^{(eff)T}_{F,Four,C_\alpha} = \sum_{k=0}^{2} A^{(k)0}(C_\alpha H_{\beta_1} H_\alpha) T^{(k)0}(C_\alpha H_{\beta_1} H_\alpha) + \sum_{\lambda = C_\alpha, H_{\beta_1}, H_\alpha} B^{(1)0}(\lambda).iT^{(1)0}(\lambda) \tag{4.16}$$

In contrast to first-order based schemes, the ^{1}H$-^1$H dipolar interactions play an influential role in the propagation of spin polarization in second-order CP experiments. When the magnitude of the homonuclear coupling (among protons) exceeds the heteronuclear coupling, truncation (through second-order cross-terms) is observed both in first-order and second-order based schemes. On the contrary, as illustrated through models depicted in Figures 4.1(C) and 4.1(D), the dipolar truncation between heteronuclear spin pairs (^{13}C$-^1$H) facilitates the propagation of spin polarization in first-order based CP schemes. Hence, dipolar truncation remains the main driving force behind the propagation of polarization among spins in strongly coupled systems.

4.4 Conclusions

In summary, the current study elucidates the important role of dipolar truncation in the propagation of polarization from protons to carbons in CP experiments. Based on the phenomenon of truncation, an alternate framework in the form of truncated effective Hamiltonians is proposed to describe the propagation of spin polarization in strongly coupled systems. In contrast to the effective Hamiltonian approach, the present model facilitates the analytic description even in strongly coupled systems. Employing this approach, polarization transfer in first-order based CP experiments is described by a pseudo two-spin model comprising of the active (^{13}C, ^1H) and passive spins. The effects of the ^{1}H$-^1$H dipolar interactions are incorporated through the longitudinal single-spin operators (protons) within the two-spin framework. In contrast to first-order based schemes, the ^{1}H$-^1$H-

dipolar interactions play a dual role in the propagation of the spin polarization in second-order schemes. Hence, in a strongly coupled network, propagation of spin polarization across the sample is predominantly facilitated through the weakly coupled protons (^{1}H$-^1$H interaction) in the system. The current study presents a probable mechanism of propagation of spin polarization in CP experiments and could well be employed to build theoretical models for quantifying polarization transfer in strongly coupled spin systems.

Appendix-4

In the following page Table 4.1 depicts the Second-order corrections to the effective Hamiltonian for a model three-spin system $I_1 I_2 S$. The spherical tensor operators have been constructed by sequential coupling[23] of the angular momentum vectors between the spins[24]. The constant 'N' in the pre-factors associated with the operators represents the number of spins and the results presented could be generalized for N-coupled (spin 1/2) systems. The indices p and r (can be integers/fractions) defined in the operators are due to $\omega_{RF,I} = p\omega_r, \omega_{RF,S} = r\omega_r$. In all the calculations and simulations in this chapter the following values of p and r have been employed: $p = \frac{2}{3}, r = \frac{1}{3}$ (in first-order schemes) and $p = r = 1$ (in second-order schemes). The indices p and r correspond to the indices n_1 and n_2 in eq. 4.5.

Table 4.1: Summary of Second-order corrections

Types of commutators	Coefficients	Operators
Single-spin operators		
(i) $\underbrace{\left[T^{(1)\pm1}_{m\pm p}(I_1), T^{(1)\mp1}_{-m\mp p}(I_1)\right]}_{\mathrm{CSA}\times\mathrm{CSA}}$	$\frac{G^{(1)\pm1}_{m\pm p}(I_1).G^{(1)\mp1}_{-m\mp p}(I_1)}{m\omega_r \pm \omega_{RF,I}}$	$\mp\left(\frac{1}{\sqrt{2}}\right)^{N-2}\frac{i}{2}T^{(1)0}_{\{1\}}(I_1)$
(ii) $\underbrace{\left[T^{(2)\pm2}_{m\pm2p}(I_1I_2), T^{(2)\mp2}_{-m\mp2p}(I_1I_2)\right]}_{\mathrm{DQ_{Homo}}\times\mathrm{DQ_{Homo}}}$	$\frac{G^{(2)\pm2}_{m\pm2p}(I_1I_2).G^{(2)\mp2}_{-m\mp2p}(I_1I_2)}{m\omega_r \pm 2\omega_{RF,I}}$	$\pm\left(\frac{1}{\sqrt{2}}\right)^{N-2}\frac{i}{2}\left[T^{(1)0}_{\{1\}}(I_1)+T^{(1)0}_{\{1\}}(I_2)\right]$
(iii) $\underbrace{\left[T^{(2)\pm2}_{m\pm p\pm r}(I_1S), T^{(2)\mp2}_{-m\mp p\mp r)}(I_1S)\right]}_{\mathrm{DQ_{Het}}\times\mathrm{DQ_{Het}}}$	$\frac{G^{(2)\pm2}_{m\pm p\pm r}(I_1S).G^{(2)\mp2}_{-m\mp p\mp r)}(I_1S)}{m\omega_r \pm \omega_{RF,I} \pm \omega_{RF,S}}$	$\pm\left(\frac{1}{\sqrt{2}}\right)^{N-2}\frac{i}{2}\left[T^{(1)0}_{\{0\}}(I_1)+T^{(1)0}_{\{0\}}(S)\right]$
Three-spin operators		
(i) $\underbrace{\left[T^{(2)\pm2}_{m\pm2p}(I_1I_2), T^{(2)\mp2}_{-m\mp p\mp r}(I_1S)\right]}_{\mathrm{DQ_{Homo}}\times\mathrm{DQ_{Het}}}$	$\frac{G^{(2)\pm2}_{m\pm2p}(I_1I_2).G^{(2)\mp2}_{-m\mp p\mp r}(I_1S)}{m\omega_r \pm 2\omega_{RF,I}}$	$\left(\frac{1}{\sqrt{2}}\right)^{N-3}\frac{i}{2}\begin{bmatrix}\pm\frac{1}{2\sqrt{5}}T^{(3)0}_{\{2\}}(I_1I_2S)+\frac{1}{2\sqrt{2}}T^{(2)0}_{\{2\}}(I_1I_2S)\pm\frac{1}{2}\sqrt{\frac{3}{10}}T^{(1)0}_{\{2\}}(I_1I_2S)\\ \\ -\frac{1}{2\sqrt{6}}T^{(2)0}_{\{1\}}(I_1I_2S)\mp\frac{1}{2\sqrt{2}}T^{(1)0}_{\{1\}}(I_1I_2S)-\frac{1}{2\sqrt{3}}T^{(0)0}_{\{1\}}(I_1I_2S)\end{bmatrix}$
(ii) $\underbrace{\left[T^{(2)\pm2}_{m\pm2p}(I_1I_2), T^{(2)\mp2}_{-m\mp p\mp r}(I_2S)\right]}_{\mathrm{DQ_{Homo}}\times\mathrm{DQ_{Het}}}$	$\frac{G^{(2)\pm2}_{m\pm2p}(I_1I_2).G^{(2)\mp2}_{-m\mp p\mp r}(I_2S)}{m\omega_r \pm 2\omega_{RF,I}}$	$\left(\frac{1}{\sqrt{2}}\right)^{N-3}\frac{i}{2}\begin{bmatrix}\pm\frac{1}{2\sqrt{5}}T^{(3)0}_{\{2\}}(I_1I_2S)+\frac{1}{2\sqrt{2}}T^{(2)0}_{\{2\}}(I_1I_2S)\pm\frac{1}{2}\sqrt{\frac{3}{10}}T^{(1)0}_{\{2\}}(I_1I_2S)\\ \\ +\frac{1}{2\sqrt{6}}T^{(2)0}_{\{1\}}(I_1I_2S)\pm\frac{1}{2\sqrt{2}}T^{(1)0}_{\{1\}}(I_1I_2S)+\frac{1}{2\sqrt{3}}T^{(0)0}_{\{1\}}(I_1I_2S)\end{bmatrix}$
(iii) $\underbrace{\left[T^{(2)\pm2}_{m\pm p\pm r}(I_1S), T^{(2)\mp2}_{-m\mp p\mp r}(I_2S)\right]}_{\mathrm{DQ_{Het}}\times\mathrm{DQ_{Het}}}$	$\frac{G^{(2)\pm2}_{m\pm p\pm r}(I_1S).G^{(2)\mp2}_{-m\mp p\mp r)}(I_2S)}{m\omega_r \pm \omega_{RF,I} \pm \omega_{RF,S}}$	$\left(\frac{1}{\sqrt{2}}\right)^{N-3}\frac{i}{2}\begin{bmatrix}\pm\frac{1}{2\sqrt{5}}T^{(3)0}_{\{2\}}(I_1I_2S)\mp\frac{1}{\sqrt{30}}T^{(1)0}_{\{2\}}(I_1I_2S)+\frac{1}{\sqrt{6}}T^{(2)0}_{\{1\}}(I_1I_2S)\\ \\ -\frac{1}{2\sqrt{3}}T^{(0)0}_{\{1\}}(I_1I_2S)\pm\frac{1}{\sqrt{6}}T^{(1)0}_{\{0\}}(I_1I_2S)\end{bmatrix}$

Types of commutators	Coefficients	Operators
Three-spin operators		
(iv) $\underbrace{\left[T^{(2)0}_{m}(I_1I_2), T^{(2)0}_{-m\mp p\pm r}(I_1S)\right]}_{\mathrm{ZQ_{Homo}\times ZQ_{Het}}}$	$\frac{G^{(2)0}_{m}(I_1I_2).G^{(2)0}_{-m\mp p\pm r}(I_1S)}{m\omega_r}$	$\left(\frac{1}{\sqrt{2}}\right)^{N-3}\frac{i}{2}\left[-\frac{1}{2\sqrt{2}}T^{(2)0}_{\{2\}}(I_1I_2S)+\frac{1}{2\sqrt{6}}T^{(2)0}_{\{1\}}(I_1I_2S)-\frac{1}{2\sqrt{3}}T^{(0)0}_{\{1\}}(I_1I_2S)\right]$
$\underbrace{\left[T^{(2)0}_{m}(I_1I_2), T^{(2)0}_{-m\mp p\pm r}(I_2S)\right]}_{\mathrm{ZQ_{Homo}\times ZQ_{Het}}}$	$\frac{G^{(2)0}_{m}(I_1I_2).G^{(2)0}_{-m\mp p\pm r}(I_2S)}{m\omega_r}$	$\left(\frac{1}{\sqrt{2}}\right)^{N-3}\frac{i}{2}\left[-\frac{1}{2\sqrt{2}}T^{(2)0}_{\{2\}}(I_1I_2S)-\frac{1}{2\sqrt{6}}T^{(2)0}_{\{1\}}(I_1I_2S)+\frac{1}{2\sqrt{3}}T^{(0)0}_{\{1\}}(I_1I_2S)\right]$
(v) $\underbrace{\left[T^{(2)0}_{m}(I_1I_2), T^{(0)0}_{-m\mp p\pm r}(I_1S)\right]}_{\mathrm{ZQ_{Homo}\times ZQ_{Het}}}$	$\frac{G^{(2)0}_{m}(I_1I_2).G^{(0)0}_{-m\mp p\pm r}(I_1S)}{m\omega_r}$	$\left(\frac{1}{\sqrt{2}}\right)^{N-3}\frac{i}{2}\left[-\frac{1}{2}T^{(2)0}_{\{2\}}(I_1I_2S)-\frac{1}{2\sqrt{3}}T^{(2)0}_{\{1\}}(I_1I_2S)\right]$
$\underbrace{\left[T^{(2)0}_{m}(I_1I_2), T^{(0)0}_{-m\mp p\pm r}(I_2S)\right]}_{\mathrm{ZQ_{Homo}\times ZQ_{Het}}}$	$\frac{G^{(2)0}_{m}(I_1I_2).G^{(0)0}_{-m\mp p\pm r}(I_2S)}{m\omega_r}$	$\left(\frac{1}{\sqrt{2}}\right)^{N-3}\frac{i}{2}\left[-\frac{1}{2}T^{(2)0}_{\{2\}}(I_1I_2S)+\frac{1}{2\sqrt{3}}T^{(2)0}_{\{1\}}(I_1I_2S)\right]$
(vi) $\underbrace{\left[T^{(2)0}_{m\pm p\mp r}(I_1S), T^{(2)0}_{-m\mp p\pm r}(I_2S)\right]}_{\mathrm{ZQ_{Het}\times ZQ_{Het}}}$	$\frac{G^{(2)0}_{m\pm p\mp r}(I_1S).G^{(2)0}_{-m\mp p\pm r}(I_2S)}{m\omega_r}$	$\left(\frac{1}{\sqrt{2}}\right)^{N-3}\frac{i}{2}\left[-\frac{1}{\sqrt{6}}T^{(2)0}_{\{1\}}(I_1I_2S)-\frac{1}{2\sqrt{3}}T^{(0)0}_{\{1\}}(I_1I_2S)\right]$
(vii) $\underbrace{\left[T^{(2)0}_{m\pm p\mp r}(I_1S), T^{(0)0}_{-m\mp p\pm r}(I_2S)\right]}_{\mathrm{ZQ_{Het}\times ZQ_{Het}}}$	$\frac{G^{(2)0}_{m\pm p\mp r}(I_1S).G^{(0)0}_{-m\mp p\pm r}(I_2S)}{m\omega_r}$	$\left(\frac{1}{\sqrt{2}}\right)^{N-3}\frac{i}{2}\left[\frac{1}{2}T^{(2)0}_{\{2\}}(I_1I_2S)-\frac{1}{2\sqrt{3}}T^{(2)0}_{\{1\}}(I_1I_2S)\right]$
(viii) $\underbrace{\left[T^{(0)0}_{m\pm p\mp r}(I_1S), T^{(2)0}_{-m\mp p\pm r}(I_2S)\right]}_{\mathrm{ZQ_{Het}\times ZQ_{Het}}}$	$\frac{G^{(0)0}_{m\pm p\mp r}(I_1S).G^{(2)0}_{-m\mp p\pm r}(I_2S)}{m\omega_r}$	$\left(\frac{1}{\sqrt{2}}\right)^{N-3}\frac{i}{2}\left[-\frac{1}{2}T^{(2)0}_{\{2\}}(I_1I_2S)-\frac{1}{2\sqrt{3}}T^{(2)0}_{\{1\}}(I_1I_2S)\right]$
(ix) $\underbrace{\left[T^{(0)0}_{m\pm p\mp r}(I_1S), T^{(0)0}_{-m\mp p\pm r}(I_2S)\right]}_{\mathrm{ZQ_{Het}\times ZQ_{Het}}}$	$\frac{G^{(0)0}_{m\pm p\mp r}(I_1S).G^{(0)0}_{-m\mp p\pm r}(I_2S)}{m\omega_r}$	$\left(\frac{1}{\sqrt{2}}\right)^{N-3}\frac{i}{2}\left[\frac{1}{\sqrt{3}}T^{(0)0}_{\{1\}}(I_1I_2S)\right]$

References

[1] U. Haeberlen, *High-Resolution NMR in Solids: Selective Averaging*, Academic, New York, 1976.

[2] M. Mehring, *Principles of High Resolution NMR in Solids*, Springer Verlag, Berlin, 1999.

[3] A. Abragam, *The Principles of Nuclear Magnetism*, Clarendon, Oxford, 1961.

[4] M. J. Bayro, M. Huber, R. Ramachandran, T. C. Davenport, B. H. Meier, M. Ernst and R. G. Griffin, *J. Chem. Phys.*, 2009, **130**, 114506.

[5] B. Meier, *Chem. Phys. Lett.*, 1992, **188**, 201 – 207.

[6] C. P. Slichter, *Principles of Magnetic Resonance*, Springer, Heidelberg, 1990.

[7] M. Veshtort and R. G. Griffin, *J. Magn. Reson.*, 2006, **178**, 248 – 282.

[8] M. Maricq and J. S. Waugh, *J. Chem. Phys.*, 1979, **70**, 3300–3316.

[9] E. Stejskal, J. Schaefer and J. Waugh, *J. Magn. Reson.*, 1977, **28**, 105 – 112.

[10] J. Schaefer and E. O. Stejskal, *J. Am. Chem. Soc.*, 1976, **98**, 1031–1032.

[11] J. Schaefer, E. Stejskal, J. Garbow and R. McKay, *J. Magn. Reson.*, 1984, **59**, 150 – 156.

[12] R. Ramachandran and R. G. Griffin, *J. Chem. Phys.*, 2006, **125**, 044510.

[13] M. K. Pandey and R. Ramachandran, *Molecular Physics*, 2011, **109**, 1545–1565.

[14] A. Lange, I. Scholz, T. Manolikas, M. Ernst and B. H. Meier, *Chem. Phys. Lett.*, 2009, **468**, 100 – 105.

[15] J. R. Lewandowski, G. De Paëpe and R. G. Griffin, *J. Am. Chem. Soc.*, 2007, **129**, 728–729.

[16] M. Bjerring and N. C. Nielsen, *Chem. Phys. Lett.*, 2003, **382**, 671 – 678.

[17] M. Bjerring, J. T. Rasmussen, R. Schultz Krogshave and N. C. Nielsen, *J. Chem. Phys.*, 2003, **119**, 8916–8926.

[18] M. Bjerring, A. B. Nielsen, Z. Tosner and N. C. Nielsen, *Chem. Phys. Lett.*, 2010, **494**, 326 – 330.

[19] C. P. Jaroniec, B. A. Tounge, C. M. Rienstra, J. Herzfeld and R. G. Griffin, *J. Am. Chem. Soc.*, 1999, **121**, 10237–10238.

[20] C. P. Jaroniec, C. Filip and R. G. Griffin, *J. Am. Chem. Soc.*, 2002, **124**, 10728–10742.

[21] R. Ramachandran, V. Ladizhansky, V. S. Bajaj and R. G. Griffin, *J. Am. Chem. Soc.*, 2003, **125**, 15623–15629.

[22] V. Ladizhansky and R. G. Griffin, *J. Am. Chem. Soc.*, 2004, **126**, 948–958.

[23] B. C. Sanctuary, *J. Chem. Phys.*, 1976, **64**, 4352–4361.

[24] R. Ramachandran, V. S. Bajaj and R. G. Griffin, *J. Chem. Phys.*, 2005, **122**, 164503.

Chapter 5

Summary and Conclusions

Development of analytic methods to study the dynamics of coupled spins in NMR spectroscopy is essential for both quantifying experimental results as well as designing new experiments. With the advent of higher magnetic field strengths and faster spinning modules, the stringent conditions of synchronization (between the MAS rotor period and the cycle time of a multiple pulse scheme) imposed by AHT seem less useful in the optimal design/implementation of ssNMR experiments. As an alternative, we explore the role of Floquet theory in the design of NMR experiments. In the past, analytic descriptions based on Floquet theory were limited primarily owing to the complexity arising from the infinite dimensionality of the problem in the Floquet Hilbert space. However, the advent of effective Hamiltonians derived from the contact transformation procedure seems to have totally mitigated the problem of infinite dimensionality in Floquet descriptions. For demonstrative purposes, the CPMAS experiment is employed as a case study in this thesis. In contrast to existing descriptions based on AHT, the effective Floquet Hamiltonians derived in this thesis predict the existence of several matching conditions that presumably would be impractical within the AHT

framework. The matching conditions (both zero-quantum and double-quantum) derived from our theory facilitate the implementation of CP experiments at faster spinning frequencies with nominal RF requirements. The predictions emerging from our theory are thoroughly substantiated using numerical simulations under different experimental conditions.

The second stage of our study focuses on the development of an analytic approach for describing multiple-pulse experiments under MAS. In contrast to descriptions involving constant RF amplitudes, analytic theory of multiple pulse experiments is complicated due to varying RF amplitudes in the rotating frame. In a typical multiple-pulse sequence, the phase and amplitude of the oscillating magnetic field plays an important role in the time-evolution of the spin system of interest. In particular, understanding the role of the modulation frequency (encountered during phase modulation/amplitude modulation experiments) with respect to the sample spinning frequency is essential in the optimal design of experiments. Often the synchronization condition imposed by the requirements of AHT seem to be the main hindrance in the design of new experiments. To address this issue, an alternate framework based on multimode-Floquet theory is presented in this thesis for describing multiple pulse experiments in ssNMR. As a test case, phase modulated CP experiment was employed in our study. The framework presented in this thesis is quite general and well suited for analytic description of schemes that involve modulations both synchronous and asynchronous with respect to the sample spinning frequency. The interplay between the modulation frequency and spinning frequency is outlined in terms of effective Hamiltonians

are well corroborated through exact numerical simulations. The final stage of our study focussed on developing mathematical models for quantifying polarization transfer among spins in ssNMR. As the number of constraints available in the solid state is limited due to limited spectral resolution, the accuracy of the measurements/interpretation of the experimental results becomes very critical. Based on the phenomenon of "dipolar truncation", truncated effective Hamiltonians are proposed to account for the multi-spin effects observed in a strongly coupled network. In contrast to the effective Hamiltonian approach, this model facilitates analytic description even in strongly coupled systems. Employing this approach, polarization transfer in first-order based CP experiments is described by a pseudo two-spin model comprising of the active (^{13}C, ^{1}H) and passive spins. The effects of the ^{1}H$-^{1}$H dipolar interactions are incorporated through the longitudinal single-spin operators within the two-spin framework. Hence, in a strongly coupled network, propagation of spin polarization across the sample is predominantly facilitated through the weakly coupled protons (^{1}H$-^{1}$H interaction) in the system. To test the validity of the models, analytic simulations are compared with numerical simulation programs based on SPINEVOLUTION. The current study presents a probable mechanism of propagation of spin polarization in CP experiments and could well be employed to build theoretical models for quantifying polarization transfer in strongly coupled spin systems. Such possibilities need to be explored in the near future.

Publications

(1) "Understanding cross-polarization (CP) NMR experiments through dipolar truncation"

Manoj Kumar Pandey, Zeba Qadri, and Ramesh Ramachandran,

Journal of Chemical Physics, **138**, 114108 (2013)

(2) "Description of amplitude and phase-modulations in heteronuclear recoupling experiments in solid-state NMR"

Zeba Qadri and Ramesh Ramachandran (*Manuscript under preparation*)